A STUDY OF LOW ENERGY COSMIC RAYS AT 1 A.U.

JAMES H. KINSEY

SEPTEMBER 1969

GSFC ——— GODDARD SPACE FLIGHT CENTER ———
GREENBELT, MARYLAND

APPROVAL SHEET

Title of Thesis: A Study of Low Energy Cosmic Rays at 1 A. U.

Name of Candidate: James Humphreys Kinsey
                    Doctor of Philosophy, 1970

Thesis and Abstract Approved: _____
                              Frank B. McDonald
                              Professor of Physics
                              Part Time

Date Approved: September 2, 1969

ABSTRACT

Title of Thesis: A Study of Low Energy Cosmic Rays at 1 A. U.

James H. Kinsey, Doctor of Philosophy, 1970

Thesis directed by: Frank B. McDonald

Professor of Physics, Part Time

The results from the two scintillator ΔE versus $E - \Delta E$ telescopes on IMP-III and IMP-IV and the solid state telescope on IMP-IV are analyzed and the resulting proton and alpha particle fluxes presented. The low energy flux time histories and energy spectra are shown for the energy interval 18.7 to 81.7 MeV/nucleon from June 1965 to April 1967, and in the interval from 5.2 to 81.7 MeV/nucleon from May 1967 to August 1968.

A comparison of the quiet time spectra of both protons and alpha particles is made.   It is shown that the results after solar minimum in 1965 do not agree with currently accepted theory in the low energy region of the spectrum considered.   Further, it is shown that the reason for this may be because of a hysteresis in the particle fluxes with respect to energy.

In September of 1966 a very abrupt decrease in proton fluxes at energies of 70 MeV and below is shown to have occurred which did not recover again to its previous level.   This decrease is attributed to a change in the properties of the propagation medium following the large solar proton event of 2 September 1967.

It is found that there is a fairly flat ratio of He^3 to $He^3 + He^4$ in the energy range considered, with a value of about 7%.

Further evidence is presented for the existence of both recurrence events with 27 day periods which are related to large calcium plage regions on the sun and co-rotating regions which produce discrete proton events observed at earth. These observations serve further to establish the source of protons with MeV energies.

A two component model of low energy cosmic rays is investigated in relation to the IMP-IV proton and alpha particle data. This model treats the observed cosmic ray flux as the sum of two power laws in energy, one with a negative exponent which is taken as the solar component and the other with a positive exponent which is identified with the modulated galactic primary component. It is shown that this model fits the observed spectra extremely well in the energy and time intervals considered.

A STUDY OF LOW ENERGY COSMIC

RAYS AT 1 A. U.*

by
James H. Kinsey

Dissertation submitted to the Faculty of the Graduate School
of the University of Maryland in partial fulfillment
of the requirements for the degree of
Doctor of Philosophy
1970

ACKNOWLEDGEMENTS

TABLE OF CONTENTS

LIST OF TABLES

LIST OF FIGURES

I. INTRODUCTION

A. General

Until 1958, with the launching of the first scientific satellite, all measurements of the energetic particle population in the solar system came from ground based, balloon borne, or rocket borne particle detectors. Balloon experiments measured the fluxes of primary cosmic ray particles in the range of kinetic energies from $\sim 10^8$ to 10^{10} ev/ nucleon. Above this energy it was necessary to rely on the measurements of the secondary cascade particles created in the earth's atmosphere by high energy primaries with kinetic energies of between 10^{15} and 10^{20} ev/ nucleon using ground based air shower experiments. Below about 10^8 ev/ nucleon and also in the range between the balloon and air shower measurements, little was known of the particle populations. Artificial satellites quickly became extremely attractive as particle experiment platforms since it is possible to get completely above the last vestiges of atmosphere for long periods and in some cases to get outside the earth's magnetosphere. This is a vast improvement over balloons, which can only reach altitudes where there is still a few g cm^{-2} of air remaining above them and only for periods of tens of hours.

The motivation and justification for putting particle detection experiments aboard satellites is several-fold. First of all it is desirable to study the intrinsic particle populations at 1 A. U. free of as much of the effects of the atmosphere and magnetosphere as possible. Further, one would like to ascertain the interstellar spectrum of particles and in order to do this it is advantageous to start with as few extraneous effects as possible. Finally, it is of interest to study

1

the propagation of particles coming from the sun as well as the sun as a source of energetic particles.

The actual form of the interstellar particle energy spectrum is not directly measurable near the earth because of the solar modulation of particles passing into the solar system. It is also now known that the sun itself accelerates copious quantities of particles in conjunction with solar flares and at low energies is producing a quasi-continuous component of energetic particles. This is contrary to the previously made assumption that during solar quiet times the observed energy spectrum of cosmic rays was predominantly the solar modulated galactic spectrum. Such energy spectra for both protons and alpha particles are shown in Figure 1 for the period in 1965 near the minimum of solar modulation. A local minimum in the neighborhood of 50 MeV/nucleon complicates the behavior of this spectrum in the energy interval below about 300 MeV/nucleon. The problems of the form of the solar modulation and the amount of solar particle contribution to the lower energy portion of the cosmic ray spectrum must be solved in order that the true interstellar spectrum may be determined, as well as contributing to the understanding of the sun as a source of energetic particles and the understanding of the large scale structure of the interplanetary medium.

The importance of knowing the true interstellar particle energy spectra, particularly for protons, with energies below 300 MeV/nucleon is quite apparent. Because of the steepness of the spectrum at higher energies, it is possible that most of the energy transported by cosmic rays in interstellar space is resident in protons having kinetic energies below 1 GeV. Cosmic rays have an energy density in space that is comparable to the energy density resident in all forms of electromagnetic radiation.

The amount and form of this energy is most important for the equilibrium balance of energy in the galaxy, for instance. Balasubrahmanyan et al. (1967) have shown that the observed heating of interstellar HĪ clouds using an assumed rate for the heating can be accomplished by the coulomb interactions of cosmic rays with the matter in these clouds if the low energy fluxes are high enough. Theory shows that the lower energy component of the cosmic rays would do most of the heating.

Since the sun plays so important a role in controlling the particle fluxes seen at earth, it is of interest to compare cosmic rays and solar activity with respect to time. Figure 2 shows the average of the smoothed sunspot numbers for cycles 1 through 19 superimposed on the current cycle number 20. On this plot is also shown the monthly averages of the Deep River hourly neutron rates with an inverted rate scale. There appears to be a time lag of about one year of the neutron rates behind the sunspot numbers. It has been shown by several workers that this apparent hysteresis between solar activity and neutron rates is probably not significant in itself. Simpson and Wang (1967) and Hatton et al. (1968) have shown that the coronal FeXXVI green line at $\lambda 5303$ correlated very well with the cosmic rays and with no apparent time lag. Balasubrahmanyan (1969) showed that the magnetic index A_p, which is closely correlated with the solar wind velocity, also correlates well with the neutron rates during solar cycle 19.

Since the observations of Lange and Forbush (1942) that there was a correlation between sea level ion chamber counting rates and solar flares, it has been known that the sun was a source of energetic particles. Although these solar particles are sometimes referred to as "solar cosmic rays," the term "cosmic rays" is usually reserved for

particles originating outside of the solar system. There is substantial evidence that non-flare associated particles are released by the sun in so-called recurrence events with a 27 day period as well as in connection with isolated solar active regions of less than 27 days lifetime (Fichtel and McDonald, 1967). The 27 day period is the equatorial rotation period of the sun. The proton flux increases associated with this rotation occur approximately when a large persistent calcium plage region passes central meridian each rotation.

Briefly, then, the observed characteristics at 1 A. U. of these four different classes of particles are

1. Galactic cosmic rays which make up the bulk of particles detected at energies of about 50 MeV/nucleon and above during solar quiet times.

2. Solar flare particles which are a transient component with increases of as many as 6 orders of magnitude above quiescent rates at low energies. These particles show very rapid rise times in their fluxes followed by exponential decays of the order of days. The energy spectra of flare particles is steep and of negative slope.

3. Recurrence event particles whose fluxes rise slowly to a plateau for several days and then decay again so that the flux-time profile is quite symmetrical. These particles are recognized by their 27 day recurrence pattern usually coinciding with the time of meridian transit of large persistent calcium plage regions on the solar disk.

4. Increases in low energy fluxes during quiet times similar in character to the 27 day recurrence events, but which occur only

occasionally. These particles are associated with large active regions near the central solar meridian.

The interplanetary magnetic field is composed of the various magnetic flux loops originating in the sun and transported radially outward by the solar wind. Near the sun, as shown by Parker (1963), the mean field has the configuration of an archimedian spiral, which much of the time dominates the propagation of low energy particles moving from the sun outward. On the other hand, the irregularities that exist in these fields cause scattering of particles and give rise to diffusion-like flux characteristics. The cosmic rays coming into the solar system interact with these moving fields and their irregularities, and it is the form of these interactions that determines the form of the flux modulations.

The earth's field also dominates the motion of charged particles entering the magnetosphere. The interactions are such that at a given latitude there exists a critical momentum below which particles are deflected back into interplanetary space rather than being able to penetrate near to the earth's surface. This critical momentum, or rigidity, is inversely proportional to geomagnetic latitude. This effect is used in balloon latitude surveys such as carried out by Neher (1967) as a naturally existing magnetic analyzer to determine the spectrum of cosmic rays.

Most cosmic ray experiments detect charged particles by measuring the signal produced when they lose energy in passing through the material of the detector. Knowing the effective area and solid angle subtended by the detector for incident particles and the number of particles counted during a specific time period, it is possible to

express the observation as a specific flux, or intensity, of particles with units of number per unit time, unit area and unit solid angle. Such fluxes may be studied in terms of essentially four experimental observables:

1. Energy dependence.

2. Charge and mass composition.

3. Time dependence.

4. Directional dependence

Over the past few years there has been a several fold improvement in resolution of these observables because of continually improving experimental techniques.

B. Galactic Cosmic Rays

During periods of minimal solar activity when there are few, if any, major flares, the residual particle flux was generally accepted to be coming from outside the solar system. The modulation effect becomes small at higher energies than $\sim$ 12 GeV and the differential particle flux, i.e., the flux per unit energy interval, has been found to fit a power law in kinetic energy per nucleon quite well at higher energies and is usually expressed as

$$dJ/dE = KE^{-\gamma} \qquad (1),$$

where the nominal value of the power law index is $\gamma \simeq 2.5$. The integral flux $J(> E_0)$, which is the quantity measured when using the geomagnetic latitude effect, is defined as the total flux above some energy E_0 and is related to the differential flux by

$$J(> E_0) = \int_{E_0}^{\infty} (dJ/dE) \, dE = K'E_0^{-(\gamma-1)} \qquad (2).$$

The outstanding features of the galactic component at 1 A. U. can be characterized by the following general observations:

1. A very long term time variation with a period of 11 years, which is the period of the solar cycle itself. The cycle of the particle fluxes lags the sunspot cycle by about one year.

2. Nearly an isotropic distribution of particle arrival directions is observed.

3. A monotonically decreasing energy spectrum above 300 MeV which approaches quite well a power law in energy with an index of -2.5 above about 12 GeV.

4. A composition which differs quite markedly from universal abundances in that there are more heavy nuclei than would be expected.

5. The energy density of cosmic rays is approximately .5 eV cm^{-3} which is comparable to other forms of energy in the galaxy such as that contained in electromagnetic radiation and the interstellar magnetic fields.

6. Frequent decreases in counting rates of a temporary nature associated with magnetic storms and frequently following solar flares and closely coinciding with the arrival of the resultant plasma wave at the detector. These decreases are called Forbush decreases.

Any model for the production of cosmic rays must invoke sources energetic enough to account for the total energy observed and must also provide a means of transforming such energy into kinetic energy of the particles. Several source mechanisms have been considered in the literature. One of the earliest such mechanisms discussed was the Fermi

acceleration mechanism, a process in which particles could increase their energies by multiple reflections from moving magnetic fields. A very clear discussion of this mechanism is given by Morrison (1961). One of the most attractive sources up to the present has been the supernova, which provides adequate energy and has a frequency and spatial distribution in the galaxy, such as to account for the isotropy observed in cosmic ray fluxes, as well as being a potentially good source of heavy nuclei which are abundant in the cosmic ray primaries. Supernova acceleration models have been discussed by Burbidge, Burbidge, Fowler, and Hoyle (1957), Colgate and Johnson (1960), Colgate and White (1963), and Arnett (1966). Most recently since the discovery of pulsars there has been some discussion that these objects could be the source of cosmic rays. Of the above source mechanisms, the Fermi process is probably the least likely since the energy spectrum of particles that can be calculated using this model is steeper by at least an order of magnitude than is observed.

The nuclear composition of cosmic rays and their comparison to universal abundances is a very important source of information about not only the source of the particles themselves, but also about the propagation of these particles through the interstellar medium and the nature of this medium itself. The abundances of heavy nuclei with respect to protons is much higher in cosmic rays than in the universal scale. This fact can be interpreted either as being due to sources rich in heavy elements, which would be the case for supernovae since they have evolved their element burning up to iron, or the superabundance of heavies can be attributed to preferential acceleration of heavies over the lighter nuclei (Ginzburg and Syrovatskii, 1964). The latter

is not likely on the basis of solar particles which are deficient in heavies. Further, there is an anomolous abundance of the light elements He^3, Li, Be, and B in cosmic rays. These are most easily accounted for by fragmentation of the heavy nuclei on the interstellar hydrogen in their propagation from the source through the interstellar medium to the observer. Assuming that the source abundances of all components are the same as the universal abundances, it can be shown that the superabundances of this light component can be accounted for if the integrated hydrogen along the path of propagation is of the order of 4.1 g cm^{-2} (Ramaty and Lingenfelter, 1969).

Very closely related to the nuclear content of cosmic rays is the electron component and its relation to the electromagnetic radiation associated with cosmic rays. One might expect to find equal numbers of electrons and positive ions present in cosmic rays. On the contrary the ratio of electrons to protons observed in cosmic rays is about 1%. For a time it was believed that the electrons might be produced locally in interstellar space by the high energy interaction of cosmic rays, such as p - p reactions and neutron decay (Ramaty and Lingenfelter, 1966). L'Heureux (1967) has shown that this theory is not consistent with observed results, because the spectra of electrons and positrons produced by this mechanism fall well below the observed spectra. Further, the collision theory predicts that there should be an excess of positrons in the cosmic rays. That this is indeed not the case has been shown (Hartman, et al., 1965). One is left then with the conclusion that electrons are probably accelerated by a hierarchy of sources. Evidence that this is true is exhibited in supernovae remnants such as the Crab Nebula, which is a strong emitter of polarized radio emission consistent

with synchrotron emission from electrons trapped in the remnant's magnetic fields. Recent advances in x-ray and gamma ray astronomy indicate an abundance of sources for these forms of radiation in the galaxy (Fazio, 1967; Morrison, 1967). The assumption is that these observed sources of photons are probably where the cosmic rays are being accelerated, or at least part of them.

C. Cosmic Ray Modulation

Any theory that would attempt to infer properties about interstellar space and the galaxy in general from the observed cosmic rays in the vicinity of 1 A. U. must include a means to account for the changes in the cosmic ray fluxes. Observed cosmic ray fluxes are modulated with a period of 11 years. Webber (1967) has summarized and compared the observations of a number of workers very well up to the minimum in solar modulation in 1965. The general assumption has been that in the absence of solar flares and recurrence events, the quiet time observed particle fluxes are primarily the modulated galactic component (Gloeckler and Jokipii, 1966). There has been to date a small amount of evidence that at very low energies there might be a quiet time solar contribution (Meyer and Vogt, 1963; Fan et al., 1968, 1969). Neher (1967) by means of latitude surveys of ionization rates with balloon borne ionization counters has set an upper bound of approximately a factor of 4 to the change in the integral flux of particles for energies > 100 MeV between solar maximum and minimum. Vogt (1962) and Meyer and Vogt (1963) found primary proton spectra in 1960 and 1961 following the previous solar minimum which were considerably higher below 100 MeV than any of the other observations to date. Furthermore, they found a relative minimum at about 100 MeV as compared to the one at about 50 MeV. There has

been speculation as to whether the present spectrum could return to values such as they observed.

Parker (1958, 1963, 1966) has treated modulation as both a convective process whereby the scattering centers in the magnetic fields are being strongly affected by solar activity, and in terms of adiabatic deceleration of incoming particles due to the effectively expanding magnetic field in the solar wind. Theoretical treatments of solar modulation have been done by Gleeson and Axford (1968), Jokipii (1967, 1968), and Jokipii and Parker (1967). A good summary of the critical aspects of the various theories with respect to the observations is given by Webber (1968).

Parker's theoretical relation for modulation (1963) may be expressed as

$$dj_e (P,t) = dj_\infty(P) e^{-\int_{1 \ a.u.}^{\infty} \frac{w}{\kappa} \, dr} \tag{3},$$

where the differential flux at the orbit of earth dj_e is a function of particle rigidity and time, dj_∞ is the unmodulated flux beyond the solar system and w and κ are the solar wind velocity and diffusion coefficients, respectively. Gloeckler and Jokipii (1966) have shown that the diffusion coefficient is separable into the produce of a function of rigidity and velocity and a function of radial distance and time, thus

$$\kappa = f(P,\beta) \, g(r,t) \tag{4}.$$

Using this last relation it is possible then to express (3) in the form

$$dj_e (P,t) = dj_\infty (P) \, e^{-\eta(t)/f(P,\beta)} \tag{5}.$$

Following Nagashima et al. (1966), it is convenient for comparison of spectra at different epochs t and t' to take the logarithm of the ratios of the two fluxes using equation (5) to get

$$\ln \frac{dj_e\ (P,t)}{dj_e\ (P,t')} \ = \ \frac{\Delta\eta}{f(P,\beta)} \tag{6},$$

with

$$\Delta\eta \ = \ \eta(t') \ - \ \eta(t) \tag{7}.$$

Webber (1962) shows that using the relation in equation (6) with t corresponding to the solar minimum in 1965 and t' for the fluxes prior to this time that the form of $f(P,\beta)$ is $P\beta$ for $P > 1$ GV. The $1/P\beta$ and $1/\beta$ dependency of the logarithmic ratio of fluxes holds for both protons and alpha particles; however, the modulation constant for protons is larger. For the time period considered, Webber shows that the observations support a mixture of both the diffusion-convection and the energy loss theories.

D.   Solar Proton Events

As mentioned above, there are large bursts of particles following solar flares. These particles come as a rapid increase in the low energy fluxes and occur shortly after a large solar flare reaching flux values at the lowest measured energies of as many as 6 orders of magnitude above quiet time levels. These large increases in counting rates are caused primarily by the proton component and hence large particle producing flares and the attendant high proton fluxes are often referred to as "solar proton events." Such events are characterized by the following features:

1.   An intense brightening of hydrogen alpha emission in the

vicinity of a solar active region in the solar chromosphere.
This brightening is almost always accompanied, or preceded, by
a Type IV solar microwave burst.

2. Production of x-rays of several kilovolts energy in the same
region as the optical flare.

3. Arrival of protons of relativistic energies at the earth
within a few minutes following the optical and radio flare.

4. A very rapid increase in counting rates for all lower energies
until a maximum counting rate is reached some hours after the
flare. The arrival times of the particles of different energies
usually show a dispersion in velocity, but there are also some-
times complex variations in the counting rates that may last for
days. In some events the low energy particles show no increase
in counting rate until after the arrival of the flare blast wave.

5. Following the peak flux an exponential decay in the counting
rates commences with pre-flare levels being reached in several
days to a week.

6. A monotonically decreasing rigidity spectrum which can be
fitted by an exponential in rigidity over much of its range
(Fichtel and McDonald, 1967).

7. Alpha particle to proton ratios of the order 10^{-3} to 10^{-1}
with the ratio decreasing with energy (Fichtel and McDonald, 1967).

E. The Scope of This Study

In the following chapters it is intended that an analysis of the
proton and alpha particle fluxes obtained from the Goddard cosmic ray
experiments aboard the satellites IMP-III and IMP-IV will help illuminate
some of the problems discussed in the foregoing. Because of the nature

of the experiments themselves and their times of execution, the following

constraints were imposed on the analysis:

1. The times considered were the rising portion of a solar cycle,

going from mid-1965 to mid-1968.

2. The kinetic energies were in the range of 4 to 80 MeV/nucleon.

3. The charge dependence extended only as far Z = 2.

4. The radial dependence from the sun as origin was fixed at 1 A. U.

and there was no directional information available.

In Chapter II a discussion of the experiments is given in which both

the theory of operation and the practical aspects of these particular

experiments are considered. The general operating parameters of the in-

dividual detectors are indicated and the anomolies of the experiments

during their lifetimes are discussed.

A discussion of the techniques used in analyzing the satellite data

is presented in Chapter III. Here also the problem of calibration of

the detectors is considered. Most of the mathematical derivations are

carried out in the appendices.

In Chapter IV the results of this analysis are presented in two

forms:

1. time histories, and

2. energy spectra.

The time histories are examined for regularities and anomalies during

the three year period immediately following the minimum of solar activ-

ity. It is found that on the basis of a number of large particle events

observed, the most active times was in late 1966, and early 1967, while

the quietest periods were early 1965 and late 1967.

Upon examination of two of the higher energy proton fluxes from the scintillator telescope on a monthly average basis, an anomalously large decrease in flux level was noted occurring in September 1966. It was noted that the higher energy flux was depressed by a significant amount more than the lower fluxes. Also the flux after the large decrease never returned to its pre-flare values. Further, these same monthly fluxes, which were at about 50 and 71 MeV, definitely showed a lag of about 1 to 2 months behind the sea level neutron rates, indicating some amount of hysteresis of the particle fluxes with respect to energy.

An examination of the lower energy fluxes, at 8 and 24 MeV, considered in the experiments show that the lowest energy fluxes vary by a greater amount than those fluxes at higher energies. Considered with the foregoing results of the monthly higher energy fluxes, at 50 and 71 MeV, a positive dependency on energy, this opposite behavior of the lower energy fluxes seems anomalous. As it turns out, these results are the basis for later consideration of the lower and higher energy fluxes as being of different origins.

The long term proton and alpha particle spectra are considered. They are compared on the basis of the diffusion-convection formalism. Whereas pre-1965 spectra agreed with theory in that they showed an exponential modulation with the exponent proportional to $1/\beta$, the results of the present study show a behavior that is proportional to β, or P which is equivalent in the range considered, for protons. The modulation of the alpha particles, though present, did not fit any simple model. It is suggested that a possible solution to the anomoly of the proton modulation would be that the power spectrum of irregularities in the interplanetary magnetic field might be a function of time such that $_LM(K) \propto 1/K^3$.

Chapter V constitutes the formulation and examination of a two component model of cosmic rays at 1 A. U. to explain the difference in behavior of the fluxes above and below the relative minimum observed in most quiet time low energy spectra that have been presented to date. The operationally convenient fit of the sum of two power laws in energy, one with positive exponent, the other with negative, is made. The tentative association of the positive power component with modulated galactic primary cosmic rays, and the negative power with solar particles is made. Statistical analysis of the results of fitting the observed fluxes to the model agree remarkably well with the predictions of the model.

The picture that finally emerges from the analysis of the data on the basis of the two component model, is that indeed the low energy fluxes up to the observed relative minimum in the spectrum are predominantly of solar origin. Above this minimum, where the level of solar activity is low enough that the minimum can be observed, the spectrum is taken to be all of galactic primary origin. The short time resolution of 4 days used in the analysis is very much shorter than the 11 year modulation of cosmic rays. Because of this, what is seen is that the galactic component is modulated very little, while at the same time the solar component is changing fairly rapidly and over many orders of magnitude. If found to be correct through further testing as the solar cycle proceeds, this model provides a means at low energies of separating the effects of the solar particles from galactic primaries.

In support of the sun as a quasi-continuous source of energetic particles of energies of about 10 to 20 MeV/nucleon, it was also undertaken to show that very good correlation of non-flare related proton

flux enhancements with solar features having both a periodic property and magnetic activity was possible. It is shown that a number of reasonably frequent events of this nature did occur, and that these kept the low energy particle fluxes up to significant levels.

II. THE EXPERIMENTS

A. Theory of the Detection Technique

When an energetic charged particle passes through matter it interacts with the atoms of the material losing energy by ionization of these atoms. The theory of the collision processes involved has been worked out in great detail by various workers. A summary of the literature on the subject is given by Rossi (1952). Using the resulting stopping power formula for particles much heavier than the electron (Barkas and Berger, 1964) one may write for the energy lost per unit path length by a particle of kinetic energy E and charge z,

$$
-\frac{dE}{dx} = \frac{2\pi N Z e^4 z^3}{A \beta^3 mc^2} \left(\ln \frac{4m^2 c^4 \beta^4}{(1-\beta^2)^2 I^2} - 2\beta^3 - \frac{2C}{Z} - \delta \right) \tag{1},
$$

where N is Avogadro's number, Z is the atomic charge of the material, e the electron charge, A the molecular weight of the material, m the electron mass, and β is the velocity of the particle relative to c the velocity of light. The quantity I represents the adjusted effective ionization potential of the material. In theory this latter quantity can be derived from weighted excitation energies, but in practice it must be obtained by performing actual stopping power, or range, experiments. The empirically derived results of such measurements may be expressed as functions of the electronic charge of the material Z such that

$$
I = 12Z + 7; \quad \text{for } Z \leqq 12 \tag{2a}
$$

$$
I = 9.76Z + 58.8Z^{-0.19}; \quad \text{for } Z > 12 \tag{2b},
$$

in which the units are eV. The remaining two terms inside the brackets are the shell correction term C/Z and the density correction term δ. These two quantities are second order effects and are also determined in most cases from experiment.

From equation (1) it is readily seen that for a given material the rate of energy loss is a function only of the particle charge z and its velocity β. It is therefore possible to write the general relationship

$$dE/dR = z^2 f_1 (\beta) \tag{3},$$

so that once the stopping power for one species of particle in a material is known as a function of velocity, those of different charges are easily found by comparison. Equation (3) may be rewritten as

$$\frac{dE/m}{dR/m} = z^2 f_1 (\beta) = z^2 f_2 (E/m) \tag{4},$$

which may be integrated to give the following relation for the range of the particle:

$$R = \frac{m}{z^2} f_3 (E/m) \tag{5}.$$

Below approximately 1 GeV/nucleon it is possible to represent E/m as a power law in R so that

$$E = k z^{2n} m^{1-n} R^n \tag{6},$$

with $n \lesssim 0.6$ depending on the properties of the material. In general then one can write the approximate relation for two particles a and b of different charge and mass passing through a particular material as

$$E_b = (z_b/z_a)^{2n} (m_b/m_a)^{1-n} E_a \tag{7},$$

by which the two particles may be compared. If particle *a* is taken to be a proton then

$$E = z^{2n}m^{1-n}E_{proton} \qquad (8),$$

which may be used as a scaling relation to scale range, stopping power, or energy loss of a proton passing through a particular material to other nuclei passing through the same material.

As suggested in the last chapter the charge, mass, and energy distribution, as well as the arrival directions of cosmic rays are quantities of very great interest. The device that has proven to be of the greatest utility in studying low energy cosmic rays has been the dE/dx versus E telescope. This is a device which measures two parameters for a given charged particle passing through the device which make it possible to determine the energy of the particle and its charge and mass. The telescope is so constructed that a particle that obeys the proper detection criteria is known to have entered within a narrow cone defined by the geometry of the instrument. A schematic of such a device as used to detect cosmic rays in the experiments reported on herein is shown in Figure 3. The basic features of any such telescope are the three separate detectors labeled A, B, and C in the diagram.

Consider a particle having a trajectory such as the one labeled 2 in the schematic. The range of this particle would be greater than the thickness of A, but less than the thickness of A and B taken together. Such a trajectory may be termed a stopping trajectory as opposed to penetrating trajectories such as the tracks labeled 3 and 4. Detector A is usually about 5 - 10% of the thickness of B. As a

charged particle of kinetic energy E penetrates detector A it deposits
an amount of energy ΔE. It then enters B and comes to rest giving up
the remainder of its kinetic energy therein of the amount $E - \Delta E$. The
energy deposited in each of these detectors produces electrical signals
which may be amplified and analyzed. For example, if A and B are made
of scintillator material the number of photons emitted will be propor-
tional to the energy deposited and hence can be detected and amplified
by means of photomultipliers looking at each detector.

To show that the measurement of ΔE and $E - \Delta E$ can indeed determine
the charge and mass of the particle note that equation (6) may be solved
for R as a function of E such that

$$R(E) = Kz^{-2}m^{1-q}E^q \qquad (9),$$

where

$$q = 1/n \qquad (10),$$

and K is a constant for a particular detector material. The range of
a particle of incident energy E after losing an amount ΔE in A is just

$$R(E-\Delta E) = Kz^{-2}m^{1-q}(E-\Delta E)^q \qquad (11).$$

It is also true then that if detector A has a thickness Δx that

$$R(E) = \Delta x + R(E-\Delta E) \qquad (12).$$

Equations (9) and (11) may be substituted into (12) and solved for ΔE
as a function of $E - \Delta E$ with the result

$$\Delta E = \left[(\Delta x z^2/Km^{1-q}) + (E-\Delta E)^q\right]^{1/q} - (E-\Delta E) \qquad (13).$$

It is easily seen that equation (13), for a given particle telescope, represents a unique and distinct function for each set of values of z and m. The plots of several of these relations are shown in Figures 4 and 5. The particle "lines" in Figure 4 are relatively flatter for small values of E - ΔE than might be expected for the idealized telescope depicted in Figure 3. The reason for this is that in actual practice there are other layers of absorbers present in the construction of such telescopes in front of all of the detectors which are unavoidable because of the need for mechanical strength of the assembly. Energy is deposited in these materials as well as in the detectors themselves, but this energy is not detected. The lines for hydrogen and helium in Figure 5 are closer to theory since there is not as much extraneous material through which the particles must pass in the telescope for which these curves were plotted. In both of these figures the solid curves represent the ΔE versus E - ΔE responses for stopping particles, while the dashed curves show the continuation of the response for penetrating particles.

In order to select only those particle events that correspond to stopping particles coincidence circuitry is designed such that the desired events may be designated by the logical requirement $AB\overline{C}$. In Figure 3 it is seen that of the four tracks shown only track 2 would satisfy this logical criterion. By restricting the analysis of events to those of stopping particles the following points are noted:

1. The energy falls within the limits defined by the thicknesses of the two detectors A and B.

2. Analyzed particles must enter the telescope within an aperture cone defined by the diameters and separation of the detectors A and B.

3. Spurious events are kept to a minimum by the anticoincidence requirement on detector C.

4. The particles of different z and m will be easily distinguishable because of their different lines.

It should also be noted that for either stopping, or penetrating particles continuous in-flight calibration of the detectors and their associated electronics is provided because of the unique "endpoint" existing for each stopping particle. This endpoint is defined by the materials and geometry of a particular telescope and must represent a unique incident energy for a given species of particle.

B. CsI Scintillator Telescope for IMP-III and IMP-IV

A mechanical layout of the CsI scintillator telescope used in both the IMP-III and IMP-IV experiments is shown in Figure 7. As viewed, an incident stopping particle would enter the telescope from the right penetrating the light baffle and passing into the A detector labeled ΔE scintillator in the figure. The particle would continue through the second light baffle and stop in the B detector labeled as the $E - \Delta E$ scintillator. Note that each of the three photomultiplier tubes is coupled through the open regions adjacent to each of the three detectors. As shown the assembly is very compactly designed with associated high voltage power supplies and pre-amplifiers attached to the photomultiplier housings.

In order to accurately compute the response curve ΔE versus $E - \Delta E$ as shown in Figure 4 it is necessary to take into account all of the material in a particle track through the telescope up to but not including the C detector. A diagram showing the dimensions and composition of the scintillator telescope used is shown in Figure 8. The aluminum and

plastic foam sandwich shown preceding the A detector and the one between

the A and B detectors are primarily responsible for the flattening of

the curves at small energies as mentioned earlier.

To compute the response curves it was assumed that an isotropic

flux of particles would enter the front end of the telescope. Such

particle tracks would generally be inclined to the axis of the

telescope. Ideally in order to find the average response curve the

energy losses for a large number of tracks of varying obliquity should

be computed and the average of these energy losses for each value of

incident energy computed. This is however not a practical approach

since the effect of oblique tracks is second order. Rather it is

sufficient to compute the average slant angle for a track of an iso-

tropic distribution of entrant particle directions and use the path

lengths so computed through the various layers of material in the range

energy calculations. The computation of the factor by which all of the

telescope material thicknesses must be multiplied is outlined in Appendix

B. For the scintillator telescope in question the average correction for

oblique tracks was computed to be $1/<\cos \theta> = 1.02$. Using the semi-

empirical relations for range and energy of Barkas and Berger (1964) in

a digital computer program, the computations of the energy loss in the

various materials indicated in Figure 8 including the detectors were

carried out. The results are those plotted in the response curves in

Figure 4. The thickness values used in these computations were those

obtained by multiplying each measured thickness by the obliquity factor

given above.

Using equation (11) in Appendix A the geometry factors for varying

penetration depths of tracks into the B detector were computed. These

are plotted in Figure 9, which has specific incident energies marked along the curve indicating the incident energy of a particle having that geometry factor.

The design of this telescope was such that the energy/nucleon range for stopping particles would nominally be between 20 and 80 MeV/nucleon. The actual telescope had a threshold for particle detection in the $\overline{ABC}$ mode of 18.7 MeV/nucleon and the cutoff for the C detector anticoincidence occurred at 81.6 MeV/nucleon.

C. Silicon Solid State Telescope for IMP-IV

In order to reach lower energies than was practicable with a scintillator telescope, it was decided to include on the IMP-IV satellite a solid state telescope using surface barrier type silicon detectors for the A and B detectors in addition to the dE/dx versus E telescope described in the last section. A schematic of the mechanical design of this telescope assembly is shown in Figure 10. The nominal values of the kinetic energy per nucleon for stopping particles in this telescope were 4 to 20 MeV/nucleon. In conjunction then with the scintillator telescope described in the last section, such an experiment would span the region of the spectrum shown in Figure 1 through the low energy minimum.

As indicated in Figure 10 two solid state detectors were required for the B detector. The reason for this was simply the unavailability of a reliable silicon surface barrier detector of the required thickness whereas it was possible to obtain detectors of half the required thickness that would meet the specifications. These two detectors then could have their signals added and were in this way equivalent to a single detector.

The A and B detectors were mounted in the two ends of a cylindrical plastic scintillator with a plastic plug of the same material after B. The signals from the silicon detectors were fed into charge sensitive preamplifiers since the number of charge pairs created by an ionizing particle would be proportional to the energy it deposited. The plugged end of the C detector was coupled to a photomultiplier. As in the case of the scintillator telescope described above the $A\overline{B}\overline{C}$ logic was invoked to discriminate against all but particles coming to rest in detector B after having passed through A.

The composition and geometry of the solid state telescope are shown in Figure 11. Note the titanium foil light shield in front of the A detector because of the sensitivity of silicon detectors to light. Also note that each of the silicon detectors has a layer each of gold and aluminum on front and back surfaces, respectively. The average obliquity factor for this assembly was $1/<\cos \theta> = 1.04$. With this factor applied to the thickness of material shown in Figure 11 the range energy program mentioned in the last section was used to compute the response curves in Figure 5.

In Figure 12 the geometry factor for this telescope is plotted as a function of the penetration depth into the B detectors, which are designated B_1 and B_2. Note that there is a pronounced jump in the value of G in going from B_1 to B_2. This latter discontinuity in G is because of the separation in the two elements of the B detector. Along the curve itself are indicated several incident energies for which the corresponding values of G occur.

The threshold energy for the actual telescope was 4.2 MeV/nucleon, while the cutoff energy was 19.1 MeV/nucleon.

In order to provide a means of measuring even lower energy proton
fluxes, particularly those originating in solar flares, an 8 level
integral analyzer was used independently from the above dE/dx versus
E arrangement to analyze the signal from the A detector. The maximum
energy for a stopping proton in A was 4.1 MeV incident on the front of
the telescope. The discrimination was set such that level 3 was the
lowest that would admit a signal, that being equivalent to about 3.32 MeV.
Level 6, which was three steps lower than 3, was set so that the integral
flux of particles would be in the range of 1.1 to 20 MeV.

D. The IMP-III Experiment

The IMP-III satellite was launched on May 29, 1965. Some of the
vital statistics for this satellite are given in Table I. The scintil-
lator telescope was mounted so that its axis was perpendicular to the
spin axis of the satellite. A block diagram of the electronics associ-
ated with the experiment is shown in Figure 13. The function of the
circuitry of interest to the present study is that part which is related
to the in-flight analysis of ABC type events and a sample of the count-
ing rate of these events.

The satellite telemetry operated in such a manner that a complete
commutation cycle was completed every 5.461 minutes. Each cycle was
divided into 4 sequences of 81.92 seconds duration, of which only the
first 3 were utilized by the cosmic ray experiment. There were 2
accumulator gates open for 39.36 seconds in each of these sequences
giving a total of 6 accumulators effectively per cycle. One such
accumulator each cycle was available for recording the number of $\overline{ABC}$
events thus providing a sample counting rate for stopping particles.
Also during each of the 3 sequences per cycle two gates of 34.24 seconds

duration were open for pulse height analysis of $\overline{ABC}$ events. When the first $\overline{ABC}$ event occurred after one of these gates was open two separate 512 pulse height analyzers analyzed the ΔE and $E - \Delta E$ signals from the A and B detectors, respectively, and stored the resultant channel numbers in the 34.24 second accumulator. During the remainder of time the gate was open, further pulse height analyses were inhibited, thus effectively limiting the number of pulse height analyzed events to a maximum of 6 every cycle.

The IMP-III experiment functioned well throughout the lifetime of the satellite. Because of temperature changes in the satellite, there was a certain amount of drift in the gain of the two detectors and their associated electronics. This drift could be compensated for quite satisfactorily in the analysis of the data on the ground by noting the shift in the channel numbers of the proton curve endpoint and computing a gain factor for each of the two parameters over some specified time period. There were at least two occasions when the scintillator crystals were temporarily saturated by very high particle fluxes. This occurred during the proton event of September 2, 1966 and again during the event of January 28, 1967. IMP-III effectively died in early May 1967, although the useful data available from this experiment reported in this study continues only until April 10, 1967.

E. The IMP-IV Experiment

IMP-IV, a somewhat improved version of the IMP series, was launched on May 24, 1967 almost providing complete coverage with IMP-III. The other pertinent flight data on this satellite is shown in Table I. The cosmic ray experiment aboard this satellite again utilized the previously discussed scintillator telescope to cover the nominal energy range of

from 20 to 80 MeV/nucleon. In what follows this telescope will hereafter be referred to as the MED for Medium Energy Detector. Besides this experiment the solid state telescope described in Section C was operated in conjunction with it. This solid state telescope will be designated LED hereafter for Low Energy Detector. The LED extended the energy range measured down to about 4 MeV/nucleon. On IMP-IV the MED was parallel to the satellite spin axis in contrast to its counterpart on IMP-III. The LED was mounted so that it looked parallel to the equatorial plane of the satellite, i.e., perpendicular to the spin axis. The experiment flight circuitry for these experiments is illustrated in block form in Figure 14. One significant difference in circuit design for this experiment was the use of 1024 channel pulse height analyzers to provide greater dynamic range in analyzing the ABC events, although the total number of channels was not available because of saturation effects.

As may be seen from the block diagram, there were two separate detector packages, one each for the LED and MED. A third package contained the combined flight circuitry for the two telescopes. In this experiment a greater degree of flexibility was designed into the electronics so that both the LED and MED could be operated in a low and a high threshold mode. The purpose for the latter change was so that in the high threshold mode the ΔE threshold would occur some 20 channels higher than in the low mode. This would permit more alpha particles to be counted during high flux rates when the normally high counting rates in the lower channels would effectively mask these counts. Also the LED circuitry provided for half the pulse height analyses per cycle being done on AB type events, i.e., on penetrating particle events.

The timing of a cycle for IMP-IV was such that there were 32 frames per commutator cycle of 5.12 seconds duration each giving a total cycle time of 2.731 minutes. Of the 5.12 seconds frame duration for 4.48 seconds the accumulator gate was open with the remaining 0.64 seconds utilized for readout. There were 8 each pulse height analyses for the LED low, LED high, MED low, and MED high modes. The time the pulse height analyzer time bins were open was the 4.48 second accumulation time. Since the AB mode was operated for the LED half the time, there were then 4 LED and 8 MED $\overline{ABC}$ pulse height analyses per commutator cycle in each of the two threshold modes. Greater signal to noise ratios for these experiments was provided by causing each accumulator to be read out twice before resetting in order to check consistency. One accumulation sample of $\overline{ABC}$ counts for 4.48 seconds was made, one for each threshold mode for the LED and the MED each cycle. Compared to the IMP-III experiment, it is seen that the MED provides 16 pulse height analyses during the same time 6 could be performed on the earlier experiment, provided the counting rate was high.

The IMP-IV experiments performed very well for the most part. Unlike the previous IMP experiments, including IMP-III, very little gain drift was noted during the effective lifetime of the satellite. Analysis of the data did show that the $\overline{C}$ provision of the LED part of the experiment failed in March of 1968. This failure has been postulated to have been caused by a cracked photomultiplier tube following the thermal shock of passing through the long period of the earth's shadow, which occurred once a year. Otherwise the experiment appeared to be functioning quite well up through the last available data acquired for this analysis which was up to August 20, 1968.

III. DATA ANALYSIS

A. General Format of Data

The raw data from current satellite experiments is in a form which is most suitable for high rates of data transmission from satellite to ground stations at high signal to noise ratios. This 4 bit PFM code is not intended for data processing in the form received, but must be converted to standard digital codes for the computers on which analysis is to be carried out. In the initial phases of data processing of the taped data as it is received from the tracking stations, this conversion must be carried out as well as the process of separating these data from different experiments and outputting this on to separate tapes for use by the individual experimenters, a process called decommutation.

Several rather tedious steps of data processing had to be performed on the decommutated tapes before these could be used in any analysis schemes. Because all of the data pertinent to an experiment that was received by ground stations was included, there was a certain amount of overlap and redundancy present in the data at this initial stage which had to be eliminated. The result of this process was a non-redundant time-ordered sequence of data. Other procedures performed on the data in this processing (pre-analysis) stage were the insertion of pertinent time and orbital information where required and the reorganization of the format and condensation of the data. The output tapes, in a form for analysis, were 800 bit per inch 9-track tapes for use on IBM series 360 computers.

For both IMP-III and IMP-IV the taped data for this study was available to the experimenter in two basic formats, which can be designated

31

here as (1) final data tapes and (2) matrix tapes. The former consisted of records corresponding to the time of one commutation cycle of the satellite telemetry system. Each record contained the U.T. time and date, satellite distance from earth, and various relative coordinates for the particular record. The cosmic ray experiment data in each record consisted of the readouts of the various experiment accumulators corresponding to the number of counts occurring for each logic requirement, e.g. $A B\overline{C}$ for one mode of the ΔE versus $E - \Delta E$ experiments, as well as the readouts of the pulse height analyzed events.

The matrix tapes were the result of a form of intermediate processing which condensed the data considerably. The matrix tape consisted of sequences of n successive records which contained the pulse height analyzed data in a compressed matrix form, as well as accumulator sums for a specified period, usually one complete orbit of the satellite. By reading any n record sequence, a complete matrix of the ΔE versus $E - \Delta E$ $A B\overline{C}$ events could be reconstructed for a particular mode of any given orbit, the number in a particular location being the number of events having the corresponding ΔE and $E - \Delta E$ channel number.

B. Calibration of ΔE Versus $E - \Delta E$ Response

As shown in Chapter II, the expected response of the cosmic ray telescopes was computed using the range-energy data of Barkas and Berger (1964). The theoretical response curves so obtained are plotted in Figures 4 and 5. The collective results from several orbits of pulse height analyzed data from one of the cosmic ray experiments can be interpreted in terms of one of these response curves in the following manner. This data can be arranged in a two dimensional array where the x and y axes represent the $E - \Delta E$ and ΔE channel numbers, respectively,

so that the number of counts occurring for a particular value of E - ΔE and ΔE is the value of the x,yth element of the array. Because of the various statistical fluctuations in energy losses of the detected particles, there will be a maximum distribution of counts in a region of the array corresponding to a particle line.

Figure 15 shows a computer printout of such an array, or matrix, for the period from 4 June 1965 to 26 October 1965 for IMP-III. The central curved line is drawn through the maximum of the distribution corresponding to the proton line in Figure 4. In order to establish a correspondence between the physical channel numbers in the x and y directions and the incident energy of a proton, it was first necessary to know the corresponding relationship between a detector's pulse height analyzed channel number and the kinetic energy deposited in that detector.

Scintillators exhibit a non-linearity in light output versus energy deposited at energies of the order of 10 MeV and greater because of a partial saturation of the available number of activation centers in the material. Preflight calibration of the IMP detectors showed that this is best expressed as a function of the differential light output versus stopping power. In the energy interval of interest for this experiment, this functional dependence could be expressed as

$$dL/dE = A - B/(dE/dx) \qquad (1),$$

with $B/A \cong 0.3$. Integration of (1) in the case of the ΔE detector produces the result

$$\Delta L = A\Delta E - B' \qquad (2),$$

with the offset B' actually being a very slowly varying function of
particle range and hence energy. Similarly a stopping particle of
incident energy E - ΔE on the E - ΔE detector will give a light re-
sponse of the form

$$L = A(E - \Delta E) - B' \tag{3},$$

in which again B' is a slowly varying function of energy.

Because of the linear form of equations (2) and (3) with an offset
it was possible then to express the overall response of the detectors
A and B in the following form:

$$E - \Delta E = a + bx \tag{4}$$

and

$$\Delta E = f + gy \tag{5}.$$

In equations (4) and (5) E - ΔE and ΔE represent the energy/nucleon
deposited in the respective crystals, and x and y are the signal out-
puts from the entire detector electronics train in terms of pulse
height channel number.

Since equations (4) and (5) each contain two undetermined con-
stants, two calibration points along the response curve are required.
The endpoint automatically provides the first of these calibration
points. Ideally, the second point, or several points, is found by
preflight calibration using a monoenergetic beam of particles. Such
a calibration was carried out. The theoretical values for ΔE and
E - ΔE for a particle with incident energy E were computed as de-
scribed in Chapter II. These values of E - ΔE and ΔE corresponded
to the channel numbers x and y found in calibration. This can be

located approximately by noting what channel the threshold of the E - ΔE

signal occurs in. The corresponding ΔE channel is the y coordinate of

the curve in the matrix having this x threshold value. More accurate

determinations of several points along this distribution have also been

made by utilizing a monoenergetic beam of protons from an accelerator.

A combination of these two methods was used to calibrate both the scin-

tillator and the solid state telescopes with agreement between the two

methods. The coefficients for equations (4) and (5) for the various

experiments are given in Table II.

Using the Barkas and Berger (1964) range energy loss expressions,

detailed tables were computed for the precise theoretical energy de-

posited in each detector for a given incident energy for each one of

the telescopes. Using these tables and the appropriate forms of equa-

tions (4) and (5), it was then possible to ascertain the incident

energies corresponding to a position on the matrix curves.

Because of possible gain shifts in the satellite electronics,

there could be a change in one, or both, of the pulse height analyzer

responses. On IMP-III this was a very noticeable effect. In order to

correct for such gain changes, the endpoint of every one orbit matrix

over the lifetime of the satellite was examined and the E - ΔE and ΔE

channel numbers of the endpoint determined in each case. Picking one

such endpoint as the standard, all other endpoints, which always cor-

respond to the same energy, could be compared to this standard and ΔE

and E - ΔE gain factors could be computed. These gain factors could

be applied to the data from the respective orbits, permitting combin-

ing of the data for longer periods. Indeed this is the process that

was used in combining the almost four months of data presented in Fig-

ure 15.

C. Matrix Histogram Analyses

Consider again the region of the proton line in Figure 15. As noted, there are two outer curves bounding a region containing the proton line. This region was originally determined using only one orbit of data following a large solar flare so that the copious quantities of energetic protons so produced would easily delineate the line. It is readily apparent that there are a number of counts outside of this proton region. The origin of the non-proton events can be mostly attributed to nuclear interactions in the telescope, and to a lesser degree in the spacecraft. These counts, though obeying the $\overline{ABC}$ criterion, are not primary protons and constitute noise that must be separated from the true primary events. An example of such a reaction causing the background counts could be a secondary neutron formed in the spacecraft by a cosmic ray primary. Such a neutron could penetrate the C detector, producing no signal in the process, and then decay in the B detector, where it would deposit a certain amount of energy and continue on through the A detector leaving there a small amount of energy. Such an event would certainly satisfy the $\overline{ABC}$ criterion, but would not be caused by a primary cosmic ray, which is what one is looking for.

If one is careful to exclude regions containing protons, alphas, or electrons in the matrix, it is found that parallel to either axis in the matrix the "background" counts, as described above, obey a power law in channel number to a very good approximation. This background flux will contaminate the region of interest, and hence must be removed. The power law behavior of the background provides a convenient method for removing this contribution in the neighborhood of the proton line, for instance, so that one can obtain a true measure of the primary proton counts.

In Figure 15 the region of the proton line has been divided up
into six boxes which in increasing order represent energy lines lying
between the incident energy values of 18.7, 29.2, 39.7, 50.2, 60.6, 71.1,
and 81.6 MeV. By taking narrow strips parallel to the proton line and
lying inside of the upper and lower energy boundaries as shown, the
number of counts in each strip can be determined. Extending the number
of these strips in either direction beyond the proton region so that
some of the background region will be included, it is possible then
to plot histograms of the counts so determined. Such histograms cor-
responding to the energy bins shown in Figure 15 are presented in Figure
16. The dashed lines show the mean values of the power law in channel
number and were obtained by plotting the strip counts on log-log paper
for several trial midpoints in channel number until the best straight
line fit was obtained for the background regions. The shaded areas re-
present the true primary proton counts in the energy interval specified.
The region below the dashed line and between the vertical lines delimit-
ing the proton region is the background component.

As discussed in the previous chapter, the LED experiment was
surrounded by a plastic scintillator cup constituting the C anticoinci-
dence detector. Histogram analyses of the LED data analogous to that
discussed above shows almost no background contamination. This justifies
the assumption that most of the background secondaries were produced in
the detectors, or the walls of the telescope housing, in the case of the
scintillators by high energy primaries with kinetic energies > 1 GeV.
Further, if histograms are produced for solar flare protons after a
large flare, when very high fluxes of protons register as events, in
the case of the scintillator telescope the relative background is

vanishingly small. This decrease in the number of secondary protons with respect to the low energy primaries is because the flux of secondaries has remained constant. This reinforces the view that secondaries are produced by nuclear interactions of high energy primaries which are not present in the solar flux and are not too highly modulated so that their flux through the spacecraft remains relatively constant.

The differential proton flux was computed from the total proton counts in a specified energy box using the relation

$$dJ_i = \frac{N_i \, N_a}{N_T \, t \, G_i \, \Delta E_i} \tag{6},$$

where N_i is the number of protons in box i, N_T the total number of counts in the matrix, N_a is the accumulated $\overline{ABC}$ counts during the accumulation time t, and G_i and ΔE_i are the geometry factor and differential energy respectively for box i. The energy E_i taken for dJ_i is just the mean of the upper and lower energy bounds of the ith box.

Using this method of histogram analysis for both proton and alpha lines, it is possible to obtain very good counting statistics. In practice, preliminary examination of the data was made to determine the quietest time periods so that contamination by solar flare protons could be avoided. Excluding solar disturbed periods, data could be combined to cover several months such as the example shown in Figures 15 and 16. For the large numbers of counts involved, Poisson statistics are applicable (See the discussion in Appendix C). The relative error is a combination of the three relative Poisson standard deviation for the N_i, N_a, and N_T, i.e.,

$$\sigma = \left(\frac{1}{N_i} + \frac{1}{N_a} + \frac{1}{N_T} \right)^{1/2} \tag{7}.$$

Examination of the background shows that it is reasonably constant over the lifetime of the satellite. This fact provides a means of making a background correction to the short time period fluxes discussed in the next section. Such a background correction can be put in terms of a flux in the same units as the particle flux to be measured. This is accomplished simply by using in place of N_i in equation (6) the number of background counts below the respective dashed lines as shown in the histograms in Figure 16. This correction is to be subtracted from flux measurements in the same energy range for which the background counts have not been separated by means of the histogram method illustrated above.

For the MED telescope the minimum flux measurable occurs when the flux and its computed standard deviation are approximately equal. Examination of 24 hour average proton flux values showed that this value occurred at about $10^{-5}/s$ cm^2 sr MeV. This is also about the average value of background flux that had to be subtracted from the MED fluxes to correct for nuclear interaction events in the spacecraft. Even though there was no background correction necessary for the LED experiment, the box method gave about the same minimum for a measurable flux.

D. Computation of Particle Flux Time Histories

With Fine Time Resolution

The methods outlined in the last section for computing fluxes have the limitation that they are good only for time periods of the order of days to months. Since many of the cosmic ray phenomena of great interest occur in times of a few minutes to times of hours, some other method of computation must be used. In principle the same prescription as given

above can be followed, but since the size of the matrices involved is quite large, it is not feasible to construct these matrices every few minutes and then examine the histograms. Instead a computational procedure amenable to coding for a high speed digital computer was developed.

The shortest time period records for the experiments were read from final data tapes and effectively the pulse height analyzed counts that fell into the various energy bin as depicted in Figure 15 were accumulated, as were the $\overline{ABC}$ counts, the total number of pulse height analyzed counts, and the $\overline{ABC}$ accumulation time. Two modes of computation were available; the first being a fixed time period process in which counts were accumulated for a predetermined time and the fluxes and errors then computed on the basis of this accumulated data. The second mode computed the fluxes and standard deviations of the fluxes after the addition of each record of data, and continued to add more data until a predetermined precision criterion had been satisfied. These two methods were designated the fixed time and variable time techniques.

To obviate constructing matrices of the $\overline{ABC}$ pulse height analyzed events as was done in the previously discussed histogram method, each event was examined to see where it would fall in such a matrix if it were to be constructed. This was accomplished by producing a mask of the region surrounding the particle line in question for a standard line including the energy boundaries of the boxes as depicted in Figure 15. The mask was simply the x values of the box boundaries for· each value of y. For instance in Figure 15 if an event had the ΔE channel number of 40 and E - ΔE channel numbers of more than 31 and less than 38 then that event would be attributed to box 2. This mask data was tabulated

on a row by row basis for a standard line and used in the computer as a "go-no go" test in the manner described.

One feature of this box counting of particle events was that it permitted the correction for gain changes in a fairly simple manner. The gain factors as described in the last section were simply applied to the masks during the applicable periods. In this way there never was any need to consider fractional counts.

Besides accumulating the individual box counts as described, the total number of $\overline{ABC}$ pulse height analyzed events was accumulated for a given energy interval being computed. Also the total $\overline{ABC}$ counts N_a and corresponding counting time t were accumulated. It is fairly obvious that in principle the box counts obtained in this way and the total analyzed $\overline{ABC}$ counts are equivalent to the total histogram particle counts N_i and total matrix counts N_T, respectively, as descussed in the previous section. The only difference is that in the present case the background counts were included as well as the desired particles. To compute the particle flux using the method under discussion, equation (6) was used with N_i replaced by the total box counts as described and N_T by the total accumulated $\overline{ABC}$ pulse height analyzed counts. N_a and t were the same as before but accumulated over a very much shorter time period.

The background rate as described in the last section was a constant throughout the lifetime of a particular satellite and hence was subtracted from the raw computed flux to give the absolute particle flux. For completeness, then, the formula used to compute the flux by this method may be written as

$$dJ = \frac{N_i \, N_a}{N_T \, t \, G_i \, \Delta E_i} - r_i \qquad (8),$$

where r_i represents the constant background component, and the other quantities are completely analogous to those used in equation (6) except for N_i which contains background as well as primary counts. Also it should be noted that N_T, although still the total number of $\overline{ABC}$ pulse height analyzed counts, is at most a small number depending, of course, on how long a period the averaging process extended for a single flux calculation.

The use of Poisson statistics for this method of flux computation is not quite so clear cut. The $\overline{ABC}$ event counts were large and reasonably unrestricted, hence the standard deviation in N_a in (8) was given by the Poisson formula (See Appendix C, equation (35)):

$$\sigma_a = \sqrt{N_a} \tag{9},$$

and the relative standard deviation by

$$S_a = \sigma_a/N_a \tag{10}.$$

In the case of N_i, however, the use of Poisson statistics is not justified because of the small number of bins N_T, which could vary anywhere from 4 to 8 per commutation cycle. As discussed in Appendix C, the appropriate formula to use is derived directly from the binomial distribution. Using equation (19) from Appendix C, the standard deviation for N_i is given by

$$\sigma_i = \lceil N_i (1 - N_i/N_T) \rceil^{1/2} \tag{11},$$

and the fractional standard deviation by

$$S_i = \sigma_i/N_i \tag{12}.$$

The additional relation, equation (20) in Appendix C, was utilized where required. Treating the two errors as given by equations (10) and (12) as independent errors, the two may be combined to give

$$S = (S_a^2 + S_i^2)^{1/2} \tag{13},$$

so that the standard deviation in dJ may be written in terms of (13) as

$$\sigma = S \cdot dJ \tag{14}.$$

The "box" method under discussion worked extremely well for obtaining proton fluxes since protons are the predominant component of cosmic rays. For alpha particle fluxes which were also determined on a short time basis, one drawback was a relative saturation of the electronics by high proton flux rates, thus making more difficult a true measurement of the alpha particle fluxes. One design feature in IMP-IV noted in Chapter II was a high threshold mode of operation which in principle would have suppressed a number of proton counts, thus enabling the counting of a higher number of alphas. As it turned out, the high threshold $\overline{ABC}$ sums were not transmitted from the satellite. Although an artificial $\overline{ABC}$ sum could be computed from the ratios of total pulse height counts in both modes and the low threshold $\overline{ABC}$ sum, the alpha pulse heights were still too scarce to compute reasonable alpha fluxes.

The very scarcity of alpha particles noted made possible the use of a computational technique that utilized the number of alpha pulse heights in a given energy interval and the time interval that the pulse height bin was open to record an event. The derivation of this technique is given in Appendix D. Using equation (13) in Appendix D, the flux of a particle based on pulse heights alone is given by

$$dJ = \frac{1}{tG\Delta E} \ln \left[N_T/(N_T - N_i) \right] \tag{15},$$

where t is the time the pulse height bin will accept a count, G is the geometry factor, and ΔE the energy interval. N_T is again the number of pulse analyzed counts. Equation (15) is valid in the limit that $N_i \ll N_T$. The standard deviation for dJ can be computed using equation (13) in Appendix D, so that

$$\sigma = \frac{1}{tG\Delta E} \left[N_i/N_T (N_T - N_i) \right]^{1/2} \tag{16}.$$

One other statistical item was considered in the short period analysis. This was the problem of upper limits when there were no counts during the averaging interval. The procedure adopted when there was no count during an averaging period was to add one artificial count and compute the appropriate flux on the basis of this one count. This flux was then considered to be the upper limit for that particular interval of elapsed time.

In Table III is a summary of the analysis parameters used for this study. These values were used for both the box method and the histogram method of analysis.

IV. THE OBSERVATIONS

A. Time Histories of Low Energy Proton Fluxes

From June 1965 to August 1968

The period concerned with in this study begins with the launch of
IMP-III spacecraft near the minimum of solar activity in 1965. There
is a certain amount of arbitrariness in speaking of a measure of solar
activity. From a solar astronomer's viewpoint the minimum of solar
activity for this current cycle occurred in October 1964 as indicated
by the minimum in sunspot number shown in Figure 2. On the other hand,
the cosmic ray flux at earth as indicated by neutron monitor counting
rates reached a first maximum in April 1965 and a secondary maximum
approximately six months later in October 1965. The current study is
concerned with the behavior of the low energy component of cosmic rays
during the period of decreasing galactic cosmic ray flux.

Figure 17 shows a history of the 24 hour proton differential fluxes
at energies of 29 and 60 MeV for the entire period of this study. Using
the results from the solid state telescope on IMP-IV a third flux value
computed at 12 MeV is shown from late May 1967 up through the middle of
August 1968 where this study ends. Because of the loss of communications
on IMP-III there is missing data from 1 May to 24 May 1967. There is an
additional block of data missing from this analysis because of a bad
data tape for the period from 10 April to 1 May 1967. This former is
unfortunate for several reasons including the loss of data for the large
proton event commencing on 24 May.

The gross features of the solar activity and production of energetic solar protons are summarized in Table IV. In this table a semi-annual count of the number of substantial increases in counting rate above the quiescent rate of protons is tabulated on an integral basis. The counts in each column are for fluxes greater than or equal to the column flux heading and therefore contain also the number in the adjacent column to the right. No account has been taken in this table as to whether the increase was flare related or a return to central meridian of an active region; however, the fluxes refer to the peak flux reached during any of the increases. The 29 MeV flux is derived from the lower two boxes of the MED experiment spanning the energy interval 18.7 to 39.7 MeV hence, should certainly indicate particles of solar origin.

Two aspects of the period of study are worth consideration. First, a maximum in activity as reflected by the high frequency of large events was reached in the first half of 1967. This was followed immediately by a minimum in number of events in the next six months and then a slow return to a higher number of events by the end of 1968. This large maximum followed by the minimum in 1967 is probably related to a concurrent decrease in quiet time fluxes to be discussed below. The second aspect of the frequencies shown in the table is the monotonically decreasing behavior with respect to peak flux of the total numbers of counts over the entire period under discussion. This latter bears a resemblance to the frequency of optical solar flares as a function of flare area (Smith 1963).

Returning again to Figure 17, it is seen that such events as are enumerated in Table IV represent enhancements of at least a factor of

10 above the quiet time rates. It is reasonable to assume then that because of the well known observed correlations of these short term proton flux increases with solar activity, either in the form of flares or returning solar active regions, that the origin of protons during such events is almost entirely solar. Conversely, it has been generally assumed that during very quiet solar periods when particle fluxes are at their minimum observed values, the composition of cosmic rays is predominantly galactic in origin. Such solar quiet times would be exemplified by the periods June through September 1965, October through December 1966, and most of September and October in 1967. It would be during these, or similar, quiet periods that one would want to study the long term variations of cosmic rays and in particular the solar modulations of the galactic cosmic rays.

It should be noted here that all observations of solar flare associated proton spectra show a very steep monotonically decreasing behavior for proton fluxes as a function of kinetic energy. With this fact in mind and referring to Figure 1, it is readily apparent that the higher energy fluxes in this study should be better able to give good statistics on galactic cosmic rays during quiet times. On this basis the flux with the next to highest energy for these experiments and the one just below it are presented in Figure 18 on a monthly basis. The highest energy value was not used here because of some lack of confidence in its overall statistics. Plotted on the same graph are the monthly averaged hourly Deep River neutron counts. The proton flux averages are based on the quietest flux periods available each month. There are several months where no points are presented simply because of the greatly disturbed nature of that period.

In examining the cosmic ray quiet time behavior in Figure 18 several marked features stand out. First of all there appears to be a lag of one to two months in corresponding features in the IMP proton fluxes with respect to the neutron rates. For instance a big minimum in neutron counts occurs in August 1965, and the corresponding minimum in proton flux does not occur until October. The second maximum in neutron rates in November 1965 is followed by the corresponding proton maximum in January of 1966. In September of 1966 there is a massive Forbush decrease, which appears to be related to the abrupt drop in proton fluxes in October and November. In this respect it is to be noted that the proton fluxes do not recover to anywhere near their previous level. Referring back to Figure 17d, it is probable that this latter behavior is associated with the large solar flare occurring on 2 September 1966, with its resultant proton event and greatly increased proton fluxes that lasted the remainder of the month. This lack of recovery is possibly directly the result of a large change in the interplanetary medium following the September solar disturbance. It is not as clear cut as the lag just discussed, but there appears to be some small displacement in time between the two IMP proton fluxes. The observed lags seen here would tend to indicate a hysteresis effect in the proton fluxes with respect to energy, similar to that suggested by Balasubrahmanyan (1965), and Balasubrahmanyan, Hagge, and McDonald (1967).

In Chapter V will be presented a model of the low energy cosmic rays based on the 4 day averages of differential fluxes spanning the energy interval from 4.2 to 81.7 MeV. This model and its analysis will be restricted to the IMP-IV data only which extends down to the lower energies. A plot of these 96 hour averages for two of the lower energies

(one each from the LED and MED experiments) is shown in Figure 19. It
is readily apparent that the fluxes for the two energies track each other
quite well. Further it will be noted that the lowest energy value varies
considerably between widely separated extremes, as compared to the higher
energy flux, on a percentage basis. This latter behavior may be inter-
preted in one of two ways. Either the lower energy particles are more
highly modulated then at higher energies, or the lower energy fluxes
represent a larger component of solar particles. Indeed this is the
very question that the present study will attempt to answer.

In view of the last point noted above, it is of interest to return
to Figure 18 and consider the relative changes for the two proton fluxes
represented there. It is easily seen that the short term month to month
changes are larger for the higher energy flux. Further the large decrease
in September 1967 produced a reduction in the higher energy flux of about
2.5 times whereas the lower energy flux was reduced by a factor of less
than 2.0. At face value this behavior seems to be just the opposite of
that encountered above for the 96 hour proton fluxes at lower energies,
in that the relative changes in fluxes is larger for the higher, rather
than the lower energy. This is not necessarily the case, however. The 96
hour averages must represent all of the data at the given energies with
no selection of quiet periods, and also is at the low end of the energy
interval where the spectrum has been observed to have a negative slope
as shown in Figure 1. On the contrary, the monthly flux averages shown
in Figure 18 were taken for the quietest periods available and lay well
above the minimum appearing in Figure 1.

The difference in the monthly averages of proton fluxes at the two
higher energies can also be satisfied by alternate explanations. If

the fluxes so presented are predominantly of galactic origin then the fact that higher energy flux changes proportionately more than the lower must be interpreted as a greater effect of solar modulation on the higher energies in the limited range considered. If on the other hand there were a monotonically decreasing steady solar component inherent in these fluxes then the modulation of the lower energy particles could be the same, or greater than, the higher energy particles and this effect would be effectively masked because of the larger solar component at the lower energy.

B. Proton and Alpha Particle Spectra

And Cosmic Ray Modulation

The time dependent behavior of cosmic rays is dominated by an 11 year modulation that has been rather well established experimentally (see discussion in Chapter I). By using the low energy MED fluxes it was possible to screen the data of both satellites for the quietest times available. Using this technique six periods as tested in Figure 20 were abstracted from the data. Using the histogram technique described in the last chapter the proton and alpha particle fluxes were determined for these periods. The results are plotted in Figures 20a and 21a.

The proton spectra presented in Figure 20a first of all show that of the data presented the June 1965 to October 1965 period and the November 1965 to March 1968 period have about the same minimum amount of modulation. These two periods represent the maximum fluxes at the 1965 solar minimum and are in extremely good agreement with the same energy interval of the spectrum shown in Figure 1, which were derived by the Chicago group (Fan et al. 1966a) and the Goddard group (Balasubrahmanyan et al. 1966a,b). The September to October 1967 spectrum is quite regular

except for the highest energy point, although two standard deviations would allow this low flux. The most recent spectrum, the one for April to May 1968, shows large modulation at the high energies but a rather peculiar double valued behavior at the low energy end.

In Figure 21a again the June to October 1965 helium spectrum compared extremely well with the corresponding energy interval in Figure 1. The fractional modulation between the protons and alphas comparing Figures 20b and 21b shows that on the energy per nucleon basis the proton fluxes are reduced by a factor of 2.7 while the alphas are reduced by a factor of 3.5 during the same time. It should be noted that the November to December 1966 alpha spectrum shows a very steep power law behavior as compared to the other alpha spectra.

Using the formulation described in Chapter I in equations (3) through (7), the logarithms of the ratios of the minimum fluxes in 1965 to the fluxes for the other periods were plotted in Figures 22 and 23, for protons and alpha particles, respectively. As indicated by Webber (1968) the low energy cosmic ray rates should fall parallel to $1/\beta$ functions. As seen in Figure 22 the proton logarithmic flux ratios have positive slopes unlike the negative slope expected. The alpha data in Figure 23 shows even more erratic behavior except for the period of October to December 1966, and in this case the ratios are parallel to a $1/\beta P$ function rather than the $1/\beta$ expected.

In light of the evidence presented in the last section for some amount of hysteresis between fluxes of different energies, one might expect the erratic behavior observed. If such hysteresis does exist, then in order for the spectra and these modulations to return to the forms observed before solar minimum as described by $\eta(t)/\beta$ behavior,

then it would be necessary for a change in the formulation of the modulation. It is at least apparent that the accepted modulation theories do not apply during the period under discussion.

As a tentative explanation to this problem consider equation (6) in Chapter I,

$$\ln \frac{dj_e (P,t)}{dj_e(P,t')} = \frac{\Delta \eta}{f(P,\beta)} \qquad (1),$$

with $\Delta \eta = \eta(t') - \eta(t)$. The exponent in equation (5) in Chapter 1 is just

$$\frac{\eta(t)}{f(P,\beta)} = \int_{1 \ A.U.}^{\infty} \frac{w}{\kappa} \ dr \qquad (2).$$

Jokipii (1966) and Roelof (1967) have independently shown that the diffusion coefficient κ in the integrand of (2) is related to the power spectrum of spatial irregularities in the interplanetary magnetic field. In other words, they have found a means of relating a property of the medium to the propagation of the particles.

The form of the diffusion coefficient derived from theory may be expressed as

$$\kappa = \frac{\beta c P^3}{3\pi M(K_o)} \qquad (3),$$

where βc is the particle velocity, and K_o designates the wave number corresponding to a particle with gyro-radius r_o:

$$K_o = \frac{1}{r_o} = \frac{B}{P} \qquad (4).$$

The power spectrum M(K) of the spatial variations is related to the time variations "seen" by a satellite by

$$M(K) = \frac{W}{2\pi} m(f) \tag{5},$$

where the frequency and wave number satisfy

$$f = \frac{W}{2\pi} K \tag{6}.$$

Measurements of the magnetic field in space (Webber, 1968), have shown that

$$M(K) \propto 1/K, \text{ or } 1/K^2 \tag{7}.$$

With this form of power spectrum, the diffusion coefficient in equation (3) has the form

$$\kappa \propto \beta P, \text{ or } \beta \tag{8},$$

and hence in (1):

$$f(P,\beta) = \beta P, \text{ or } \beta \tag{9}.$$

The contrary results exhibited by the proton spectra since solar minimum in Figure 22 show that the present theory must be modified so that

$$f(P,\beta) \propto 1/P^n \tag{10},$$

or equivalently that

$$M \propto 1/K^{n-2} \tag{11},$$

where the ΔM represents the change in the power spectrum since solar minimum until the measurement of the relative modulation. n must be 1, or greater, then for the observed flux ratios to exhibit the form predicted by theory.

C. Comparison of Quietest Time Energy Spectra

From IMP-IV with Solar Minimum Spectrum

Referring ahead to Figure 39, it is readily seen that during several time intervals in September and October 1967 the differential flux of protons at 5.2 MeV was at a minimum. Examination of these two months of proton and alpha particle fluxes in detail showed an interval from October 11 through October 26 when the alpha particle counting rate almost vanished in the LED telescope. This period then was taken to represent the time of least solar activity on the basis of the low energy alpha particle fluxes.

A combination of methods was used to obtain the fluxes during this period. Where counting rates almost vanished, but were still non-zero, the fluxes were computed from the few counts that fell into an energy bin and the total accumulation on-time for the period. In the cases where no counts occurred, one count was assumed. This one count was used to compute an upper limit to the flux. For higher counting rates, the box fluxes were averaged for the period in question.

The proton energy spectrum obtained in the manner discussed is displayed in Figure 20 (b), and the alpha particle spectrum is shown in Figure 21 (b). Superimposed on each of these plots is a solid curve representing the corresponding 1965 quiet time composite spectrum (Gloeckler and Jokipii, 1967). These composite curves are identical to the spectra indicated in Figure 1. As one would expect, the 1967 spectra occurring

during a time of increasing solar activity show appreciable modulation. Also they show a low energy "tail" which, in light of the material to follow in Chapter V, is most probably of solar origin. If only the increasing parts of these 1967 spectra are compared with the 1965 spectra, one finds that the modulation of the protons and alphas is by a factor of 1.86 and 2.23, respectively, at 50 MeV/nucleon.

V. A TWO COMPONENT MODEL FOR LOW ENERGY
COSMIC RAYS AND ITS IMPLICATIONS

A. The Model

Qualitative examination of the low energy proton fluxes during very quiet times in 1967, for instance in September in Figure 17 (g), show that there seems to be a very noticeable relative minimum at around 30 MeV. If a slightly more active period is examined, say in August 1967 in the same figure, it is apparent that the local minimum disappears as the lowest energy fluxes begin to dominate. Further, it is noticed that the lowest energy flux increases by several orders of magnitude while the adjacent flux increases by a much smaller amount and the highest energy flux by even less. This behavior immediately suggests that what one may be observing in the energy range considered is a monotonically decreasing spectrum of particles that undergoes large variations added to a relatively stabile monotonically increasing spectrum of particles. The admixture of these components would seem to be such that during very quiet times the relative minimum noted falls in the vicinity of 30 MeV. It is probably not fortuitous that the proton spectrum in Figure 1 exhibits a minimum at about this same energy.

It is very difficult not to immediately identify the decreasing low energy component as originating in the sun and the increasing component as being of galactic origin. Solar proton fluxes that are known to be associated with flares all have very steep monotonically decreasing spectra. Further, it has been generally assumed that the higher energy particles were of galactic origin as in Figure 1. It does not seem

56

unreasonable to assume then that at least part of the cosmic rays below
the relative minimum in Figure 1 are of solar origin. Fan et al. (1968,
1969) have suggested that the lowest energy proton fluxes observed by
them below 10 MeV might contain a solar component.

With the above observations in mind, it is then possible to con-
struct a two component model of the low energy cosmic rays which , as
will be seen later, fits the observations remarkably well. Solar flare
proton spectra have been shown to fit an exponential rigidity law for
a wide range of rigidities (Fichtel and McDonald, 1967), but over a
limited energy range can equally well be fitted to a power law in
energy, e.g.

$$J(E) = J_o E^{-S} \tag{1}.$$

It would seem reasonable then to assume the same form for the quiet
time solar fluxes that would apply to the model being discussed.
Further, a power law in energy with a positive exponent could equally
well apply to the increasing, or galactic, component in the limited
energy interval being considered, even though above this interval it
will no longer hold true. Very simply, then, such a model may be
expressed as

$$J(E) = F_S E^{-S} + F_G E^{G} \tag{2},$$

where F_S and F_G are the values of the fluxes at unit energy, for the
solar and galactic components, respectively, and S and G are the
magnitudes of the power law indices in the two cases. Differentiating
(2) with respect to E and setting the result equal to zero, one ob-
tains for the energy at minimum flux

$$E_{min} = (SF_S/GF_G)^{1/(G+S)} \tag{3}.$$

Asympotically on either side of the minimum, the flux becomes dominated by one component, or the other, since

$$J \cong F_S E^{-S} \quad \text{for } E < E_{min} \tag{4},$$

and

$$J \cong F_G E^{G} \quad \text{for } E > E_{min} \tag{5}.$$

The four independent parameters describing this model, F_S, F_G, S, and G, all may be functions of time. It is to be expected that F_S and S will vary more rapidly since they are related to transient solar phenomena, and the galactic component will show on the average only a comparatively slow variation, provided the averaging time is long enough to remove transient modulation effects. If indeed the galactic component is relatively constant for short periods, then the energy at which the minimum is observed should be almost entirely dominated by the variations of the solar component. Eliminating F_S between equations (2) and (3) one obtains the result that

$$J_{min} = (1 + G/S) F_E E_{min}^{G} \tag{6}.$$

If the galactic component is represented by J_G then equation (6) may be expressed as

$$J_G (E_{min}) = [(S/(S + G)] J_{min} \tag{7}.$$

Hence, if indeed the observed spectrum is due to a rapidly varying solar component plus a relatively constant galactic component, then equation (7) is to be taken as a prescription for computing the galactic component from a series of measurements of J_{min}, E_{min}, S, and G.

It is now possible to summarize the assumptions and predictions of this model. With only the basic assumption that equation (2) represents the cosmic ray fluxes in some limited energy range containing the relative minimum it follows that

1. The lowest-energy fluxes and highest-energy fluxes should be relatively independent of each other,

2. On either side of the relative minimum, the fluxes should asymptotically approach the simple power-law form as given by equations (4) and (5).

If in addition it is also assumed that the solar component will exhibit greater magnitude and more rapidly varying time dependence than the galactic component, then the following are also predicted:

3. The location of the relative minimum will be closely related to the lowest energy fluxes, and almost independent of the fluxes at high energies, as long as that minimum falls between the fluxes at the two extremes. It should be noted that when the solar component becomes large enough, it should even dominate the higher energy fluxes.

4. The envelope of the various minimum fluxes taken over a period of time should trace out a power law function related to the galactic component by the relation given in equation (7).

With the above picture of the two component model in mind, it was possible to compare this model to observed proton and alpha particle spectra.

B. Least Squares Fitting of Model to Data

In order to compare the model presented in the last section to the observed data, it was necessary to systematically fit the mathematical

formulation given to this data in order to determine the four parameters F_S, F_G, S, and G. Several independent methods of curve fitting were tried out before one method was adapted as giving the most self consistent results. The method used was conveniently available in the form of a Fortran language subroutine that made it possible to perform the calculations on a high speed digital computer.

The algorithm used is completely general in that no special functions must be used to express the desired function. The method is further very general in that any function which is a good measure of goodness of fit between the computed and observed values, such as "chi-squared," may be used for computation. The process in essence steps each parameter of the desired function iteratively until the fit measure reaches a relative minimum. After variation of one parameter achieves a minimum, then the next parameter is varied. This procedure is carried through for two cycles of variation using a process of parabolic interpolation about the minima and increasing and decreasing the step size as necessary.

For convenience it was decided to use as the measure of goodness of fit an expression for "chi-squared" given by

$$\chi^2 = \sum_{i=1}^{N} [f(x_i) - y_i]^2 / dy_i^2 \tag{8},$$

where $f(x_i)$ represents the theoretical function to be fitted, the y_i are the dependent observed variables, the x_i are the independent observed variables, and the dy_i are the standard deviations or measured errors. N is the number of data points so that if P represents the number of free parameters in $f(x_i)$, then the distribution represented by χ^2 should

have a maximum at

$$\chi^2 = N - P \qquad (9).$$

By using χ^2 then as the function to be minimized, it was possible to obtain at the same time a direct measure of the goodness of fit. Explicitly the form of equation used was

$$\chi^2 = \sum_{i=1}^{10} [F_S E_i^{-S} + F_G E_i^{G} - J_i]^2 / \sigma_i^2 \qquad (10).$$

Ideally it would have been of great interest to treat as short time averages of the fluxes as possible in order to ascertain a high resolution picture of the time dependence of the model. In an initial attempt 24 hour averages of the 10 differential fluxes for the protons and 7 values for the alpha particles were tried, but it was found that the overall statistical accuracy was too poor to give meaningful results. It turned out that 96 hour averages of the same data gave very good results and hence the resulting analysis of the data with respect to the model was carried out on this basis.

Since the computations were performed on a digital computer, it was possible to code into the same program the necessary output formats to make interpretations as simple as possible. The analysis was applied only to the IMP-IV data covering the period from 24 May 1967 to 18 August 1968, so that the model could be examined at as high a resolution as possible in the energy interval from 4 to 80 MeV. Since there were 451 days of continuous data included in the analysis, there were 113 separate spectra each for the proton and alpha particle fluxes that were fitted. It is not particularly illuminating to merely display 113 graphs

of the fitted curves, or alternatively 113 sets of the four parameters F_S, F_G, S, and G, although these were produced directly and have a certain value. Rather it was expedient to perform directly on the fitted spectra the requisite comparisons and additional calculations to concisely compare the results with the predictions of the model.

The procedure was as follows. First the least squares fitting as described was carried out providing the best values of the four parameters in question for each of the 113 proton and alpha particle spectra. Next the minimum flux and the energy at minimum flux were determined numerically using the fitted values of the function. For each 96 hour set of proton and alpha spectra, a table was produced containing among other quantities the observed fluxes, energies, standard deviations, computed fluxes, final values of the function parameters, minimum flux, energy at minimum flux, and χ^2. At the same time a graph of the computed spectra for both the protons and alpha particles was made. It contained the data points with error bars superimposed on the fitted curves. In addition the ratios of helium to proton fluxes were computed for a number of values of energy/nucleon and a graph of these results were produced.

After the above computations were performed, the results were treated collectively in order to examine the multitude of computed results. Graphs for both protons and helium nuclei were produced showing the following correlations:

1. The flux at maximum energy versus the flux at minimum energy.

2. The flux at minimum energy versus the energy at minimum flux.

3. The flux at maximum energy versus the energy at minimum flux.

4. The minimum flux versus the energy at minimum flux.

5. The power law indices versus the flux at minimum energy.

6. The power law indices versus the flux at maximum energy.

With the results in the above described form, it was then possible to examine the results in a meaningful manner.

C. Interpretation of Results

Since it is not feasible to present all of the graphic results of the curve fitting herein, four representative graphs showing proton and alpha particle spectra are shown in Figure 25. Going from left to right and top to bottom, these show the actual data and computed spectra for four periods having progressively less amounts of the low energy components. As would be expected, these correspond to progressively quieter times of solar activity. It will be noted that indeed these log-log plots of observed data show straight line behavior on either side of the minimum. Further, it is to be noted that the high energy component is completely masked by the high level of the solar component for the 13-17 June period. Also in the other three graphs the level and slope of the galactic component remains quiet constant. This latter is consistent with the assumptions made for the model. The alpha particle spectra are seen to have essentially the same behavior as those for the protons.

Figure 26(a) displays four representative alpha-to-proton ratio plots for the same dates as Figure 25. All of the ratio plots show large time variations with no apparent regularities. A plot of the means and standard deviations for several discrete energies is shown in Figure 26(b). Two important features exhibited by this long term average are

(1) A maximum ratio of about .2 at   50 MeV/nucleon,

(2) A decrease in the size of the variations for increasing energy.

Studies of flare associated events (Fichtel and McDonald, 1967) show that

the alpha-to-proton ratio varies between about 10^{-3} and 10^{-1}. At galactic cosmic ray energies (Webber, 1967) the ratio is relatively constant at 10^{-1} after falling from about .2 at 60 MeV/nucleon. The decrease in size of the fluctuations with increasing energy may be interpreted as the lower energy ratios being primarily due to solar particles, while the higher energy ratio is more likely of galactic origin. The observed maximum in the ratio and decrease above   50 MeV/nucleon is consistent with observed ratios for galactic particles.

As has already been suggested, the lowest energy flux should probably consist mostly of solar particles and the highest energy flux of galactic protons. The 76.4 MeV proton flux is plotted versus the 5.2 MeV flux in Figure 27. Up to about a flux of 10^{-2} protons/s cm^2 sr MeV at 5.2 MeV, there appears to be no correlation between the two energies. Above this flux value the correlation becomes quite good. This behavior is consistent with the prediction that during quiet times the two extremes of the spectrum come from independent sources.

With the assumptions made in the first section, the model predicts that for a relatively constant galactic component that the lowest energy flux should correlate very well with the energy at minimum flux while the flux at the highest energy would show poor correlation with this energy. This is very strikingly the effect that is brought out in Figures 28 and 29. Figure 28 shows extremely good correlation between the 5.2 MeV flux and the energy at minimum flux; while the following figure shows almost no correlation between the 76.4 MeV flux and the energy at minimum flux.

In Figure 30 is shown a monotonically increasing dependence of the minimum flux as a function of the energy at minimum flux. As pointed out earlier, if the model is correct then such an increasing dependence should be related to the galactic component by equation (7). The slope

of the distribution in this plot is approximately 1 which is in extremely good agreement with the slopes of the two quiet time galactic components shown in Figure 25. If one takes a value of $J_{min} \cong 10^{-4}$ at 10^2 MeV in Figure 30, and nominal values of G and S of 1 and 3 respectively, then from equation (7) $J_G \cong .75 \ J_{min} \cong .75 \ x \ 10^{-4}$ which is quite close to the values found in the last two plots in Figure 25.

In the next two plots, Figures 31 and 32, are shown the distribution of the power law indices as a function of the low energy flux and high energy flux, respectively. With respect to low energy flux, there appears to be no systematic feature in either index except for an indication of a very slight anticorrelation between the positive values of S and the low energy flux. This latter can be interpreted as a hardening of the spectrum during times of higher solar activity. The correlations of the indices with high energy flux are either non-existent, or very small.

It would be expected from the behavior exhibited qualitatively by the alpha particle spectra in Figure 25 that essentially the same behavior would hold for these particles as well. Indeed this is so for the most part with a few significant differences. Figure 33 shows no correlation between the high and low energy flux up to about a value of 10^{-3} particles/s cm^2 sr MeV/nucleon for the 5.2 MeV flux. Above this value there appears to be a small amount of anticorrelation which could be interpreted as the onset of modulation of the higher rigidity alphas because of the greater solar activity. Figures 34 and 35 exhibit the comparatively much greater activity of the solar alphas as compared to their galactic counterparts. The very flat spectra for the quiet time alphas shown in Figure 25 is certainly well supported by the flatness

of minimum flux distribution with respect to energy presented in Figure 26. Finally, there is no indication of any significant regularities in the distribution of the power law indices of the alpha particle spectra with respect to either the low or high energy fluxes.

D.   The Relation of the Two Component

Model to Other Observations

In the last section it was shown that the two component model is quite capable of describing the observations of proton and alpha fluxes in the vicinity of the relative minimum in the cosmic ray energy spectrum. Whether this model is justified on other than the phenomenological grounds of the data fitting the functional form presented depends primarily on some substantiating evidence that the sun is indeed producing particles with energies of at least up to about 30 MeV and on a quasi-continuous basis. From the very high correlations between large solar flares and the subsequent arrival of large proton fluxes, there is little doubt that the sun produces such particles on occasion. In the absence of flares, however, the question arises of what, if any, features and properties are present which would permit a close association between observed enhancements in particle fluxes and the sun as their source.

Examination of any time history of cosmic ray fluxes which is taken at low energies and with averaging times of from a few minutes to a few days will show that there are many flux increases of varying sizes and shapes. A few of these with very fast rise times, large peak fluxes, and exponential decays, usually can be immediately associated with solar flares with significant importances. The remaining events must be scrutinized in some detail, testing for periodicity and correlation with solar features other than flares. This latter process usually

permits assignment of the bulk of the non-flare events to either 27 day recurrence type flux increases, or less often to isolated events showing no tendency to reappear. These latter two classes of events are certainly closely associated with magnetically active regions in the solar atmospheres, which may be responsible for both the acceleration and long term storage of the particles.

In Figure 39 are presented the 24 hour averages of proton fluxes at 5.2 MeV over the period of analysis for IMP-IV. Events associated with confirmed flares of 2N to 2B importance, or greater, are marked with an F. Most of the remaining events have been associated with particular large area calcium plage regions whose central meridian passage on the sun nearly coincides with the event. The plage region numbers are used to label each of these events in the figure. The striking feature of these events so identified is their close association with the return of the same region for several solar rotations which are indicated by connection of the numbers of the returning regions with horizontal broken lines. On about 15 June and 9 July two isolated events which are not recurrent are indicated.

A better idea of the character of these two events is shown in Figure 40. The one shown in June is seen to be very symmetrical with slow rise and decay times on either side of a rather constant plateau at the lower energy. This is certainly the behavior one might expect from a broad stream of particles of constant intensity rotating past the observer. In contrast to this event, a small flare event occurred on 3 June and shows the characteristic rapid rise time and slow decay. The other isolated event occurring about 9 July is not nearly so symmetrical as the one in June, but again shows the slow rise and fall

with an intervening plateau. About 2 August a rather irregular prolonged flux increase occurs which is identified in Figure 39 as a 27 day recurrence event.

The IMP-IV data just presented shows considerable activity during the period considered. Although the two component model was applied only to this data, at a time when solar activity was quite high, it is of interest to see if at a quieter time the sun could also be a potential source. With this end in view, the integral flux of protons with energies greater than 20 MeV obtained from IMP-III is plotted on a six hourly basis from March 1966 to March 1967 in Figure 41. As in Figure 39 the flares and calcium plage region meridian transits are marked where these can be shown to be related to the observed flux enhancements. It is evident that even during the relatively quieter times represented there are recurrence events that are periodically adding their output to the particle populations.

Table IV showed that the number of events increased quite markedly the smaller the size of the event considered. From this one might conjecture that there may be even more events below the level of detection. Such a conjecture is certainly not necessary in the case of the IMP-IV data to which the two component model was fitted. For the low energy flux data available there is an ample supply of solar protons, as shown in Figure 39, to keep the low energy component of energy spectra at an appreciable level. It will be necessary to make measurements during much quieter times, such as prevailed just after IMP-III was launched and to see how these fit the model in order to determine if the low energy "tail" of the spectrum is greatly reduced.

There exists at least one case in the literature in which proton flux observations made at a different phase of the solar cycle seem to be compatable with the model up to somewhat higher energies. Meyer and Vogt (1963) present a series of differential proton energy spectra obtained from balloon-borne detectors flown in July and August of 1961. They contend that these spectra which are very steep monotonically decreasing functions of energy are primary cosmic rays. The relative minima exhibited in four of these spectra occur from about 180 MeV up to about 300 MeV, which is much higher than the minima observed since 1963 which have been in the vicinity of 30 MeV. Further, the lower energy decreasing part of their spectra which extends in energy from 100 MeV to the minima exceed by about an order magnitude the general flux levels observed from 1963 to the present time.

The above spectra of Meyer and Vogt are much more easily explained on the basis of the two component model presented here than by assuming that they are indeed galactic primaries. If the model is correct then they observed the high energy end of the solar flux component where it was of comparable value to the primary component resulting in the relative minimum. This interpretation of their results does not disagree with the IMP-IV results, since for such solar component levels the minimum would have fallen above the IMP-IV energy interval.

In closing it should be emphasized that the two component model presented is by no means confirmed by what has been discussed. Further, it has not conclusively been shown that the lowest energy fluxes are all solar protons. Rather with respect to the first of these items, it would probably suffice to say that the necessity condition of a proof has been met, but not the sufficiency criterion. Much further testing

of such a model will be required over broader energy intervals and for

the entirety of the solar cycle. As to the second point, it is prob-

ably clear that any increases above the quiet time flux levels are

of solar origin. When this latter is accounted for, what remains

is asserted to be of galactic origin.

APPENDIX A

GEOMETRY FACTOR FOR A TELESCOPE WITH CYLINDRICAL SYMMETRY

Consider the schematic of a particle telescope as shown in Figure 6, of height h and base radius R_1 and top radius R_2. Assume that the particles have an isotropic flux of J particles per unit area and solid angle. Referring to the diagram, then the differential number falling on the increment of area dA and passing through the upper end area increment dA' will be given by

$$dN = J \cos \theta \, dA \, dr \qquad (1)$$

where θ is the angle between the vertical h and s, the line connecting the two area elements, and where

$$dA = r \, dr \, d\phi \qquad (2)$$

$$dr = \frac{dA' \cos \theta}{s^2} \qquad (3),$$

and

$$dA' = r' \, dr' \, d\phi \qquad (4).$$

From the diagram it is also seen that

$$1^2 = r^2 + r'^2 - 2rr' \cos(\phi' - \phi) \qquad (5),$$

$$s^2 = h^2 + 1^2 \qquad (6),$$

and

$$\cos \theta = h/s \qquad (7).$$

Equation (1) can now be integrated using these relations with the result that

71

$$N \ = \ IG \tag{8}$$

where the geometry factor G is

$$G \ = \ 2h^2 \int_0^{R_1} rdr \int_0^{R_2} r'dr' \int_0^{2\pi} d\phi \int_\phi^{\phi+\pi} \lceil h^2 + r^2 + r'^2 - 2rr' \cos (\phi' - \phi) \rceil^{-2} d\phi' \tag{9}$$

The four integrals in (9) are easily performed going from right to left with the final result

$$G \ = \ \frac{\pi^2 h^2}{2} \left\{ 1 + \frac{R_1^2 + R_2^2}{h^2} - \left[1 + 2 \frac{R_1^2 + R_2^2}{h^2} + \frac{(R_1^2 - R_2^2)^2}{h^4} \right]^{\frac{1}{2}} \right\} \tag{10}$$

If the linear dimensions are measured in centimeters and the angles in radians, the units of G are centimeters^2 steradians (cm^2 sr). In the case of a right circular cylinder of radius R, i.e. $R_1 = R_2 = R$, equation (10) reduces to the form

$$G \ = \ \frac{\pi^2 h^2}{2} \left[1 + \frac{2R^2}{h^2} - \left(1 + \frac{4R^2}{h^2} \right)^{\frac{1}{2}} \right] \tag{11}$$

For a long slender telescope, i.e. where $R/h \ll 1$, equation (11) reduces to the approximation

$$G \ \cong \ \pi^2 R^4 / h^2 \tag{12}.$$

APPENDIX B

COMPUTATION OF AVERAGE PARTICLE PATH LENGTH

IN CYLINDRICAL GEOMETRY

If the line s in Figure 6 represents a typical particle track for a particle making an angle θ with the axis, then to find the average track length $<s>$ for an isotropic distribution of particles it is necessary to average all such tracks over an appropriate distribution. This is very easily done if it is noted that in Appendix A the computation of the geometry factor G is accomplished by integrating over all angles within the limits such that the track s passes through the two ends of the cylinder.

Using Appendix A we can write for G

$$G = \iint \frac{h^3 \; dA \; dA'}{s^4} \tag{1},$$

where $s = s(r,r',\phi,\phi')$. It is then possible to write a normalized distribution function for the angles in the form

$$w(r,r',\phi,\phi') = \frac{h^3}{G \; s^4 (r,r',\phi,\phi')} \tag{2}.$$

The average of s over an isotropic distribution is given then by

$$<s> = \iint w(r,r',\phi,\phi') \; s(r,r',\phi,\phi') \; dA \; dA' \tag{3},$$

$$<s> = \frac{h^2}{G} \iint \frac{dA \; dA'}{s^3} \tag{4}.$$

Using the equations (2) through (7) from Appendix A this can be written in the explicit form

$$\langle s \rangle = \frac{2h^2}{G} \int_0^{R_1} r\,dr \int_0^{R_2} r'\,dr' \int_0^{2\pi} d\phi \int_\phi^{\phi+\pi} \frac{d\phi'}{\left[h^2 + r^2 + r'^2 - 2rr'\cos(\phi' - \phi)\right]} \quad (5).$$

In theory equation (5) is integrable. It was found in practice that it was more convenient to perform the integration numerically on a digital computer over the range of required values. This was done quite easily using a Monte Carlo integration algorithm.

The computed values were expressed as an average value of the cosine of the angle between the average path length and the longitudinal axis of the telescope such that

$$\langle \cos \theta \rangle = h/\langle s \rangle \qquad (6).$$

The corrections for both telescopes in this study were only a few percent:

$$1/\langle \cos \theta \rangle \cong 1.03 \qquad (7).$$

THE BINOMIAL AND POISSON DISTRIBUTIONS

For most random processes, including the counting of cosmic ray particles, Poisson statistics are usually assumed. Since the statistical requirements of the several forms of data analysis described in the text are varied, it is pertinent to derive here the requisite formulae for computing the standard deviations of these experiments.

One is concerned with the counting rate r which is by definition the number of particles n counted in the time interval t, i.e.

$$r = n/t \qquad (1)$$

If the interval t is divided into b bins such that the probability of any two counts occurring in one bin is negligible, then one can write the probability that a count will occur in a bin as

$$p = \bar{n}/b \qquad (2),$$

where $\bar{n}$ is the average number of counts in the time t. Similarly one can write the probability that such a count will not occur in a bin as

$$q = 1 - p = 1 - \bar{n}/b \qquad (3).$$

The combined probability that n counts will occur in the time t, or b bins, in a particular order is simply

$$p^n q^{b-n} = \left(\frac{\bar{n}}{b}\right)^n \left(1 - \frac{\bar{n}}{b}\right)^{b-n} \qquad (4).$$

Now there are b! different ways that such a particular order can be

obtained for distinguishable counts. There are n! different ways that the n counts may be arranged among themselves and (b - n)! different ways the remaining bins may be ordered among themselves. It follows then that the number of ways n indistinguishable counts can occupy b bins is given by the expression

$$\frac{b!}{n! \ (b - n)!}$$

Multiplying equation (4) by this latter expression, one obtains for the probability that there will be n counts

$$w_b(n) \ = \ \binom{b}{n} \ p^n q^{b-n} \ = \ \frac{b!}{n!(b - n!)} \left(\frac{\bar{n}}{b}\right)^n \left(1 - \frac{\bar{n}}{b}\right)^{b-n} \tag{5},$$

where the $\binom{b}{n}$ represents the binomial coefficient.

The binomial theorem may be expressed as

$$(p + q)^b \ = \ \sum_{n=0}^{b} \ \binom{b}{n} \ p^n q^{b-n} \tag{6}.$$

From equations (2) and (3)

$$p + q \ = \ 1 \tag{7},$$

so that

$$\sum_{n=0}^{b} \ w_b(n) \ = \ (p + q)^n \ = \ 1 \tag{8},$$

and hence $w_b(n)$ is the probability distribution for counts occurring in b bins. By definition the mean value of n counts occurring in b bins is

$$\bar{n} \ \equiv \ \sum_{n=0}^{b} \ n \ w_b(n) \tag{9}.$$

Using equation (6) one may write the expression

$$(py + q)^b = \sum_{n=0}^{b} \binom{b}{n} p^n y^n q^{b-n} = \sum_{n=0}^{b} y^n w_b(n) \qquad (10).$$

Differentiating equation (10) with respect to y one obtains

$$\frac{d}{dy}(py + q)^b = b(py + q)^{b-1}p = \sum_{n=0}^{b} nw_b(n) y^{n-1} \qquad (11).$$

Setting y equal to 1 in equation (11) the expected result is

$$\bar{n} = \sum_{n=0}^{b} nw_b(n) = bp \qquad (12).$$

Differentiating equation (11) again with respect to y one obtains

$$b(b - 1)(py + q)^{b-2}p^2 = \sum_{n=0}^{b} n(n - 1) w_b(n) y^{n-2} \qquad (13).$$

Setting y equal to 1 in equation (13) the result is by definition the mean value of n(n - 1), or

$$\overline{n(n - 1)} = \sum_{n=0}^{b} n(n - 1) w_b(n) = b(b - 1)p^2 \qquad (14).$$

Expanding the left hand side of equation (14) one obtains

$$\overline{n(n - 1)} = \overline{n^2} - \bar{n} = b(b - 1)p^2 \qquad (15).$$

By definition the variance is

$$\sigma^2 \equiv \overline{(\bar{n} - n)^2} = \overline{n^2} - \bar{n}^2 \qquad (16),$$

where σ is the standard deviation. Substitution of equation (12) and (15) into (16) produces the result

$$\sigma^2 = bp(1 - p) \tag{17},$$

so that the standard deviation for n counts in b bins is simply

$$\sigma_n = [bp(1 - p)]^{1/2} \tag{18},$$

or using the probability of a single count occurring in a bin as given by equation (2), (18) becomes

$$\sigma_n = [\bar{n}(1 - \bar{n}/b)]^{1/2} \tag{19}.$$

Equation (19) is a completely general formula for the standard deviation of the random process of putting n items in b boxes. As will be shown shortly, the Poisson distribution and its resultant statistical quantities are special cases following from the binomial distribution given in equation (5), with the condition that b and n are both very large. The binomial distribution, on the other hand, is applicable in the general instance and hence holds for small b and n. One inadequacy in the binomial standard deviation as given by equation (19) is that σ_n vanishes for $\bar{n} = 0$ and $\bar{n} = b$. In practice the standard deviations may be given realistic values for these two cases by arbitrarily adding one count and one bin to n and b, respectively. Equation (19) is in these two cases

$$\sigma_n = \left[(\bar{n} + 1)[1 - (\bar{n} + 1)/(b + 1)]\right]^{1/2} \tag{20}.$$

If one considers the case where b becomes very large then one can take the limit of equation (5) as b approaches infinity. In this limit the binomial coefficient becomes

$$\lim_{b \to \infty} \binom{b}{n} = \lim_{b \to \infty} \frac{b(b - 1)(b - 2) \ldots (b - n + 1)}{n!} = \frac{b^n}{n!} \tag{21},$$

and the right most factor in equation (5) is

$$\lim_{b \to \infty} \left(1 - \frac{\bar{n}}{b}\right)^{b-n} = \lim_{b \to \infty} \left(1 - \frac{(b-n)}{1!} \frac{\bar{n}}{b} + \frac{(b-n)(b-n-1)}{2!} \frac{\bar{n}^2}{b^2} - \cdots \cdot \frac{\bar{n}^{b-n}}{b^{b-n}}\right)$$

$$= e^{-\bar{n}} \tag{22}.$$

With the two limits obtained in equations (21) and (22), the limiting case for equation (5) is given by

$$w(n) \equiv \lim_{b \to \infty} w_b(n) = \bar{n}^n e^{-\bar{n}}/n! \tag{23},$$

which is the Poisson distribution function.

In the limit of Sterling's approximation which is valid for $n \geq 10$

$$n! \cong \sqrt{2\pi} \, n^{n + \frac{1}{2}} \, e^{-n} \tag{24},$$

one may express the logarithm of (23) as

$$\ln w(n) = n \ln \bar{n} - \bar{n} - \ln \sqrt{2\pi} - (n + \tfrac{1}{2}) \ln n - n \tag{25}.$$

Differentiating equation (25) with respect to n and setting the result to zero one obtains

$$\ln \bar{n} - \ln n - (n + \tfrac{1}{2}) \frac{1}{n} + 1 = 0 \tag{26},$$

or

$$\bar{n} = n e^{\frac{1}{2}n} \tag{27}.$$

It is easily seen that in the limit of large n,

$$\bar{n} \cong n \tag{28}.$$

In this case of large n, if one expands $\ln w(n)$ in a Taylor's series about $\bar{n}$, the first derivative with respect to n vanishes because of (28).

Keeping only the first non-vanishing terms above the constant term, one

obtains

$$\ln w(n) = \ln w(\bar{n}) + \frac{1}{2!} \left(\frac{d^2 \ln w(n)}{dn^2} \right)_{\bar{n}=n} x^2 \qquad (29),$$

where $x = n - \bar{n}$. Using Sterling's approximation for $\bar{n}$, the first term

in (29) becomes

$$w(\bar{n}) = \frac{n^{\bar{n}} e^{-\bar{n}}}{n!} = \frac{n^{\bar{n}} e^{-\bar{n}}}{\sqrt{2\pi\bar{n}} \, n^{-n} e^{-n}} = \frac{1}{\sqrt{2\pi\bar{n}}} \qquad (30).$$

Differentiating equation (25) twice with respect to n, the result is

$$\frac{d^2 \ln w(n)}{dn^2} = \frac{1}{2n^2} - \frac{1}{n} \qquad (31).$$

Substituting equations (30) and (31) into (29) one obtains the result

$$\ln w(n) = -\ln \sqrt{2\pi \bar{n}} - \frac{1}{2} \left(\frac{1}{2\bar{n}^2} - \frac{1}{\bar{n}} \right) x^2 \qquad (32),$$

or keeping only the largest second order term this may be expressed as

$$w(n) = \frac{1}{\sqrt{2\pi\bar{n}}} e^{-x^2/2\bar{n}} \qquad (33).$$

Comparing equation (33) with the usual Gaussian error distribution

$$f(x) = \frac{1}{\sigma\sqrt{2\pi}} e^{-x^2/2\sigma^2} \qquad (34),$$

it is easily seen that the Poisson standard deviation is just

$$\sigma = \sqrt{\bar{n}} \qquad (35).$$

Since long counting runs are usually encountered where Poisson

statistics are valid, it is the usual practice to replace $\bar{n}$ by n in

(35). It should be noted by comparing equation (19) and (35) that for
small b one cannot use Poisson statistics as is often erroneously done.
As one would expect, however, equation (19) in the limit of large b
reduces to equation (35).

APPENDIX D

COMPUTATION OF COUNTING RATES

BY THE DEAD TIME APPROXIMATION

In the case a time bin is open for a fixed period of time to accept
one, and only one, count during this period, it is possible to compute
a counting rate if the probability of a count occurring is much less
than unity. Let r be the counting rate that is sought, and let t be the
period such that a bin may be open to receive such a count. Let $P(1,t)$
be the probability that one count will occur in the interval after the
time t. Then this may be expressed as

$$P(1,t) = P(0,t) \cdot P(1,t,dt) \qquad (1),$$

where $P(0,t)$ is the probability that no count occurred before the time
t, and $P(1,t,dt)$ is the probability a count occurred in the differential
time dt at t. If r is the counting rate then the second factor on the
right hand side of (1) may be expressed as

$$P(1,t,dt) = rdt \qquad (2).$$

If the interval t is broken up into N intervals $dt = t/N$, then the prob-
ability a count does not occur in t is given by

$$P(0,t) = \prod_{i=1}^{N} P_i (0,t_i,dt_i) \qquad (3),$$

where the probability that a count does not occur in dt_i and t_i is just

$$P_i (0,t_i,dt_i) = 1 - rdt_i \qquad (4).$$

82

Using equation (4) in (3), one may write

$$P(0,t) = \prod_{i=1}^{N} (1 - rdt_i) = \lim_{N \to \infty} (1 - rdt)^N$$

$$= \lim_{N \to \infty} (1 - r\frac{t}{N})^N = e^{-rt} \tag{5}$$

Using the results of equations (2) and (5) in (1), one finds that the probability for one count occurring after a time t is just

$$P(1,t) = re^{-rt} dt \tag{6}.$$

The total probability that one count will occur sometime during the interval t is by integrating (6) over this interval,

$$P(t) = \int_0^t re^{-rt'} dt' = 1 - e^{-rt} \tag{7}.$$

If there are b time bins of duration t and n counts such that $n \ll b$, then it is also true that

$$P(t) = n/b \tag{8}.$$

Combining equations (7) and (8), one obtains

$$e^{-rt} = 1 - n/b \tag{9},$$

or

$$r = \frac{1}{t} \ln [b/b - n)] \tag{10},$$

for the counting rate.

If equation (10) is differentiated with respect to n, the result

$$\frac{dr}{dn} = \frac{1}{t(b - n)} \tag{11},$$

is obtained. The differential may be replaced with the errors, or standard deviations in this case, of r and n, hence

$$\sigma_r = \frac{\sigma_n}{t(b - n)} \qquad (12).$$

σ_n can be evaluated using equation (19) in Appendix C, with n replacing $\bar{n}$, so that

$$\sigma_r = \frac{1}{t} \left[\frac{n}{b(b - n)} \right]^{1/2} \qquad (13).$$

REFERENCES

Anand, K. C., Daniel, R. R., Stephens, S. A., Bhowmik, B., Krishna, C. S., Mathur, P. C., Aditza, P. K., and Puri, R. K., Proc. 9th Int. Conf. on Cosmic Rays, London, 1965 (Institute of Physics and Physical Society, London) 1, 362, 1966.

Arnett, W. D., Can. Jour. Phys., 44, 2553, 1966.

Axford, W. I., Planetary Space Sci., 13, 1301, 1965.

Balasubrahmanyan, V. K., Hagge, D. E., Ludwig, G. H., and McDonald, F. B., Proc. 9th Int. Conf. on Cosmic Rays, London, 1965 (Institute of Physics and Physical Society, London), 1, 427, 1966a.

Balasubrahmanyan, V. K., Boldt, E., Palmeira, R. A. R., and Sandri, G., Can. Jour. Phys., 46, S633, 1967.

Balasubrahmanyan, V. K., Hagge, D. E., and McDonald, F. B., Can. Jour. Phys., Proceedings of 19th IUPAP International Conference on Cosmic Rays, 46, S887, 1968.

Balasubrahmanyan, V. K., Solar Physics, 1, 39, 1969.

Barkas, W. H. and Berger, M. J., "Tables of Energy Losses and Ranges of Heavy Charged Particles," National Aeronautics and Space Administration, SP-3013, Washington, D. C., 1964.

Bryant, D. A., Cline, T. L., Desai, U. D., and McDonald, F. B., Jour. Geophys. Res., 67, 4983, 1962.

Burbidge, E. M., Burbidge, G. R., Fowler, W. A., and Hoyle, F., Rev. of Mod. Phys., 29, 547, 1957.

Burlaga, L. F., Univ. of Minnesota Technical Report CR88, 1966.

Colgate, S. A. and White, R. H., Proc. Int. Conf. Cosmic Rays, Jaipur, Vol. 3, p. 335, 1963.

Colgate, S. A. and Johnson, M. H., Phys. Rev. Letters, 5, 235.

Ellison, M. A., Quart. J. Royal Astron. Soc., 4, 62, 1963.

Fan, C. Y., Gloeckler, G., and Simpson, J. A., Phys. Rev. Letters, 17, 329, 1966a.

Fan, C. Y., Pick, M., Pyle, R., Simpson, J. A., and Smith, D. R., Jour. Geophys. Res., 73, 1555, 1968.

Fan, C. Y., Gloeckler, G., McKibben, B., Pyle, K. R., and Simpson, J. A., 19th International Conference on Cosmic Rays, Calgary, 1967, Can. Jour. Phys., 46, S498, 1968.

Fan, C. Y., Gloeckler, G., McKibben, B., and Simpson, J. A., (to be presented at 11th International Cosmic Ray Conference, Budapest, 1969).

Fazio, G. G., in Annual Reviews of Astronomy and Astrophysics, Vol. 5, 481, Goldberg, L., ed., Annual Rev., Inc. Palo Alto, 1967.

Fermi, E., Phys. Rev., 75, 1169, 1949.

Fibich, M. and Abraham, P. B., Jour. Geophys. Res., 70, 2475, 1965.

Fichtel, C. E. and McDonald, F. B., in Annual Reviews of Astronomy and Astrophysics, Vol. 5, 351, Goldburg, L, ed., Annual Reviews, Inc. Palo Alto, 1967.

Freier, P. S. and Waddington, C. J., Jour. Geophys. Res., 70, 5753, 1965.

Ginzburg, V. L. and Syrovatskii, S.I., "The Origin of Cosmic Rays," MacMillan Co., New York, 1964.

Gleeson, L. J. and Axford, W. I., Ap. J., 154, 1011, 1968.

Gloeckler, G. and Jokipii, J. R., Phys. Rev. Letters, 17, 203, 1966.

Gloeckler, G. and Jokipii, J. R., Ap. J., 148, L41, 1967.

Hartman, R. C., Meyer, P., and Hildebrand, R. H., Jour. Geophys. Res., 70, 2713, 1965.

Hatton, C. J., Marsden, P. L., and Willetts, A. C., 10th International Conference of Cosmic Rays, Calgary, 1967, Can. Jour. Phys., 46, S915, 1968.

Hofmann, D. J. and Winckler, J. R., Jour. Geophys. Res., 68, 2067, 1963.

Hofmann, D. J. and Winckler, J. R., Phys. Rev. Letters, 16, 109, 1966.

Jokipii, J. R., Ap. J., 149, 405, 1967.

Jokipii, J. R., Ap. J., 152, 799, 1968.

Jokipii, J. R. and Parker, E. N., Planetary Space Sci, 15, 1375, 1967.

Krimigis, S. M., Jour. Geophys. Res. 70, L943, 1965.

Lange, I. and Forbush, S. E., Terrestrial Magnetism Atmospheric Elec., 47, 185, 1942.

L'Heureux, J., Ap. J., 148, 399, 1967.

McDonald, F. B., Phys. Rev., 109, 1367, 1958.

Morrison, P., "The Origin of Cosmic Rays," in Handbuch der Physik, (Springer-Verlog, Berlin, 1961), Vol. 46-1.

Morrison, P., in Annual Reviews of Astronomy and Astrophysics, Vol. 5, 325, Goldberg, L., ed., Annual Rev., Inc. Palo Alto, 1967.

Meyer, P., Parker, E. N., and Simpson, J. A., Phys. Rev., 104, 768, 1956.

Meyer, P. and Vogt, R., Phys. Rev., 129, 2275, 1963.

Nagashima, K., Duggal, S. P., and Pomerantz, M. A., Planetary Space Sci. 14, 177, 1966.

Neher, H. V., Jour. Geophys. Res., 72, 1527, 1967.

Ormes, J. F. and Webber, W. R., Proc. 9th Int. Conf. on Cosmic Rays, London, 1965 (Institute of Physics and Physical Institute, London), 1, 349, 1966.

Parker, E. N., Phys. Rev., 103, 1518, 1956.

Parker, E. N., Phys. Rev., 107, 830, 1957.

Parker, E. N., Phys. Rev., 110, 1445, 1958.

Parker, E. N., Interplanetary Dynamical Processes, Interscience, New York, 1963.

Parker, E. N., Planetary Space Sci., 14, 371, 1966

Parker, E. N., Planetary Space Sci., 13, 9, 1965.

Paull, S., Cancro, C. A., and Janniche, P. J., GSFC Cosmic Ray Experiments Source-Encoding Electronics for IMP-F, General System Description, NASA, GSFC Document No. X-711-67-125, 1967a.

Paull, S., Garrahan, N. M., and McGowan, R. G., Circuit Design and Operation of GSFC Cosmic Ray Experiments Source-Encoding Electronics for IMP-F, NASA, GSFC Document No. X-711-67-286, 1967b.

Ramaty, R. and Lingenfelter, R. E., Ap. J., 155, 587, 1969.

Reid, G. C., Jour. Geophys. Res., 69, 2659, 1964.

Ritson, D. M., "Techniques of High Energy Physics," Interscience, New York, 1961.

Roelof, E. C., Ph. D. Thesis, Univ. of California, Berkeley, 1966.

Roelof, E. C., (to be published in Astrophys. and Space Science, 1970).

Rossi, B., "High-Energy Particles," Prentice-Hall, Englewood Cliffs, New Jersey, 1952.

Simpson, J. A. and Wang, J. R., Ap. J., 149, L73, 1967.

Smith, H. J., in "The Physics of Solar Flares," AAS-NASA Symposium
    Hess, W. N., ed., NASA SP-50, U. S. Printing Office, Washington,
    D. C., 1964.

Sweet, P. A., Nuovo Cimento, Suppl. 8, Ser. X, 188, 1958.

Sweet, P. A., AAS-NASA Symp. Phys. Solar Flares, U. S. GPO, 409, 1964.

Vogt, R., Phys. Rev., 125, 366, 1962.

Waddington, C. J. and Freier, P. S., Proc. 9th Int. Conf. on Cosmic Rays
    London, 1965 (Institute of Physics and Physical Society, London),
    1, 339, 1966.

Webber, W. R., Technical Report CR-105, School of Physics and Astronomy,
    Univ. of Minnesota, 1967 (review paper delivered at 10th IUPAP
    International Conference on Cosmic Rays, Calgary, 1967).

Wilcox, J. M. and Ness, N. F., Jour. Geophys. Res., 70, 5793, 1965.

TABLE I

SATELLITE DATA

	IMP-III	IMP-IV
Launch Vehicle:	3-stage Delta Vehicle DSV-3C	3-stage Delta Vehicle DSV-3E
Launch Site:	Eastern Test Range	Western Test Range
Launch Time:	0700:00 May 29, 1965	1405:54 May 24, 1967
Weight:	59.4 Kg	73.8 Kg
Initial Perigee:	208 Km	248 Km
Apogee:	260,800 Km	211,116 Km
Inclination:	33.94°	67.172°
Period:	140 hrs.	104 hrs.
Spin Rate:	23 R.P.M.	23.4 R.P.M.

TABLE II

COEFFICIENTS OF TELESCOPE RESPONSE FUNCTIONS

Experiment	a	b	f	g
IMP-III	-3.104	0.776	0.0679	0.862
IMP-IV MED	0.0	0.647	0.0434	0.749
IMP-IV LED	-0.272	0.341	-0.0945	0.0645

TABLE III

ANALYSIS PARAMETERS

Bin No.	E_{min}	E_{max}	E	$\angle E$	G
IMP-III and IMP-IV MED Proton:					
1	18.7	29.2	23.9	10.5	3.26
2	29.2	39.7	34.4	10.5	3.14
3	39.7	50.2	44.9	10.5	2.99
4	50.2	60.6	55.4	10.4	2.84
5	60.6	71.1	65.8	10.5	2.67
6	71.1	81.7	76.4	10.6	2.52
IMP-III and IMP-IV-MED Alpha Particle:					
1	18.7	40.0	29.4	21.3	3.20
2	40.0	60.0	50.0	20.0	2.92
3	60.0	81.5	70.8	21.5	2.62
IMP-IV LED Proton:					
1	4.2	6.2	5.2	2.0	.764
2	6.2	9.5	7.8	3.3	.756
3	9.5	13.5	11.5	4.0	.740
4	13.5	19.1	16.3	5.6	.594
IMP-IV LED Alpha Particle:					
1	4.8	7.0	5.9	2.2	.764
2	7.0	10.0	8.5	3.0	.756
3	10.0	13.7	11.8	3.7	.740
4	13.7	18.9	16.3	5.2	.594

Note: Energies in units of MeV/nucleon. Geometry factor in units of cm^2 sr.

TABLE IV

SEMI-ANNUAL COUNT OF 29 MEV

PROTON FLUX INCREASES

Dates	$\geq 10^{-3*}$	$\geq 10^{-2}$	$\geq 10^{-1}$	$\geq 10^{0}$	$\geq 10^{1}$
Jan. - Jun. '65	0				
Jul. - Dec. '65	1	1			
Jan. - Jun. '66	4	1			
Jul. - Dec. '66	8	4	3	1	1
Jan. - Jun. '67	(18)**	(14)	(8)	(5)	(2)
Jul. - Dec. '67	7	2	2		
Jan. - Jun. '68	6	5	1	1	
Jul. - Dec. '68	(16)	(12)	(4)		
TOTALS	60	39	18	7	3

* Units are number/s cm^2 sr MeV.

** The numbers in parenthesis are normalized to 6 months where data was missing.
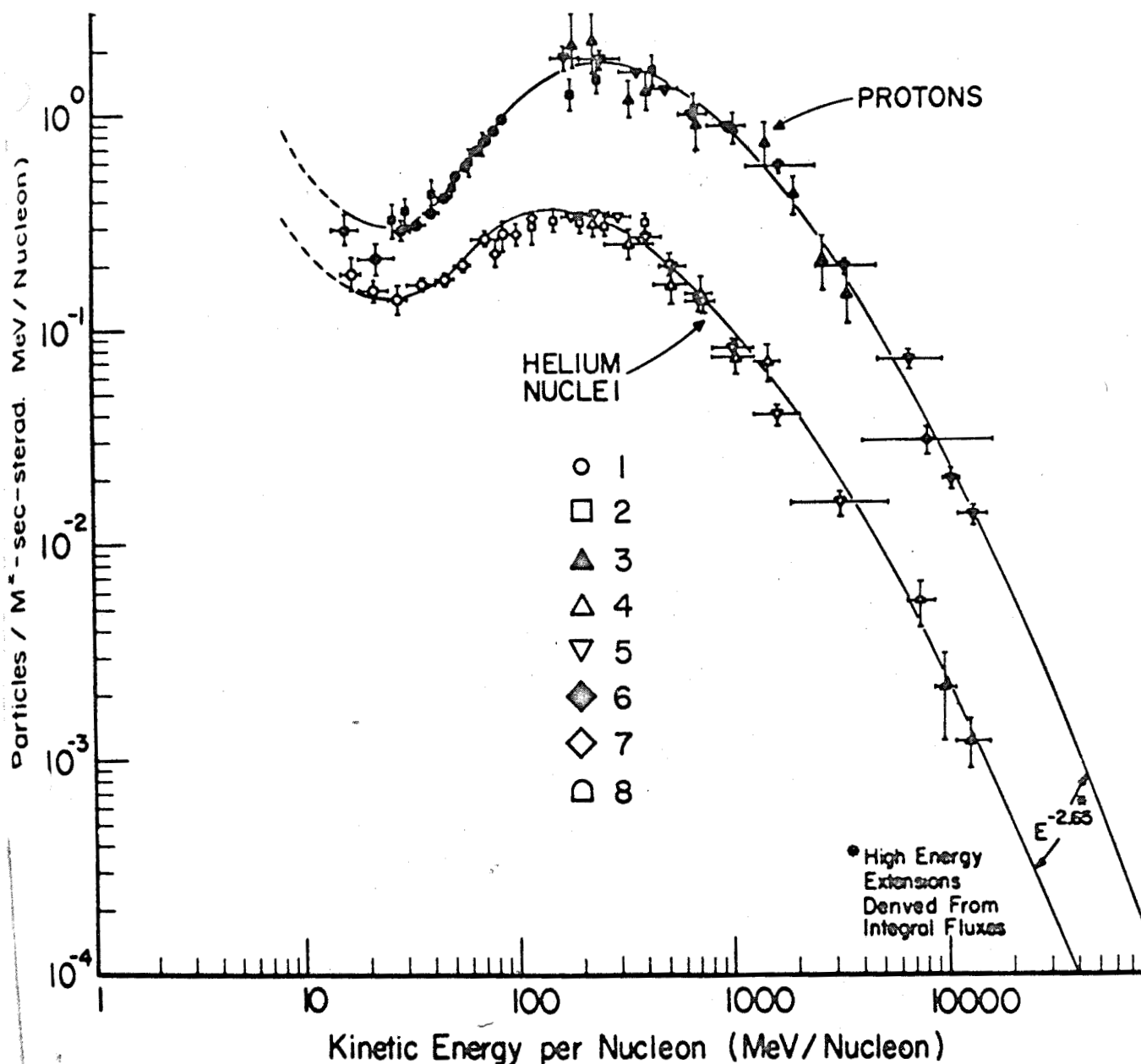
Figure 1. Primary differential energy/nucleon spectra of cosmic-ray
protons and helium nuclei observed near earth near solar
minimum in 1965. Solid and open symbols represent
measurements of protons and helium nuclei, respectively.
1. IMP-3, June-Dec. 1965, Fan et al. (1965a)
2. IMP-3 and balloon, June 1965, Balasubrahmanyan, Hagge,
   et al. (1966a,b)
3. balloon, June 1964, Waddington and Freier (1966)
4. balloon, June 1963, Freier and Waddington (1965)
5. balloon, June 1964, 1965, Ormes and Webber (1966)
6. balloon, 1954, McDonald (1958)
7. balloon, May 1965, Hofmann and Winckler (1966)
8. balloon, April 1963, Anand et al. (1966)
Only data representative of solar minimum have been used.
(from Gloeckler and Jokipii, 1967).
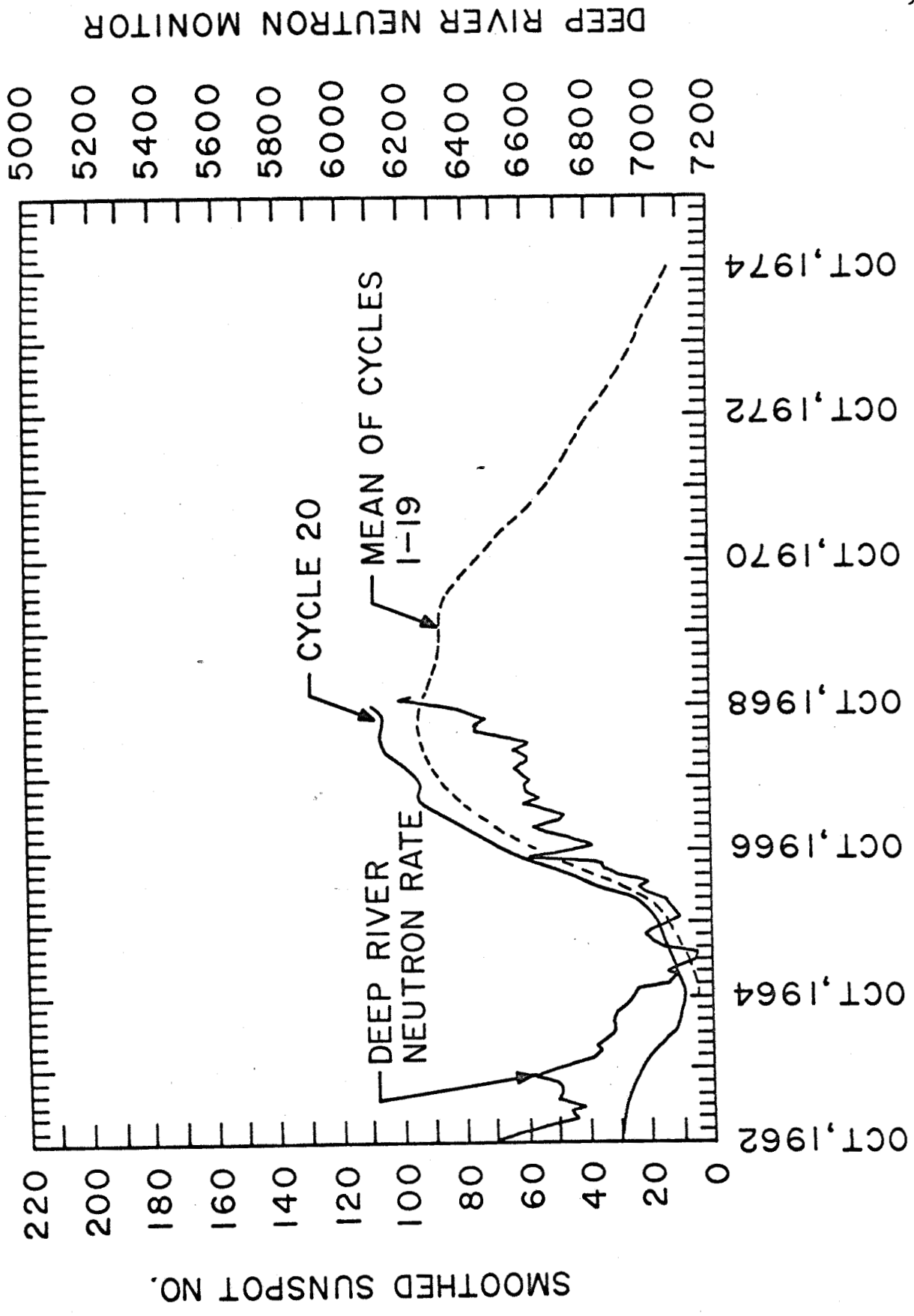
DEEP RIVER NEUTRON MONITOR

SMOOTHED SUNSPOT NO.

CYCLE 20

MEAN OF CYCLES
1-19

DEEP RIVER
NEUTRON RATE

OCT,1962
OCT,1964
OCT,1966
OCT,1968
OCT,1970
OCT,1972
OCT,1974

Figure 2. Comparison of Deep River neutron counting rate with smoothed sunspot number for the current cycle. Mean of previous 19 cycles superimposed.

Figure 2. Comparison of Deep River neutron counting rate with smoothed sunspot number for the current cycle. Mean of previous 19 cycles superimposed.
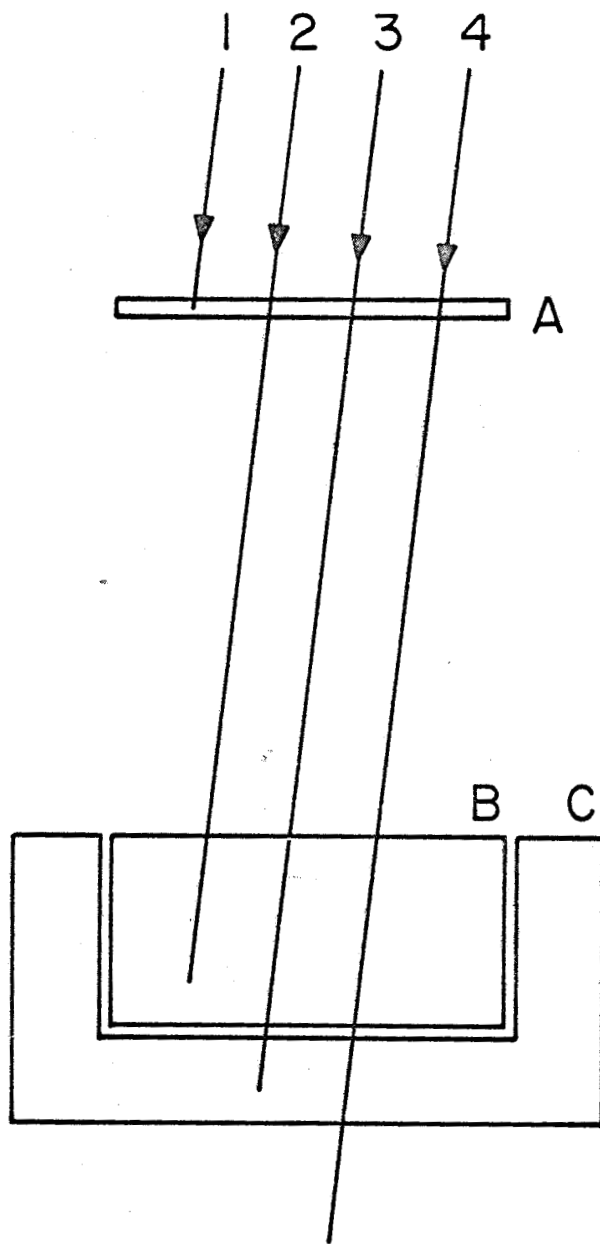
Figure 3. Schematic of ΔE versus $E - \Delta E$ particle telescope. A denotes detector measuring ΔE and B the dector measuring $E - \Delta E$. C is the anti-coincidence detector.
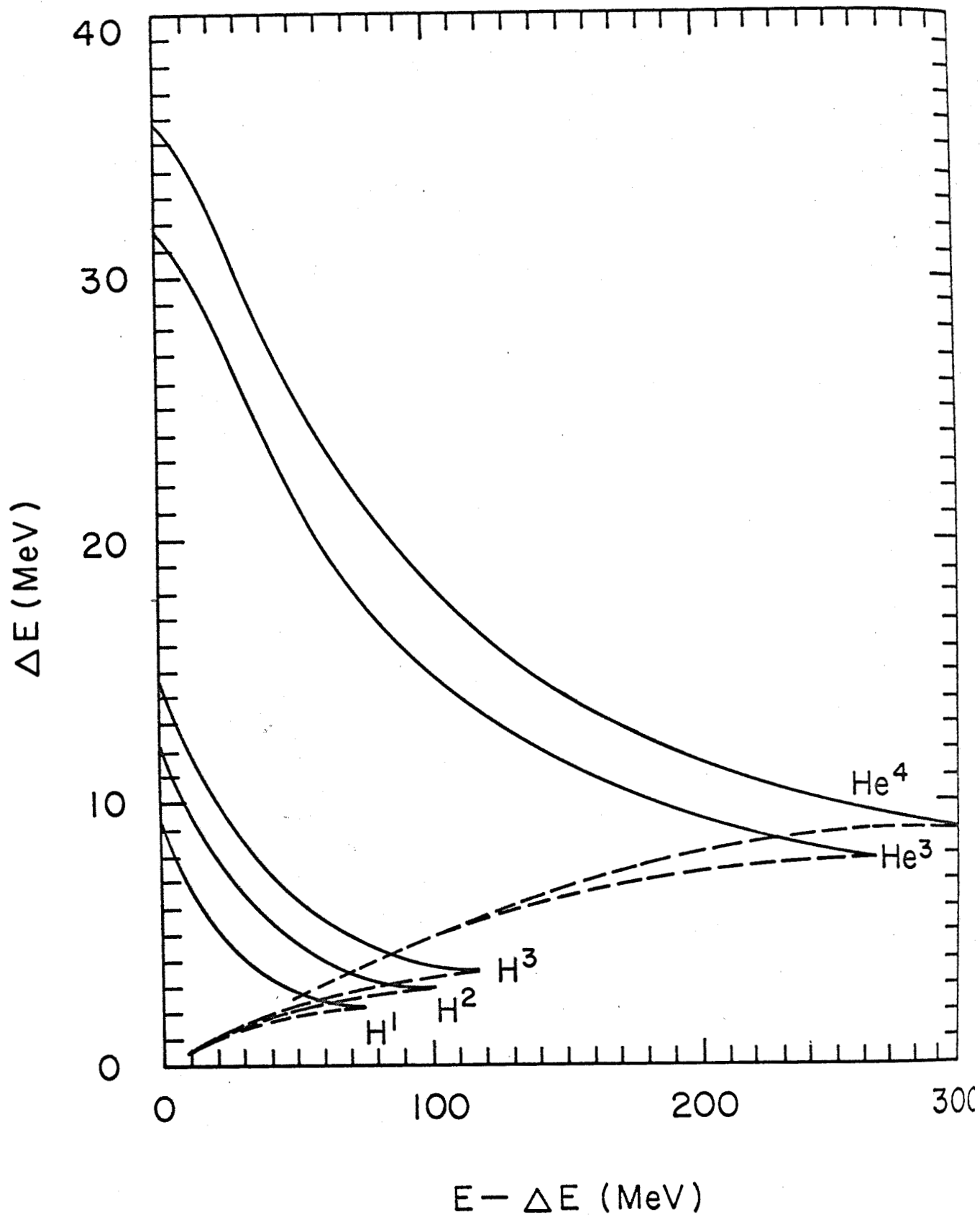
Figure 4. ΔE versus E - ΔE response curves for hydrogen and helium
isotopes for the scintillator telescope used on IMP-III
and IMP-IV.
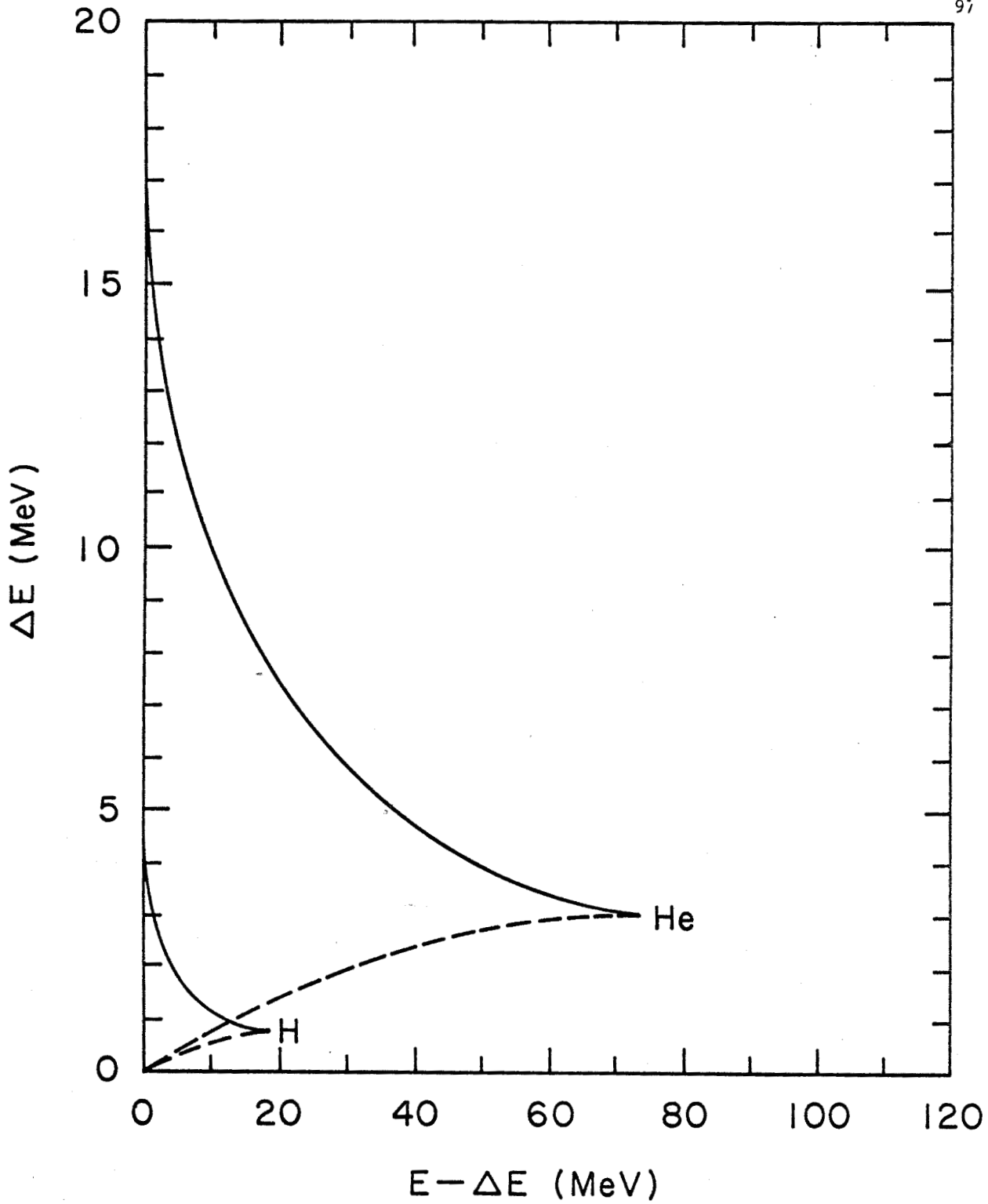
Figure 5. ΔE versus E - ΔE response curves for hydrogen and helium
for the solid state particle telescope on IMP-IV.
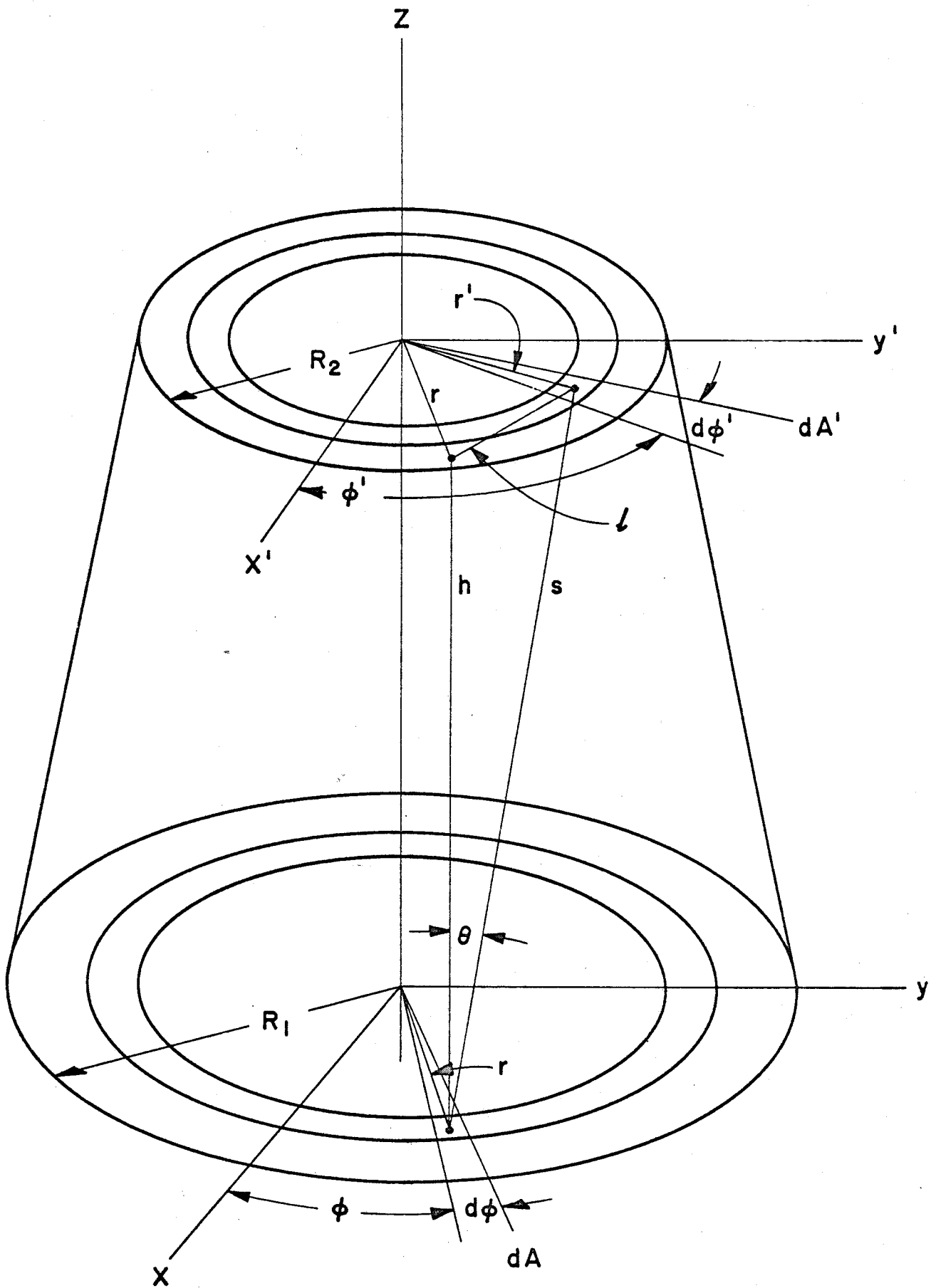
Figure 6. Schematic diagram of geometry of a generalized circular cylindrical telescope of height h and base radii of R_1 and R_2.

RTV SILICONE RUBBER (TYP. ALL TUBES)

E-ΔE SCINT. CsI(TI), 9 gm/cm²

POWER SUPPLY, PS-13/1 (3 REQ'D)

P.M. TUBE, R.C.A. C-7151 (3 REQ'D)

PLASTIC GUARD SCINT., 0.8 gm/cm²

PRE-AMP BOX
(———LINES FOR
APPROX. LOCATION)

ΔE SCINT. CsI(TI), 450 mg/cm²

AL ALLOY LIGHT BAFFLE, 25 mg/cm²

SOLID STATE LIGHT DIODES

AL ALLOY LIGHT BAFFLE, 27 mg/cm²

13.254 CM.

25.044 CM.
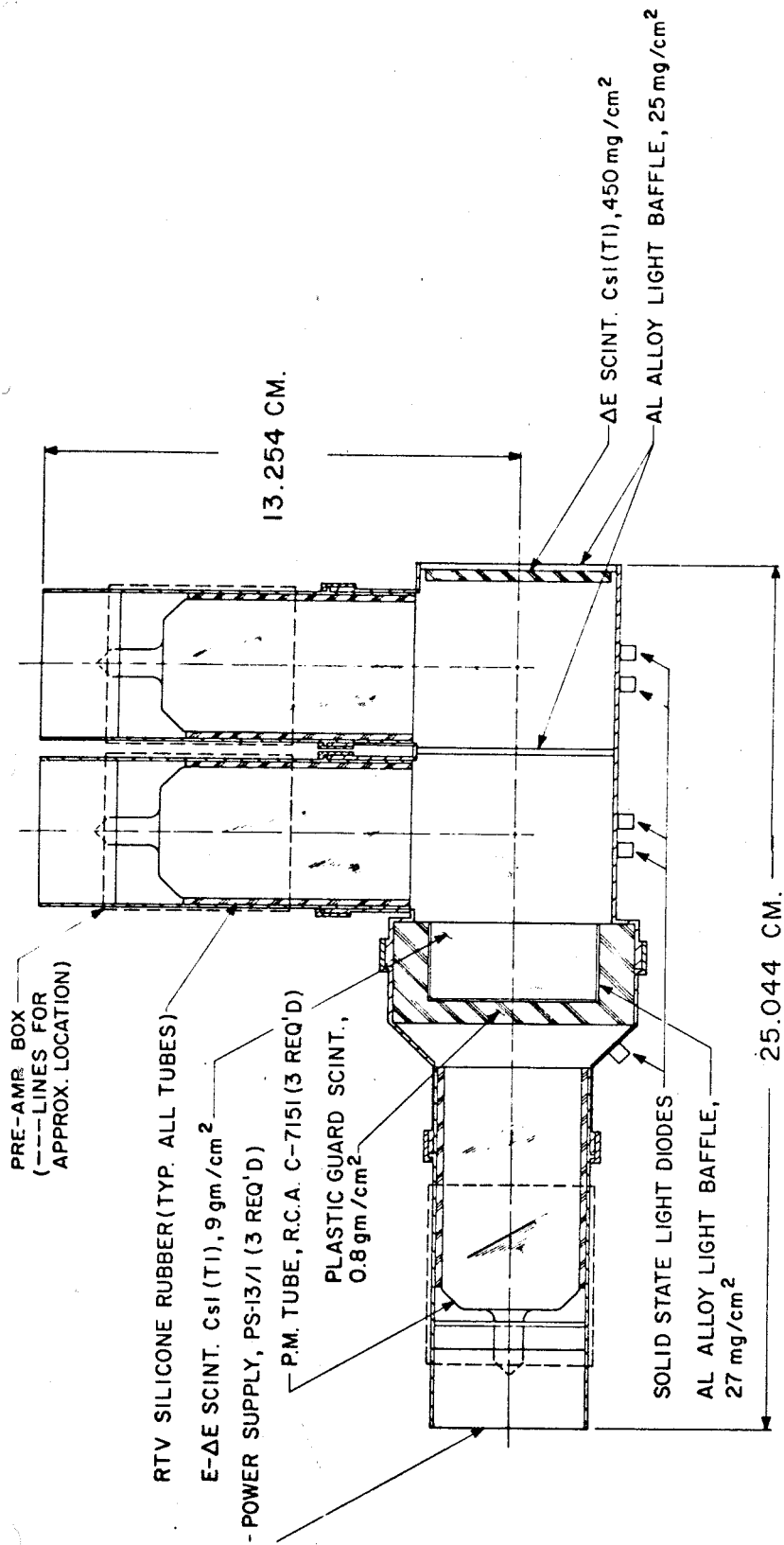
Figure 7. Schematic of IMP scintillator telescope assembly.
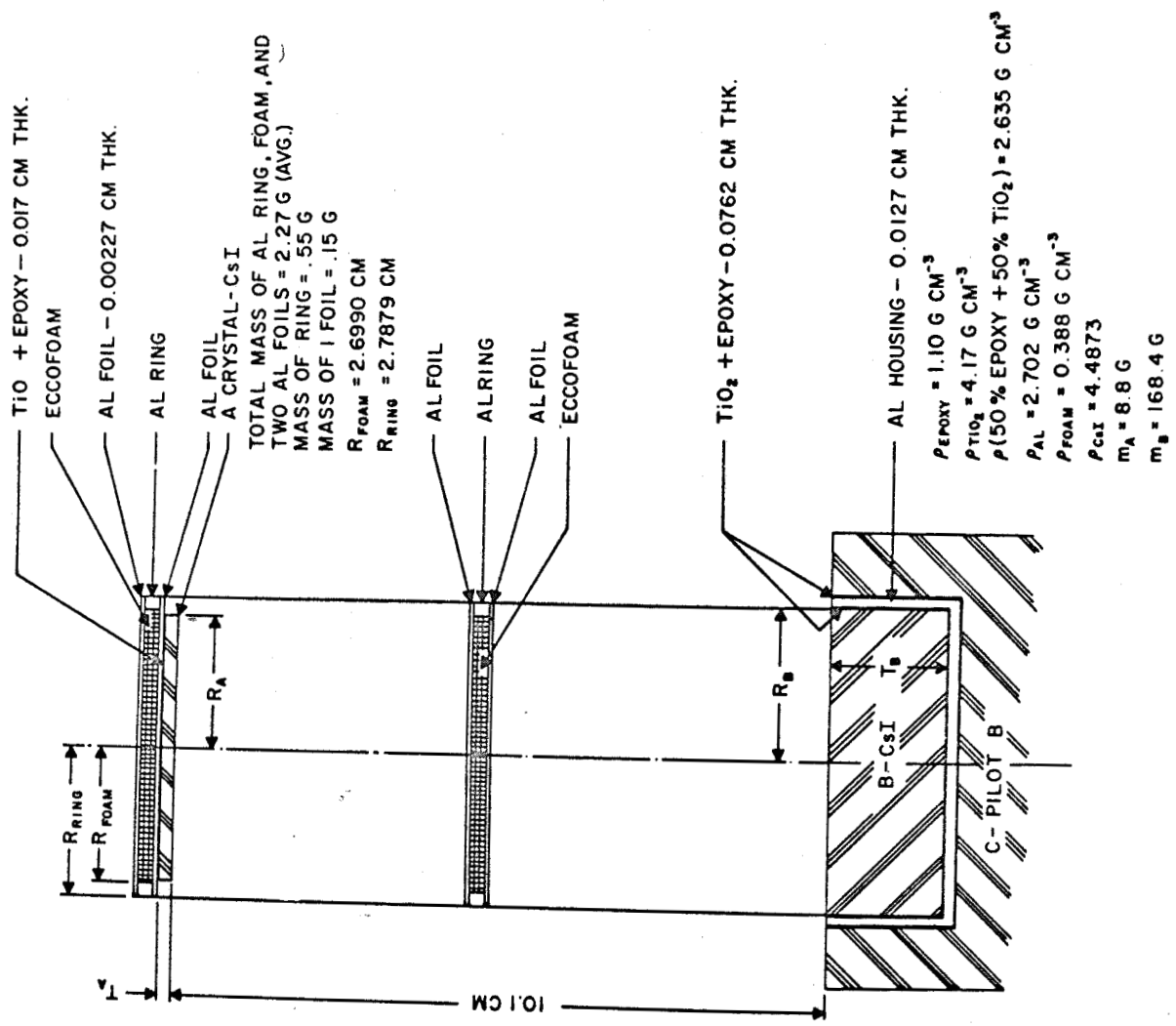
Figure 8. Schematic of IMP scintillator telescope showing critical dimensions and composition of layers.
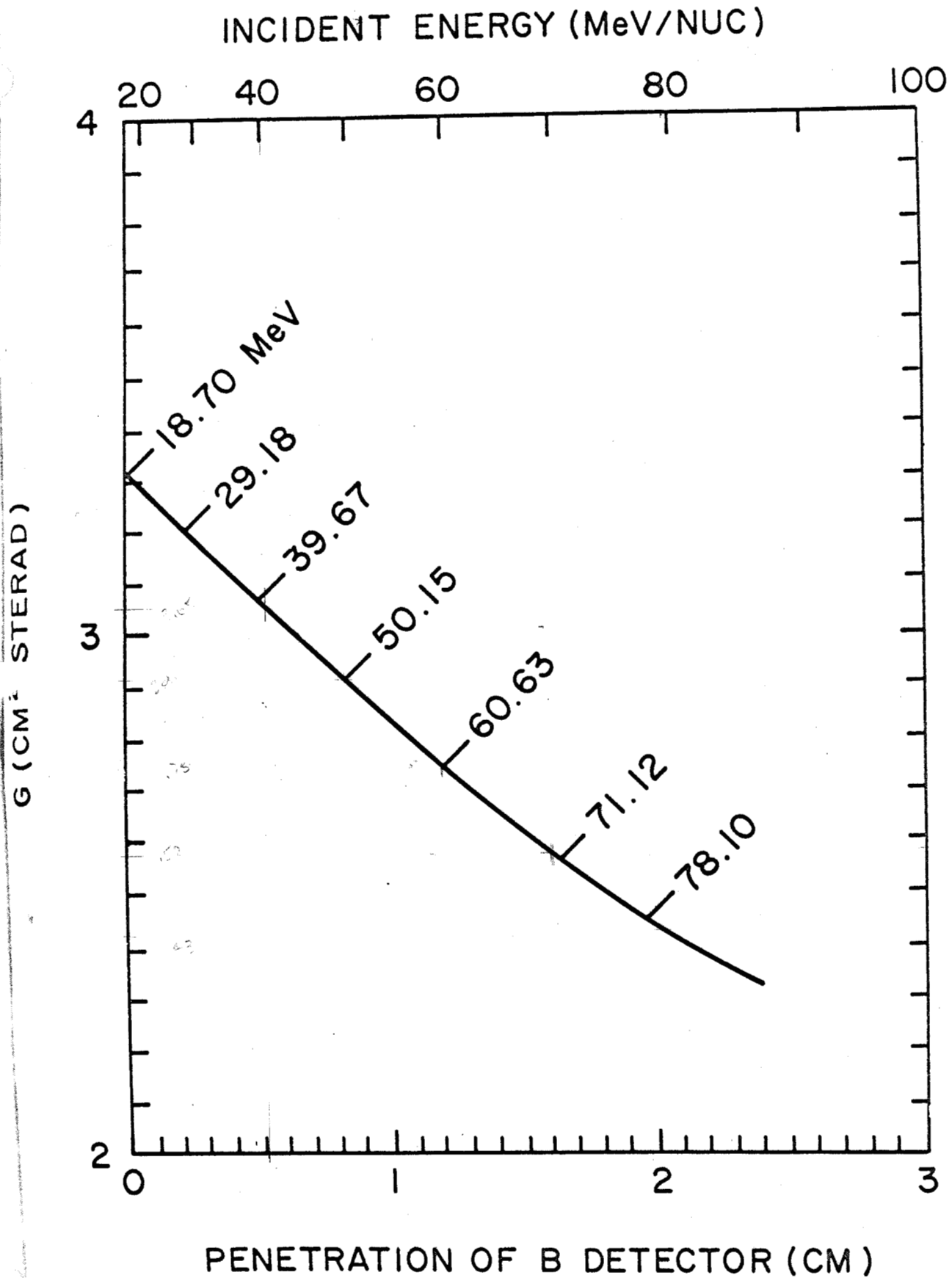
Figure 9. Geometry factor G versus penetration of particle into B
detector for IMP scintillator telescope.

END CAP (AL ALY)

COLLIMATOR (AL ALY)

LIGHT SHIELD (TITANIUM)

INSULATOR (TEFLON)

300 SQ. MM. RING MOUNTED
SURFACE BARRIER DETECTOR
150 MICRONS

INSERT (PILOT B PLASTIC
SCINTILLATOR)

DETECTOR HOUSING (AL ALY)

WASHER (SILICONE RUBBER)
(2 REQUIRED)

300 SQ. MM. RING MOUNTED
SURFACE BARRIER DETECTOR
(I MM THICK, 2 REQUIRED)

WASHER (COPPER, 5 REQUIRED)

END PLUG (PILOT B PLASTIC
SCINTILLATOR)

PHOTOMULTIPLIER TUBE
(RCA #C-7151)

RETAINING RING (AL ALY)

RTV SILICONE RUBBER

TUBE HOUSING (AL ALY)

GEOMETRY FACTOR 5 CM^2–SR

FILTER CIRCUITRY (PC BOARD)

POWER SUPPLY, PS–15/I

17.526 CM.

Figure 10. Schematic of IMP-IV solid state detector telescope assembly.

.0146 CM. Si (A CRYSTAL)

.00004 G CM^{-2} Au (TOP)
.00004 G CM^{-2} Al (BOTTOM)

R = 0.9525 CM

.00004 G CM^{-2} Au (EACH SURFACE)

0.1000 CM. Si (B₁ CRYSTAL)

0.0984 CM Si (B CRYSTAL)

.00004 G CM^{-2} Al EACH SURFACE

R

3.132 CM

.399 CM
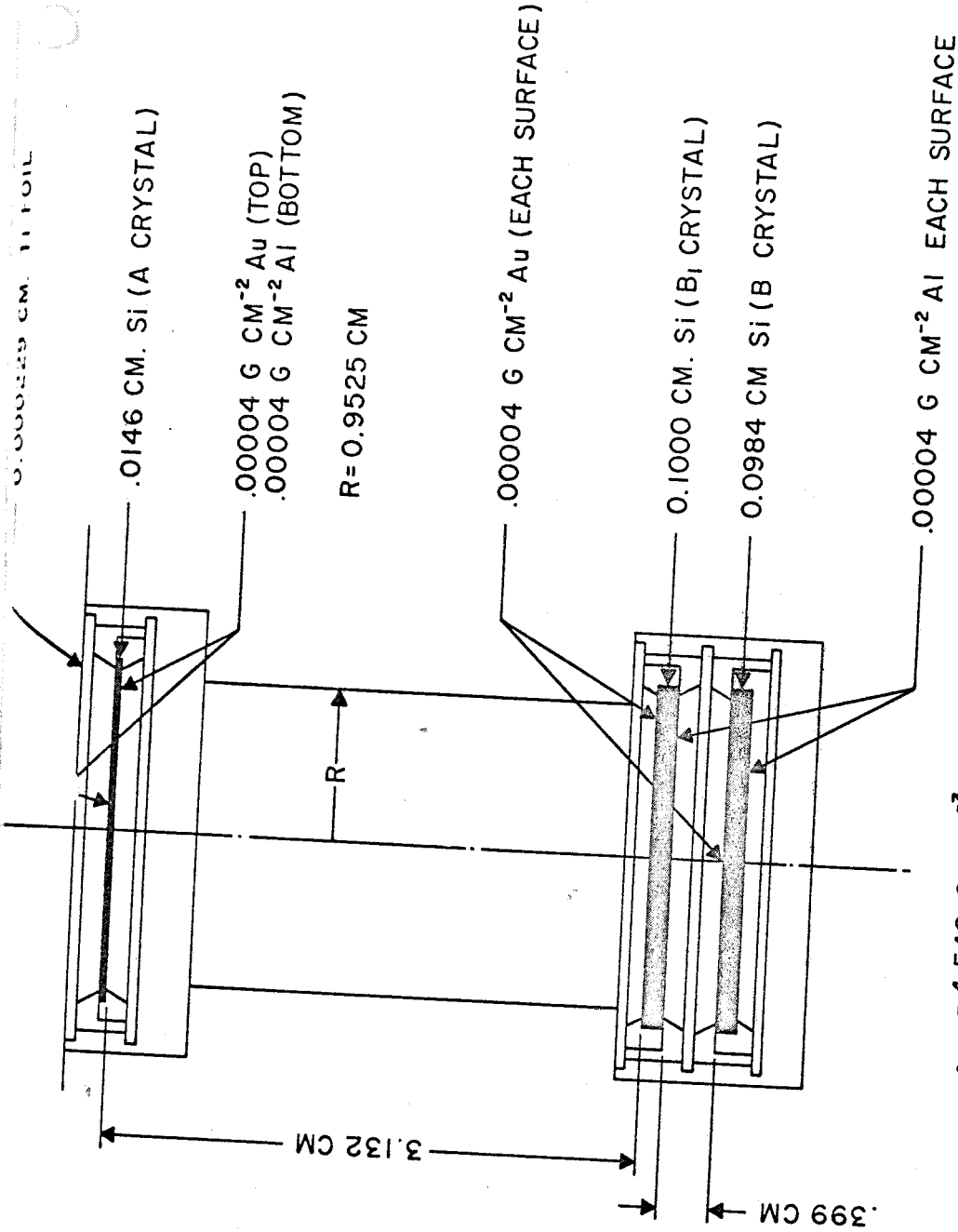
ρ_{Ti} = 4.540 G CM^{-3}
ρ_{Au} = 19.320 G CM^{-3}
ρ_{Al} = 2.702 G CM^{-3}
ρ_{Si} = 2.330 G CM^{-3}

Figure 11. Schematic of IMP-IV solid state detector telescope showing critical dimensions and composition of layers.
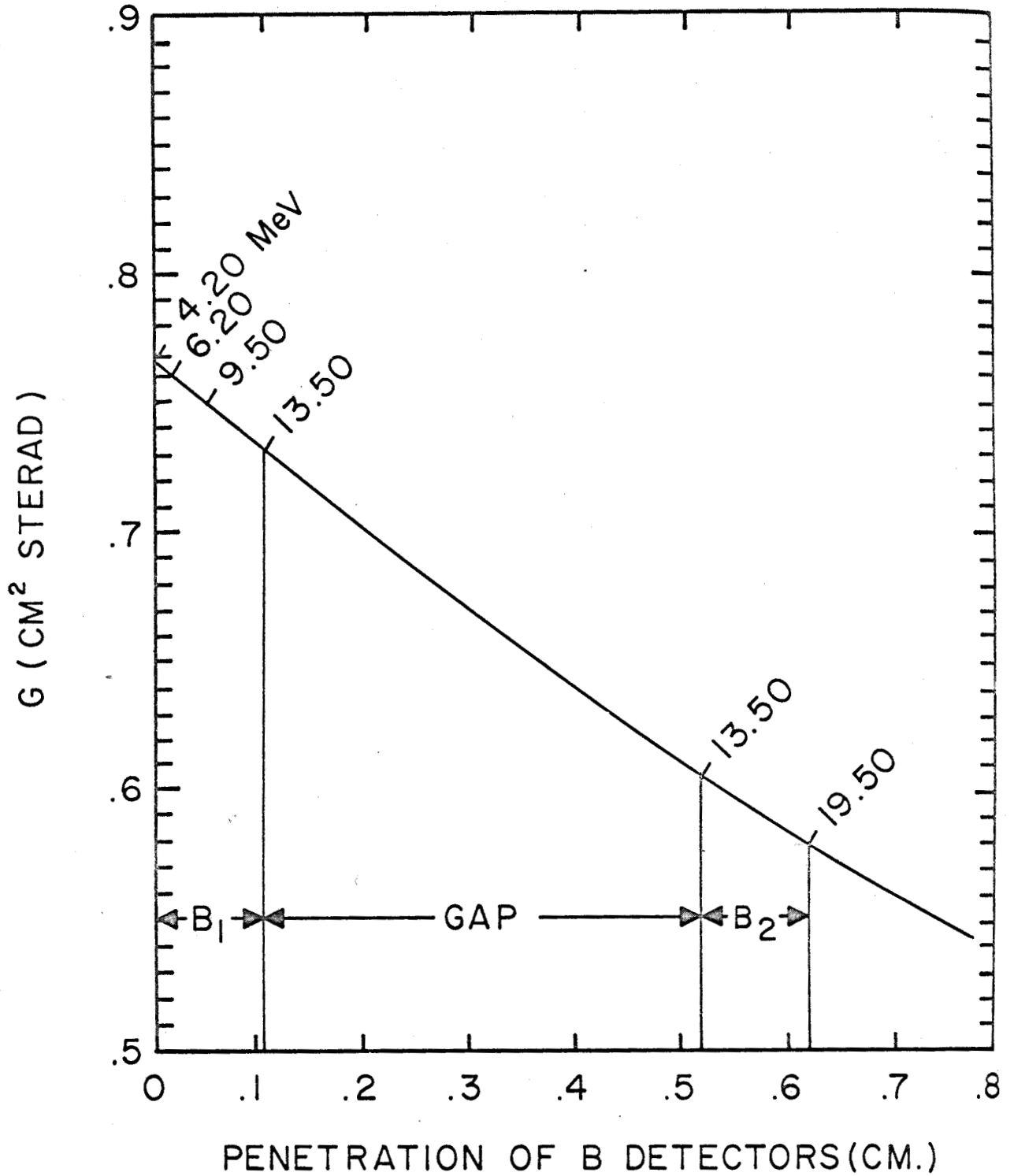
Figure 12. Geometry factor G versus penetration of particle into B
detector for IMP-IV solid state detector telescope.
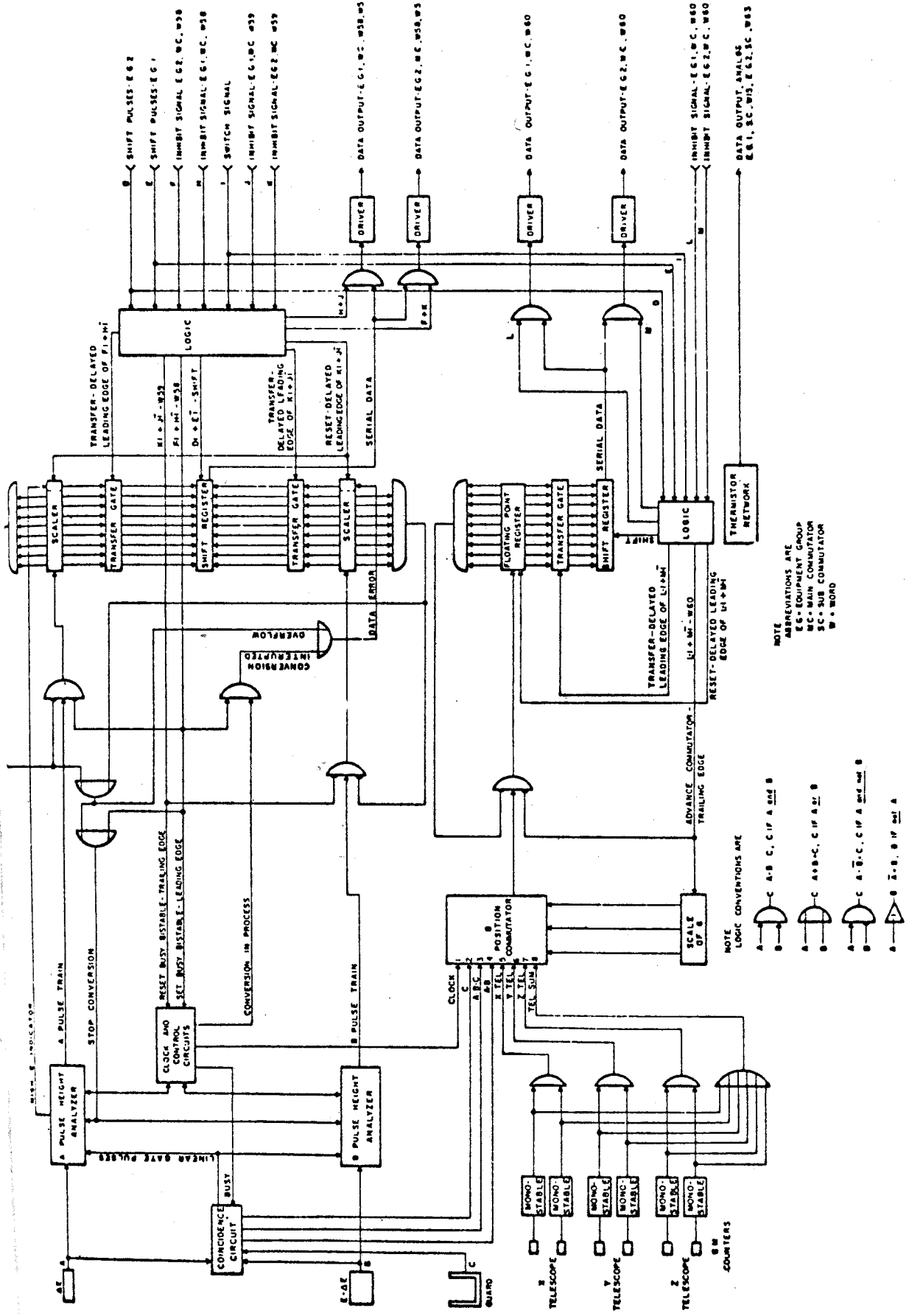
Figure 13. Block diagram of IMP-III cosmic ray experiment electronics.

Figure 14. Block diagram of IMP-IV cosmic ray experiment electronics.
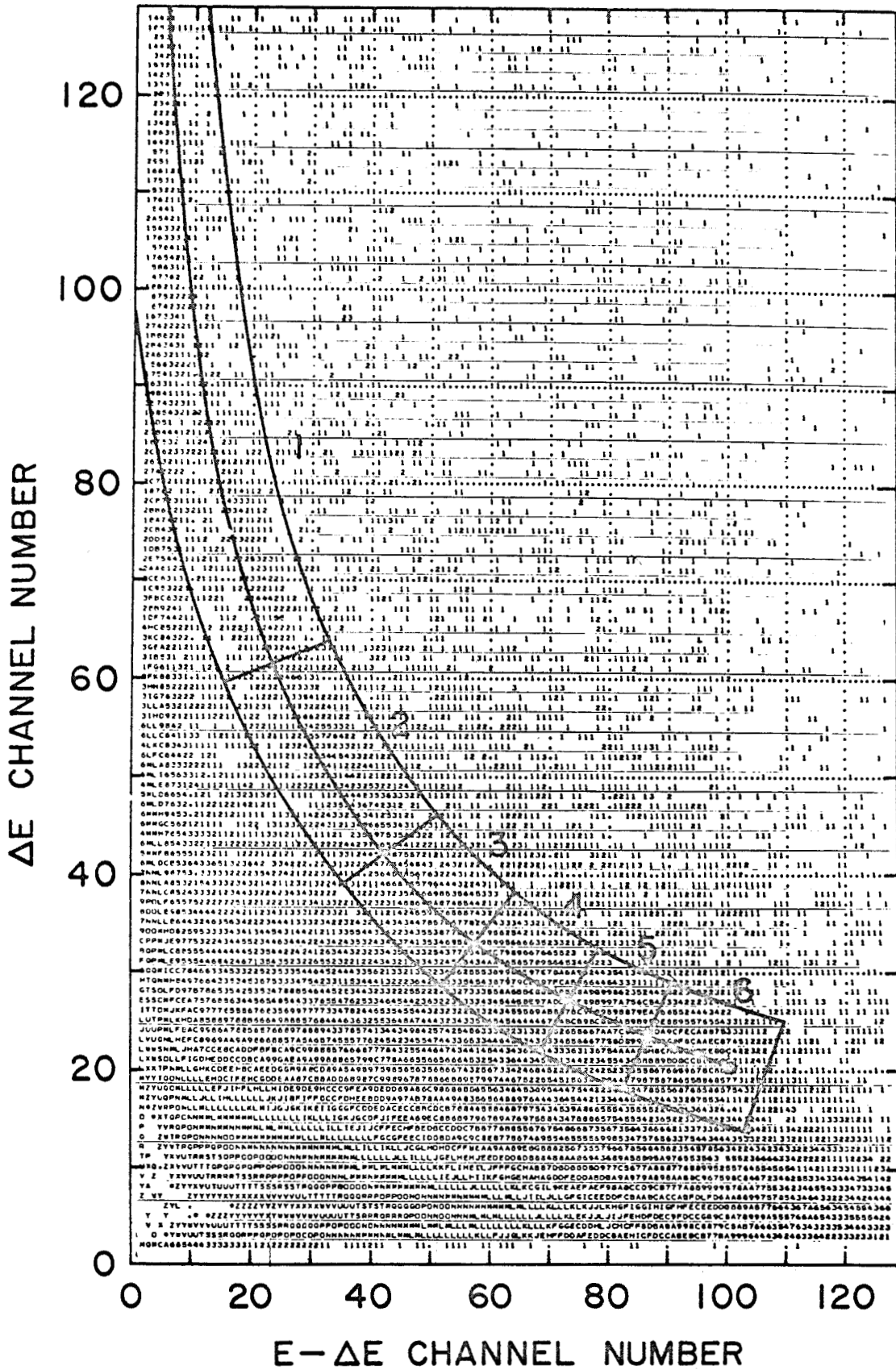
Figure 15. IMP-III ΔE versus E - ΔE matrix showing proton line and
six energy bins: (1) 18.7 - 29.2, (2) 29.2 - 39.7,
(3) 39.7 - 50.2, (4) 50.2 - 60.6, (5) 60.6 - 71.1,
and (6) 71.1 - 81.7 MeV.
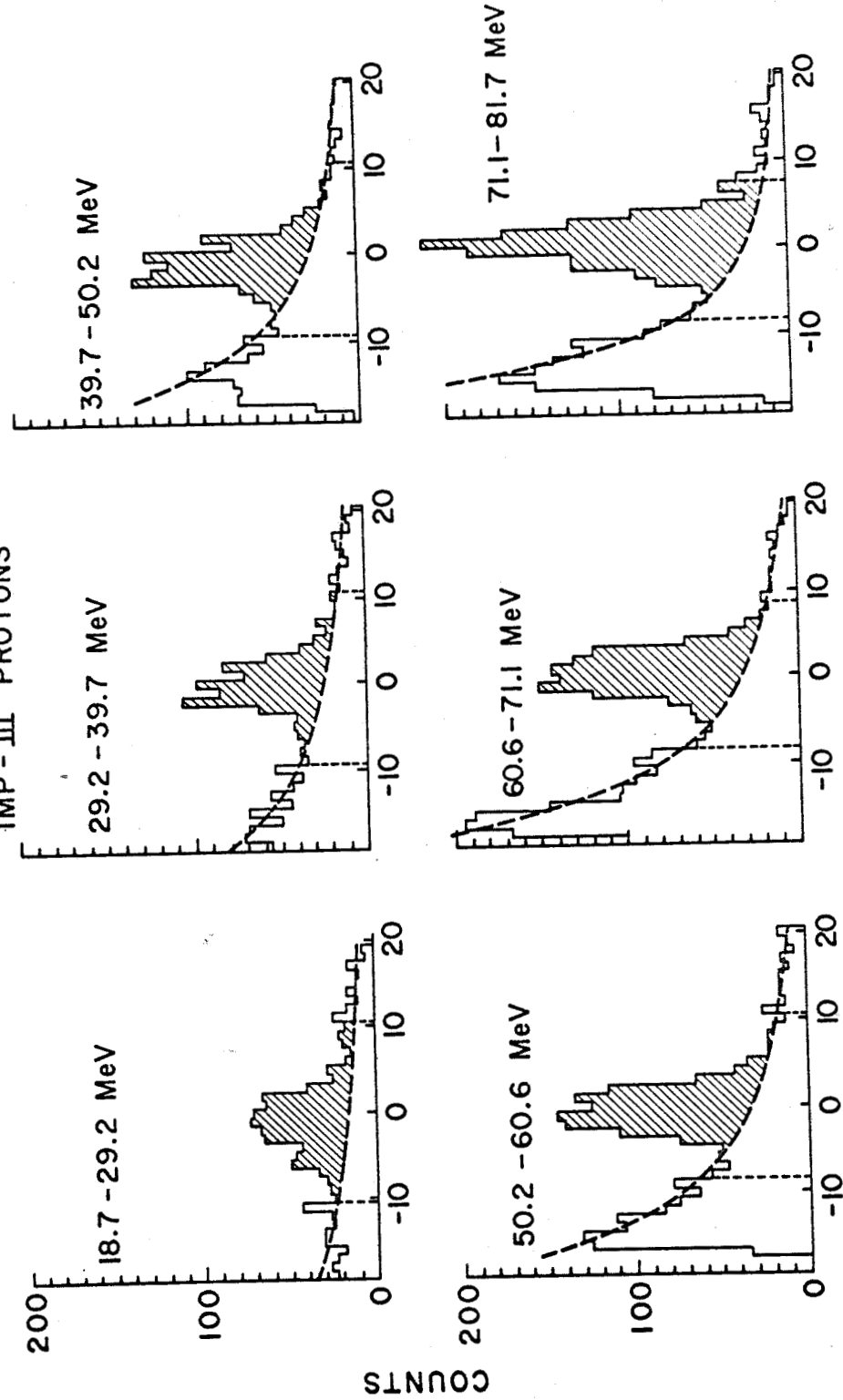
Figure 16. Proton ΔE versus E - ΔE histograms. Region under the dashed curve represents the background component. The shaded area represents the true proton component.
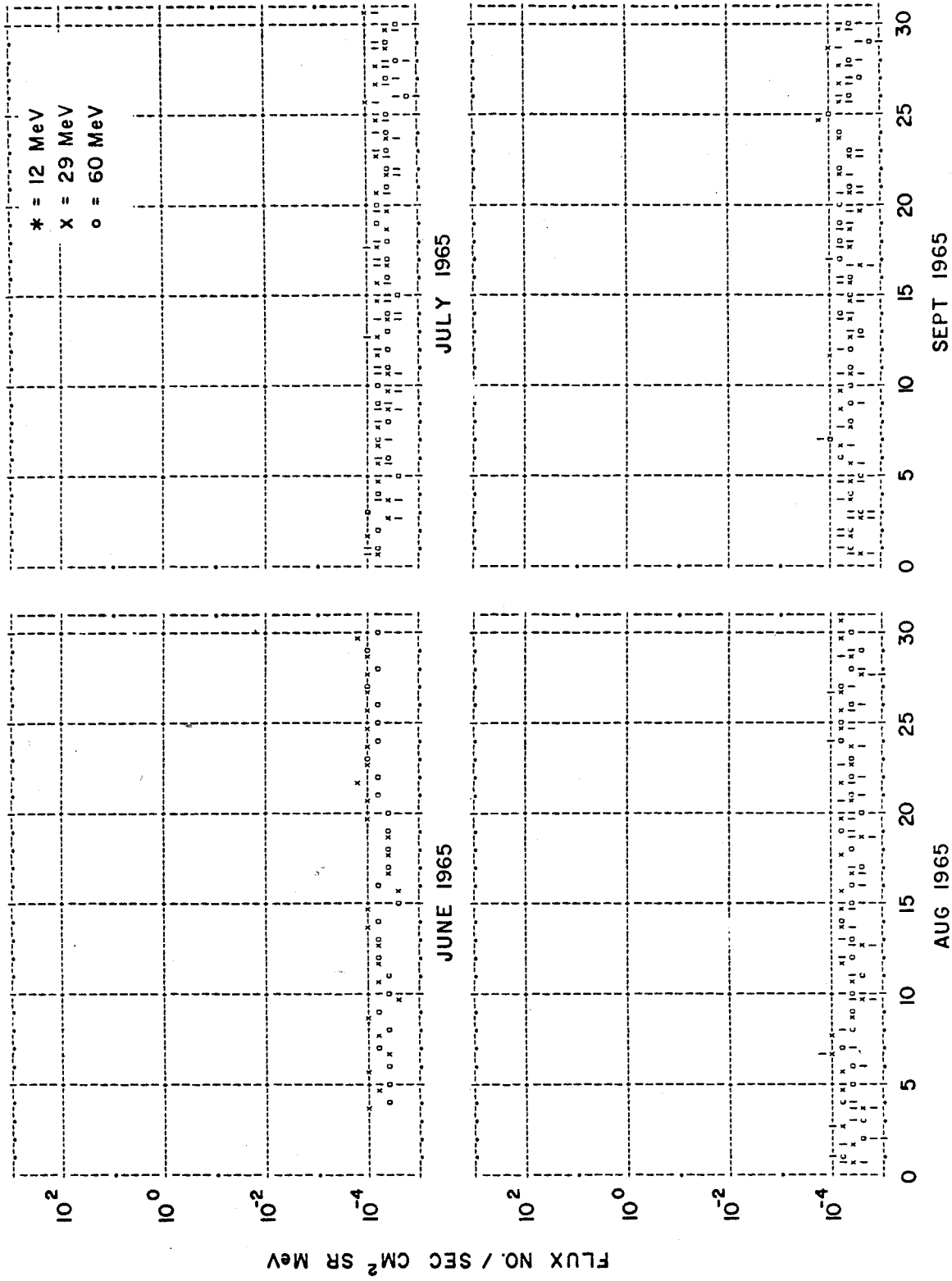
Figure 17(a). 24 hour average proton fluxes.
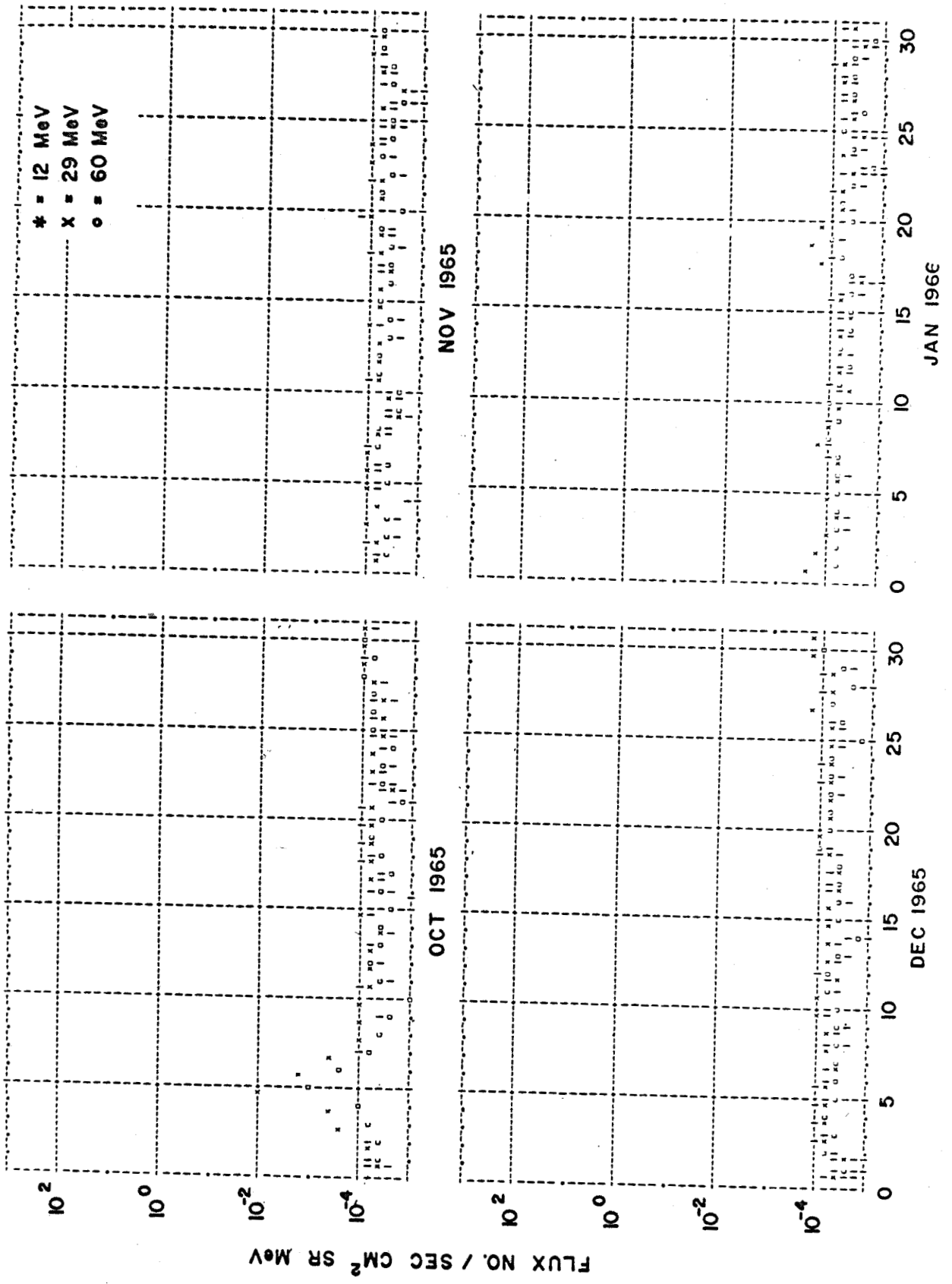
Figure 17(b). 24 hour average proton fluxes.

* = 12 MeV
X = 29 MeV
o = 60 MeV

MAR 1966

FEB 1966

MAY 1966

APR 1966

FLUX NO. / SEC CM^2 SR MeV

10^2 10^0 10^{-2} 10^{-4}
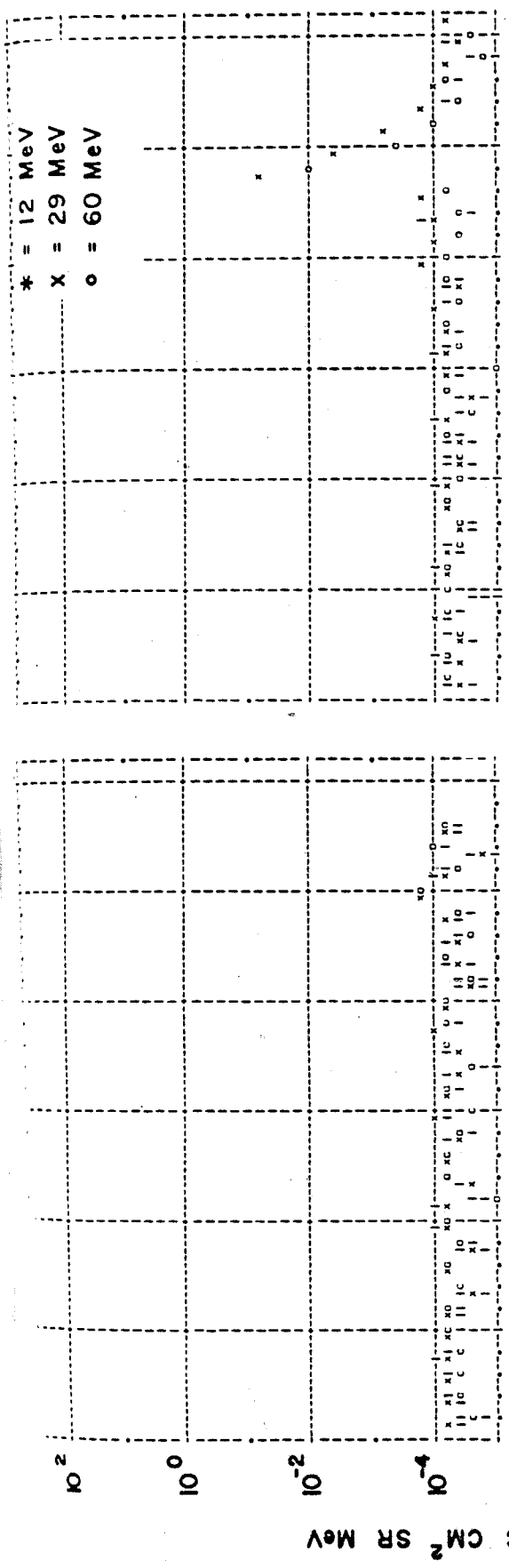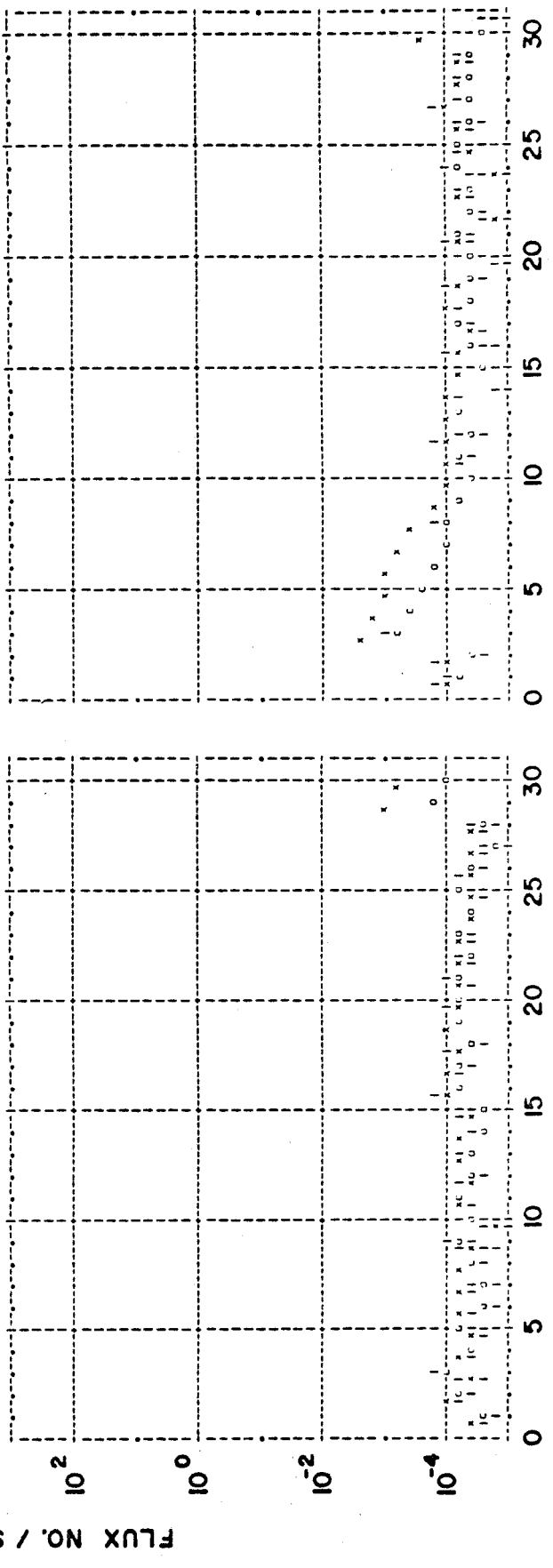
Figure 17(c). 24 hour average proton fluxes.

Figure 17(c). 24 hour average proton fluxes.
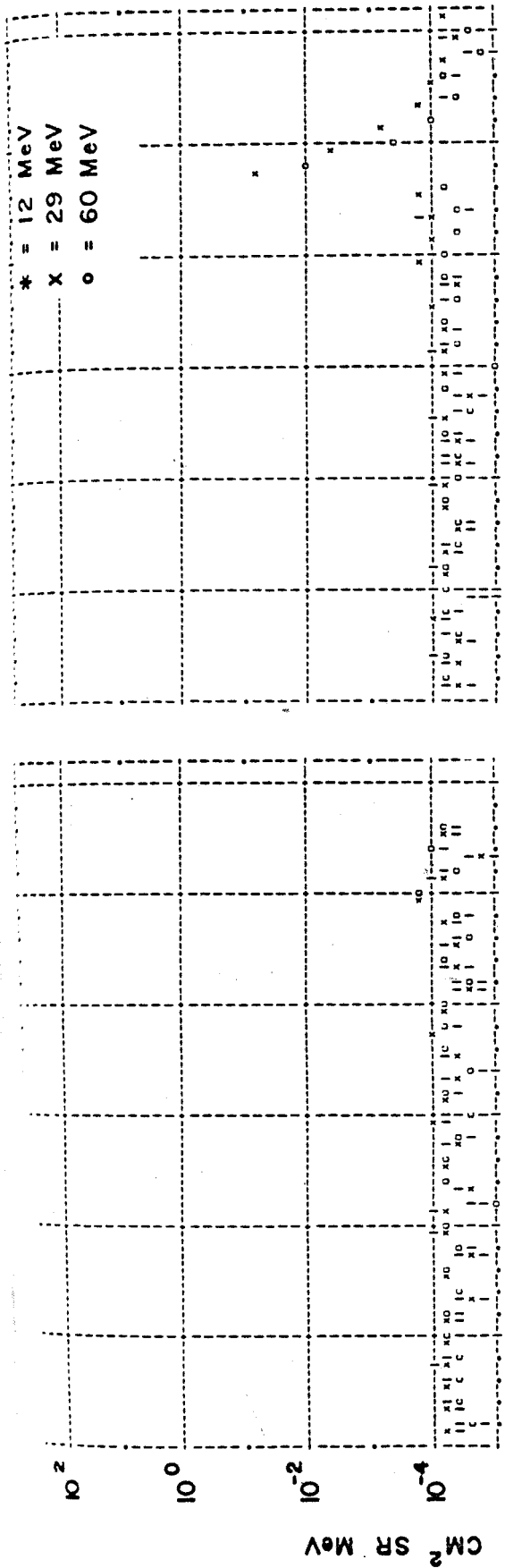
MAR 1966

MAY 1966

FEB 1966

APR 1966

* = 12 MeV
x = 29 MeV
o = 60 MeV

FLUX NO. / SEC CM² SR MeV
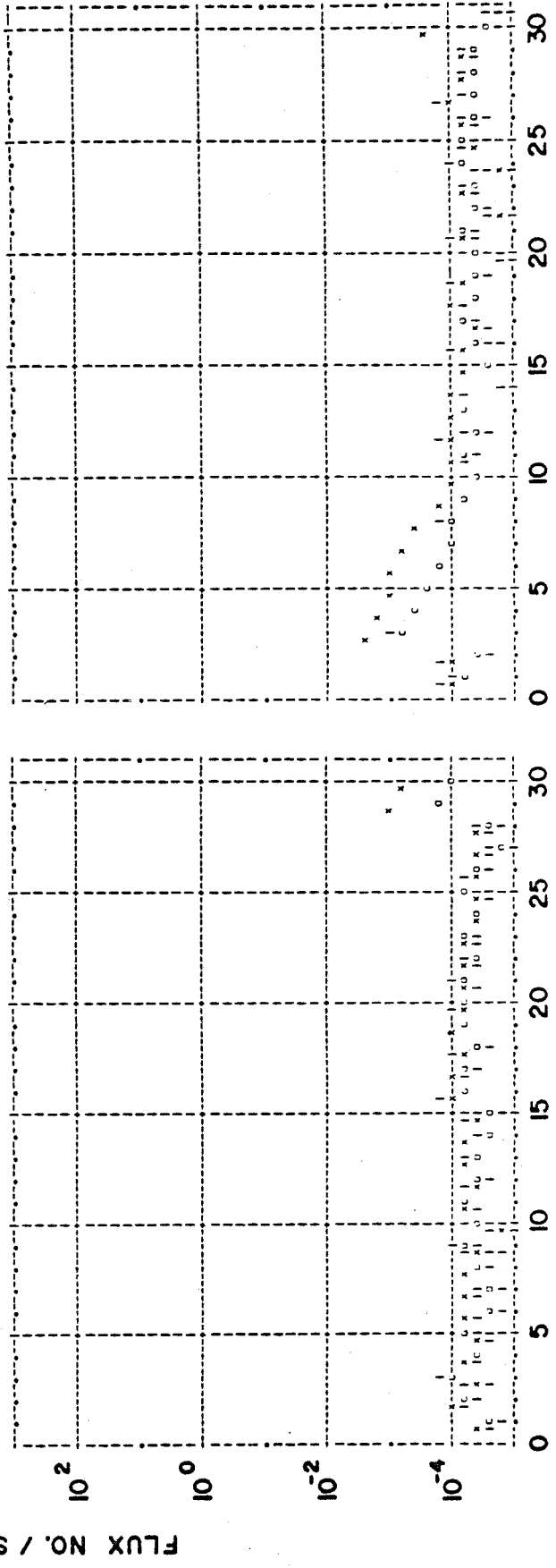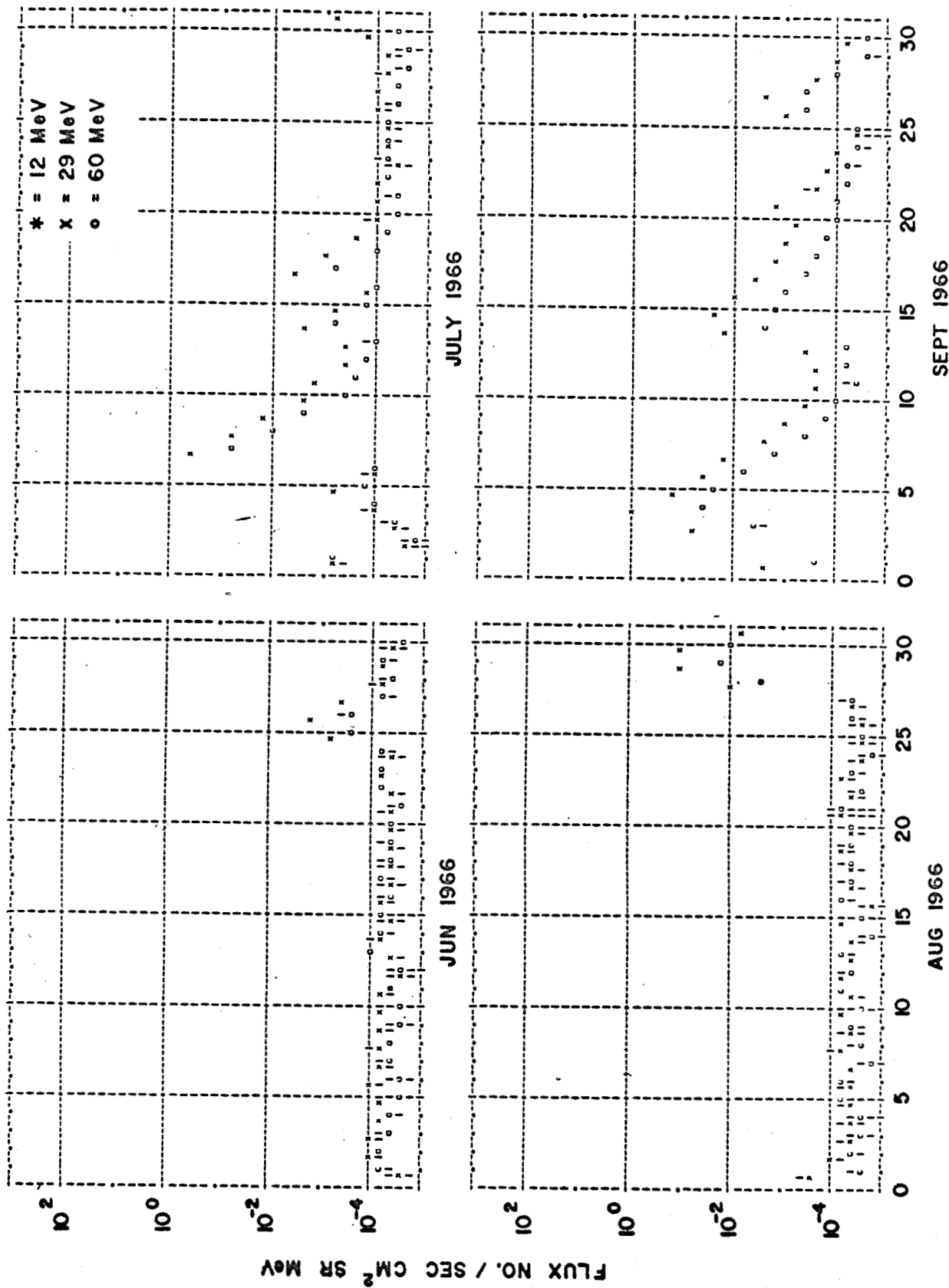
Figure 17(d). 24 hour average proton fluxes.
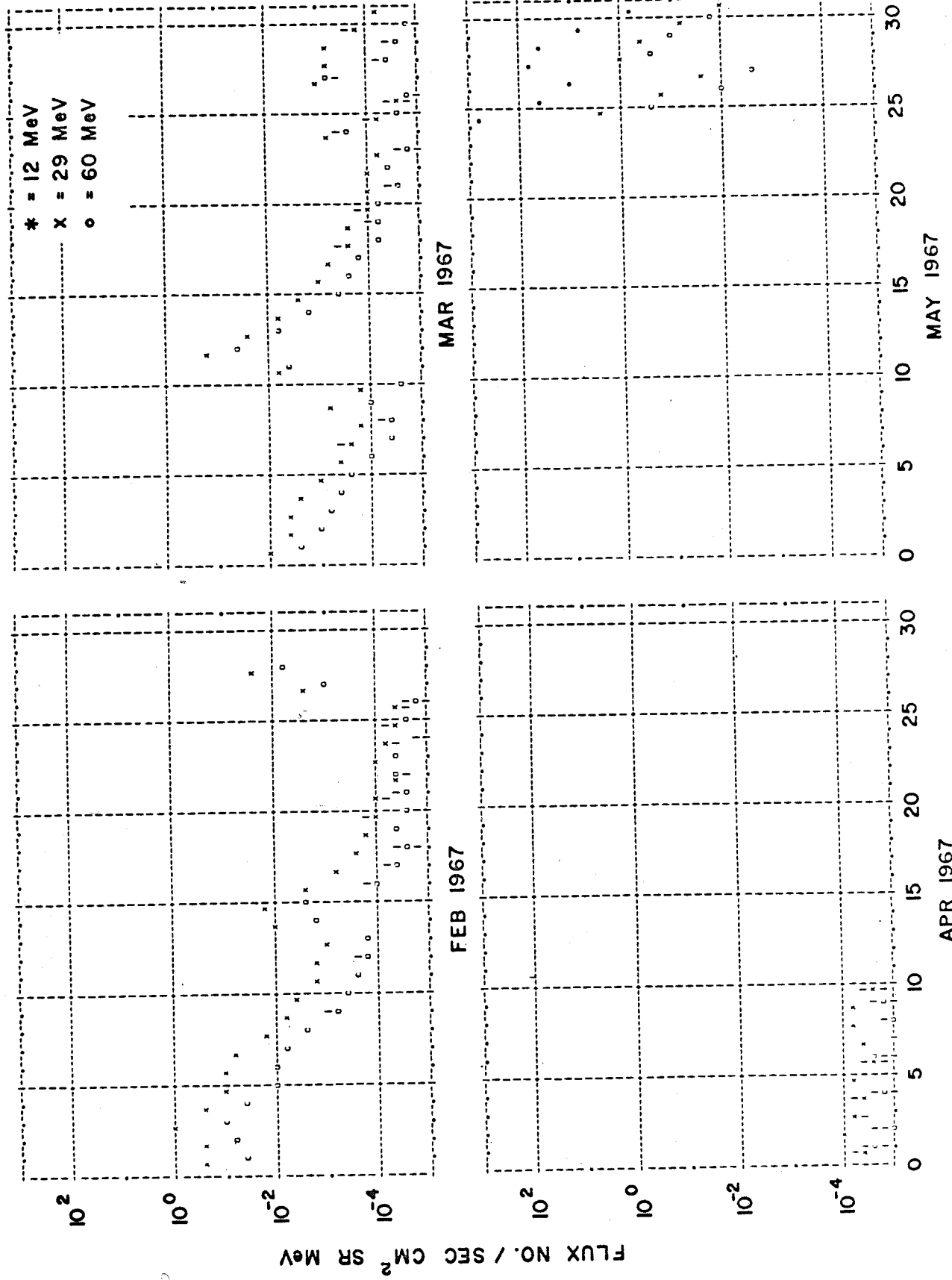
Figure 17(f). 24 hour average proton fluxes.

Figure 17(f). 24 hour average proton fluxes.

* = 12 MeV
X = 29 MeV
o = 60 MeV

JULY 1967

SEPT 1967
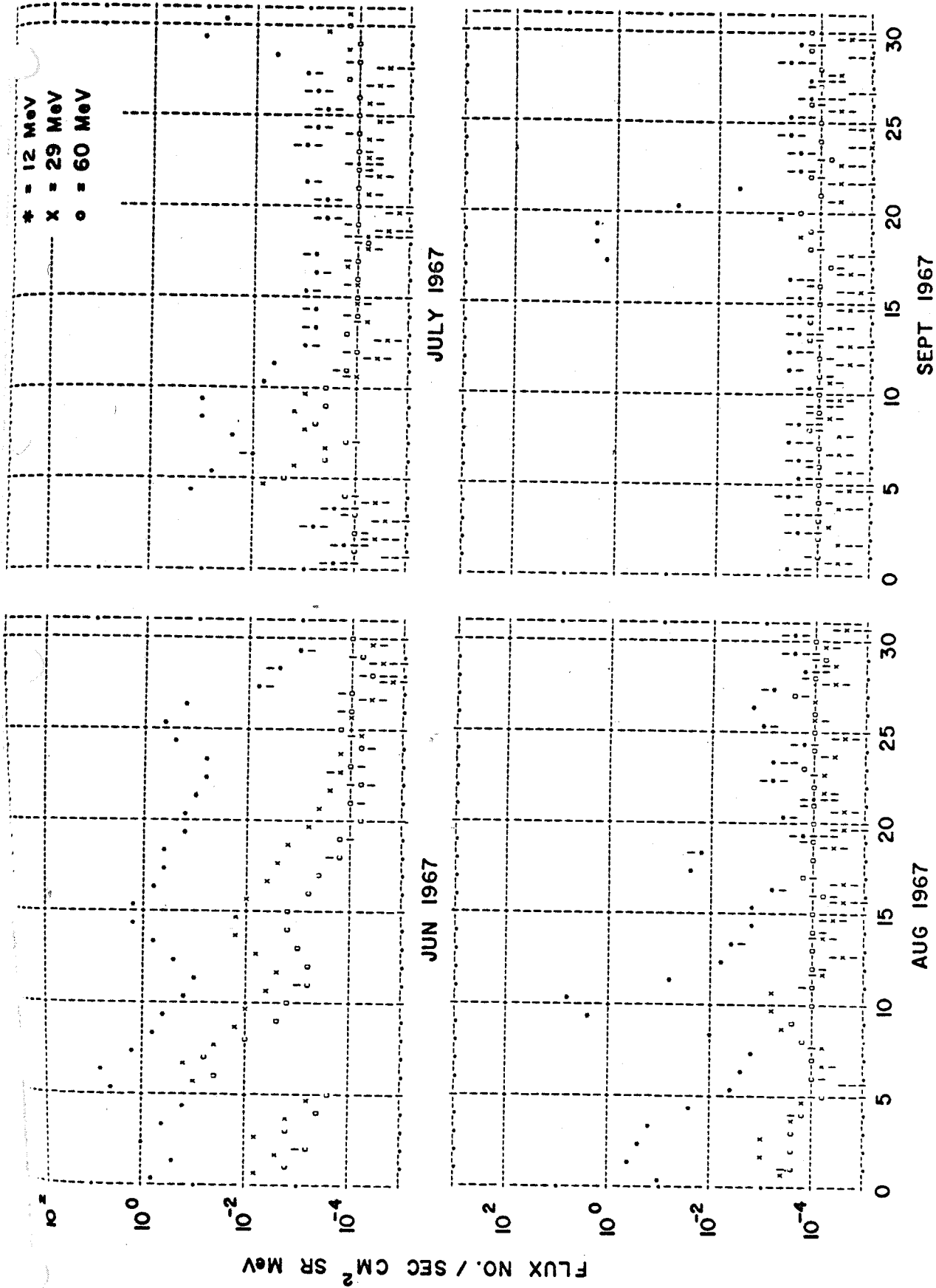
JUN 1967

AUG 1967

Figure 17(g). 24 hour average proton fluxes.

FLUX NO. / SEC CM² SR MeV
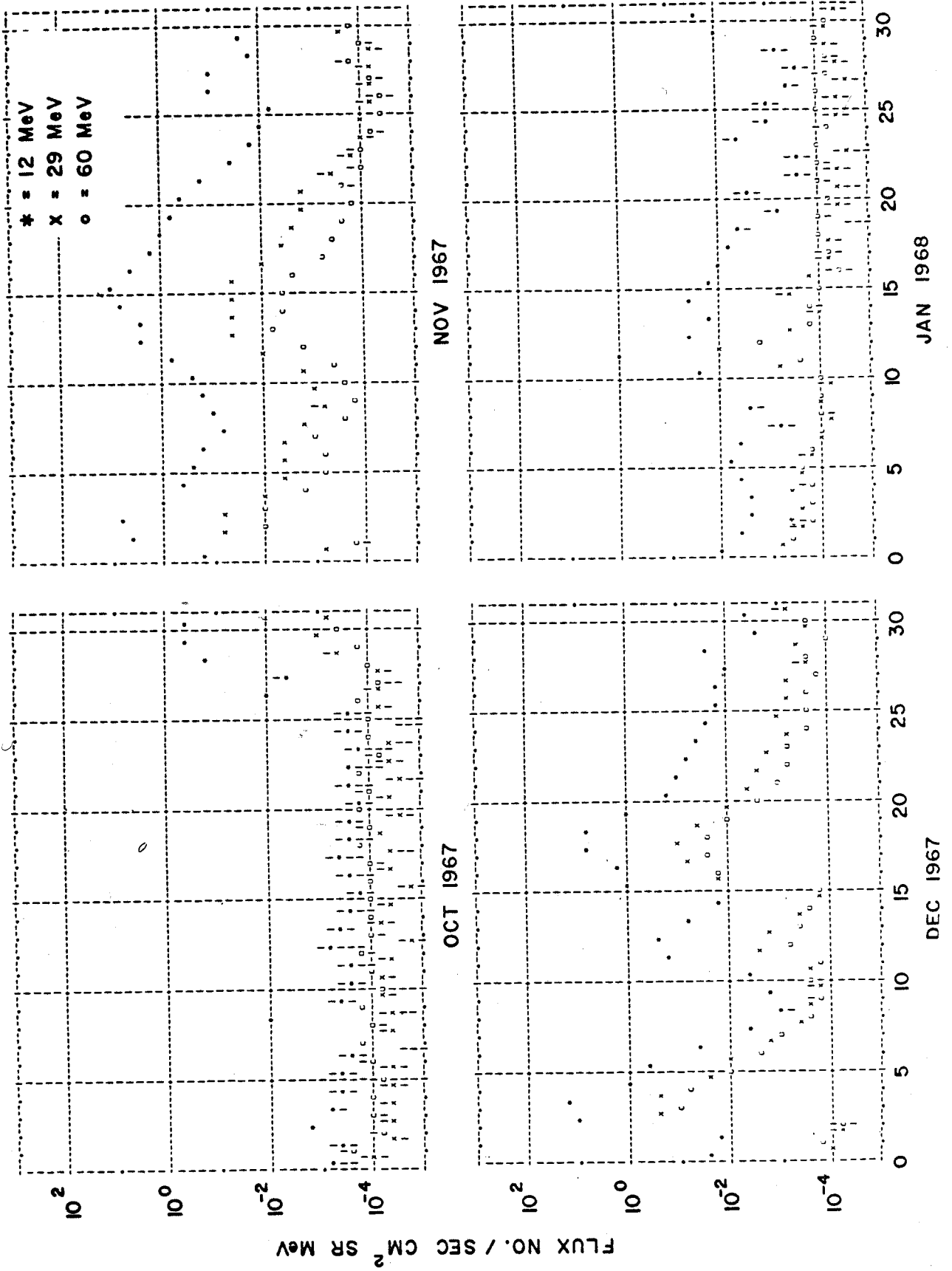
Figure 17(h). 24 hour average proton fluxes.

Figure 17(h). 24 hour average proton ~~~~
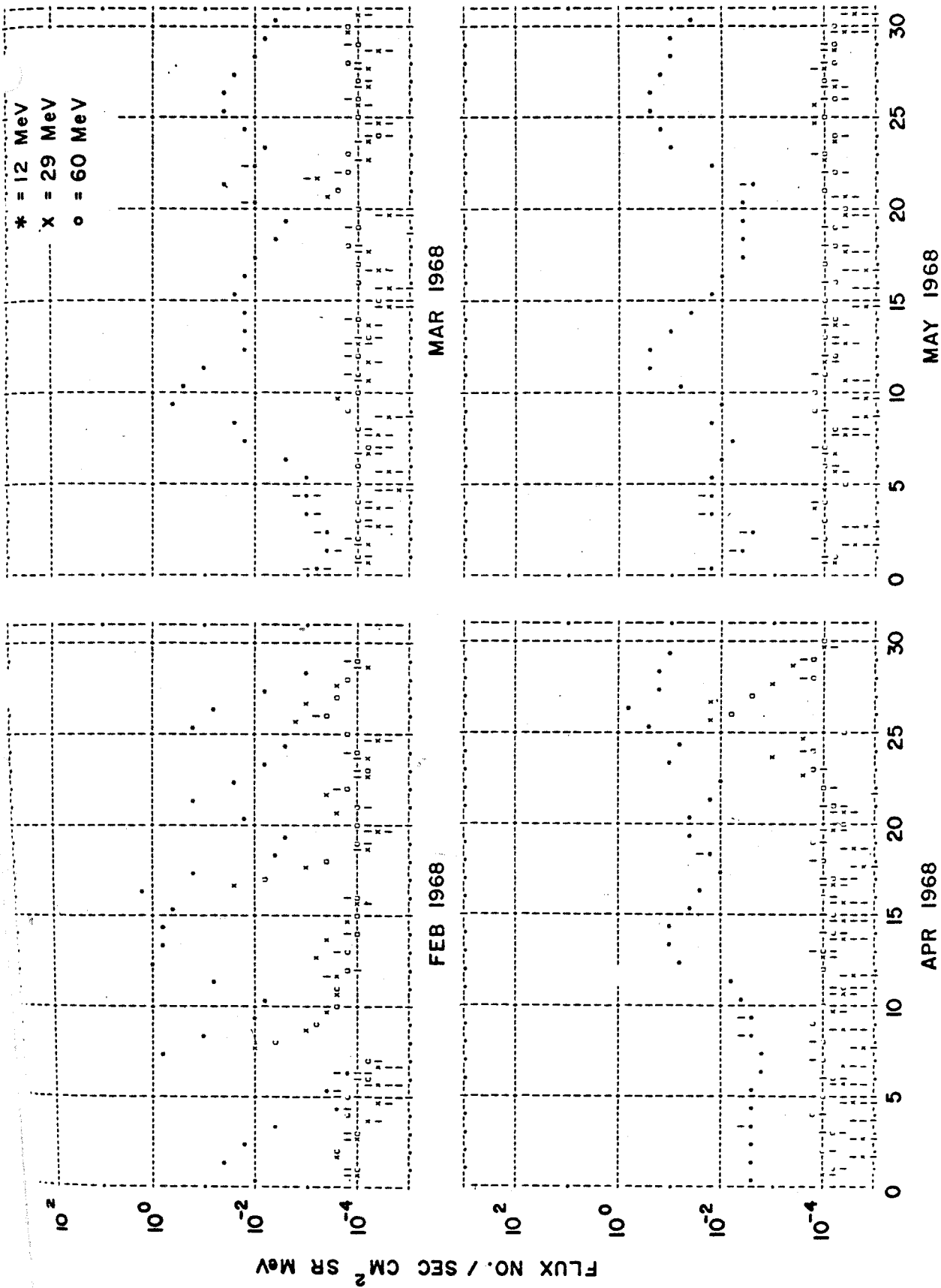
Figure 17(i). 24 hour average proton fluxes.

* = 12 MeV
x = 29 MeV
o = 60 MeV

MAR 1968

MAY 1968

FEB 1968

APR 1968

FLUX NO. / SEC CM^2 SR MeV
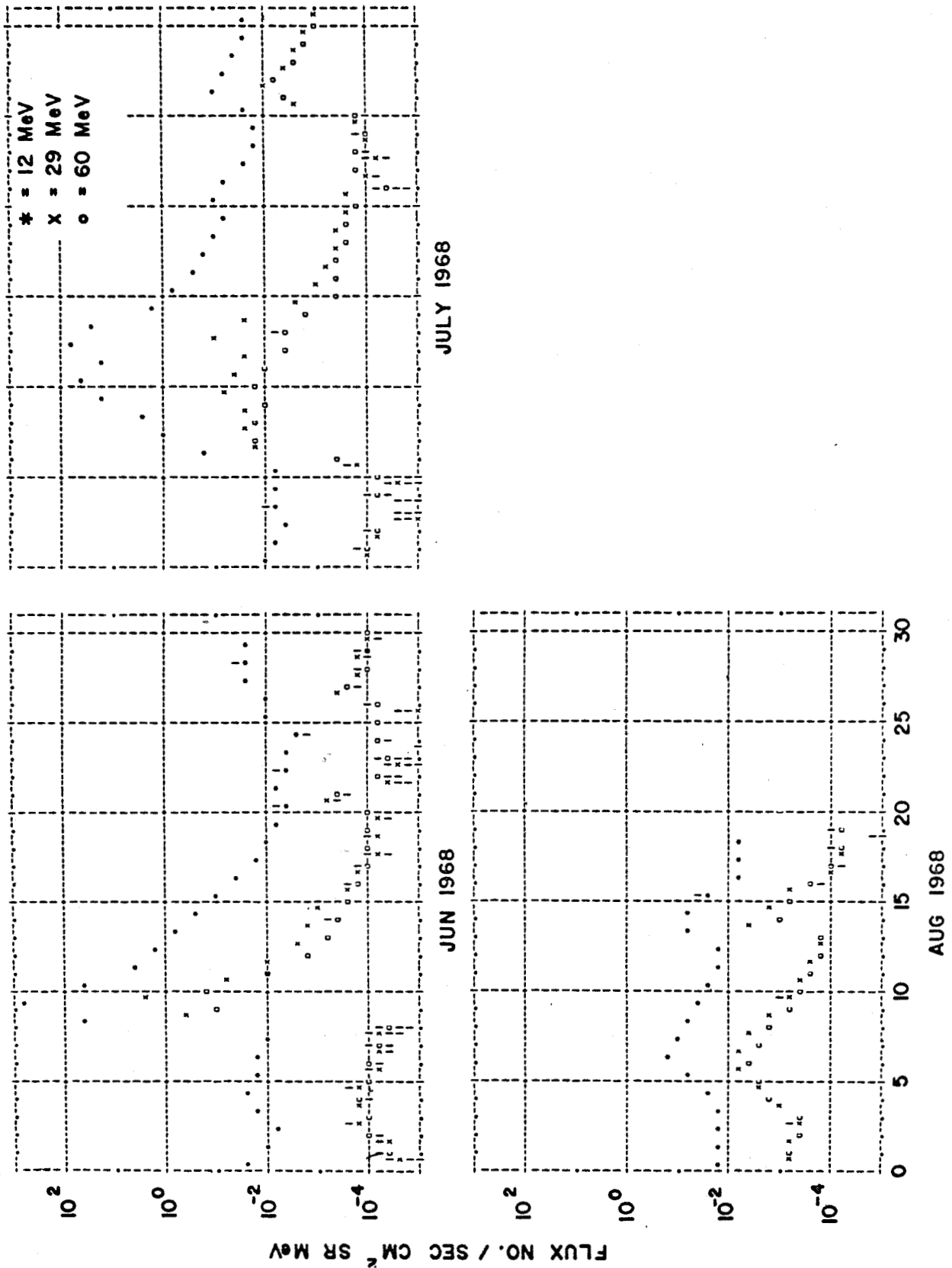
Figure 17(j). 24 hour average proton fluxes.

Figure 17(j). 24 hour average proton fluxes.
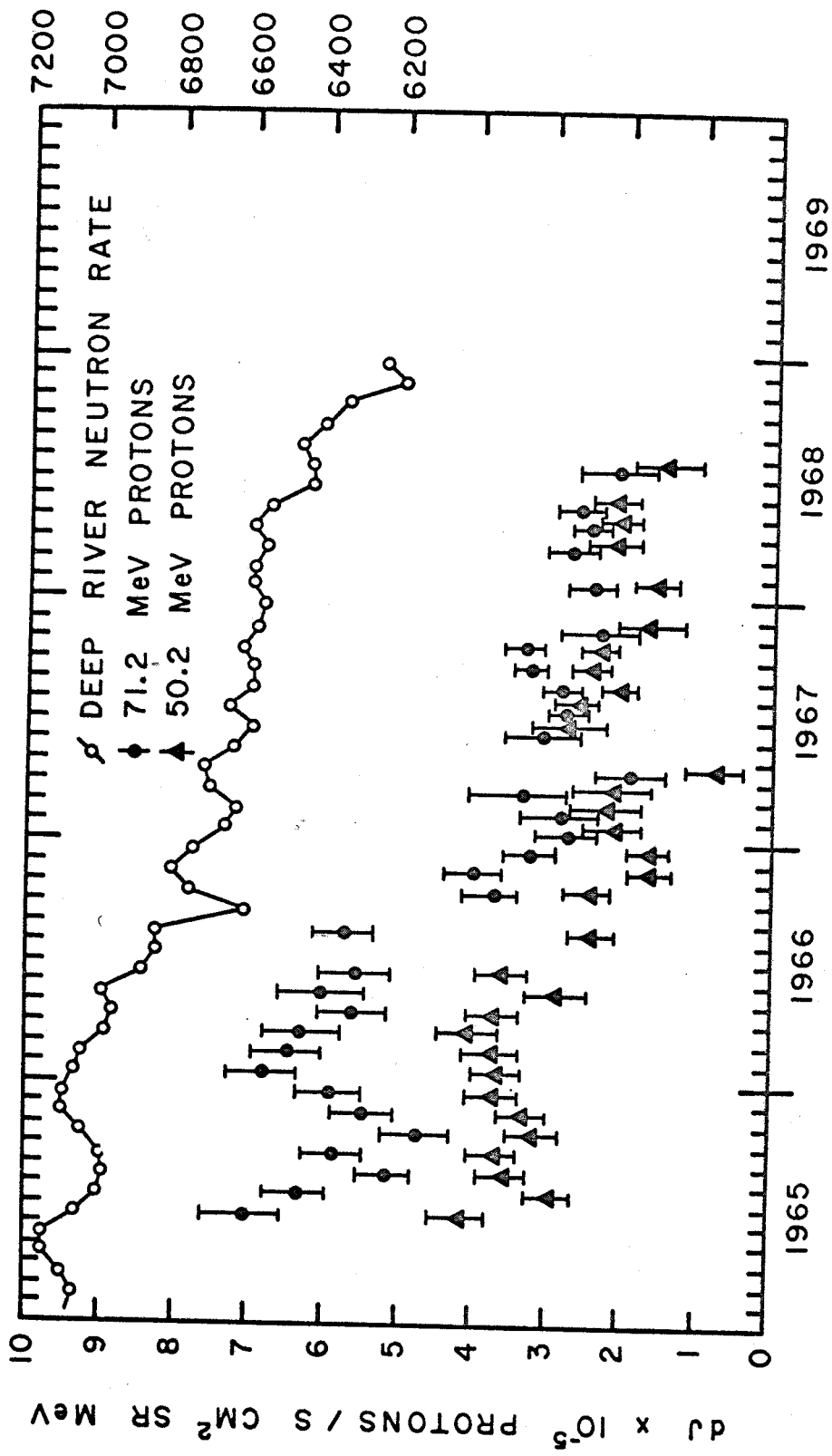
Figure 18. IMP-III and IMP-IV monthly averages of proton fluxes and monthly averages of the Deep River hourly neutron rate.
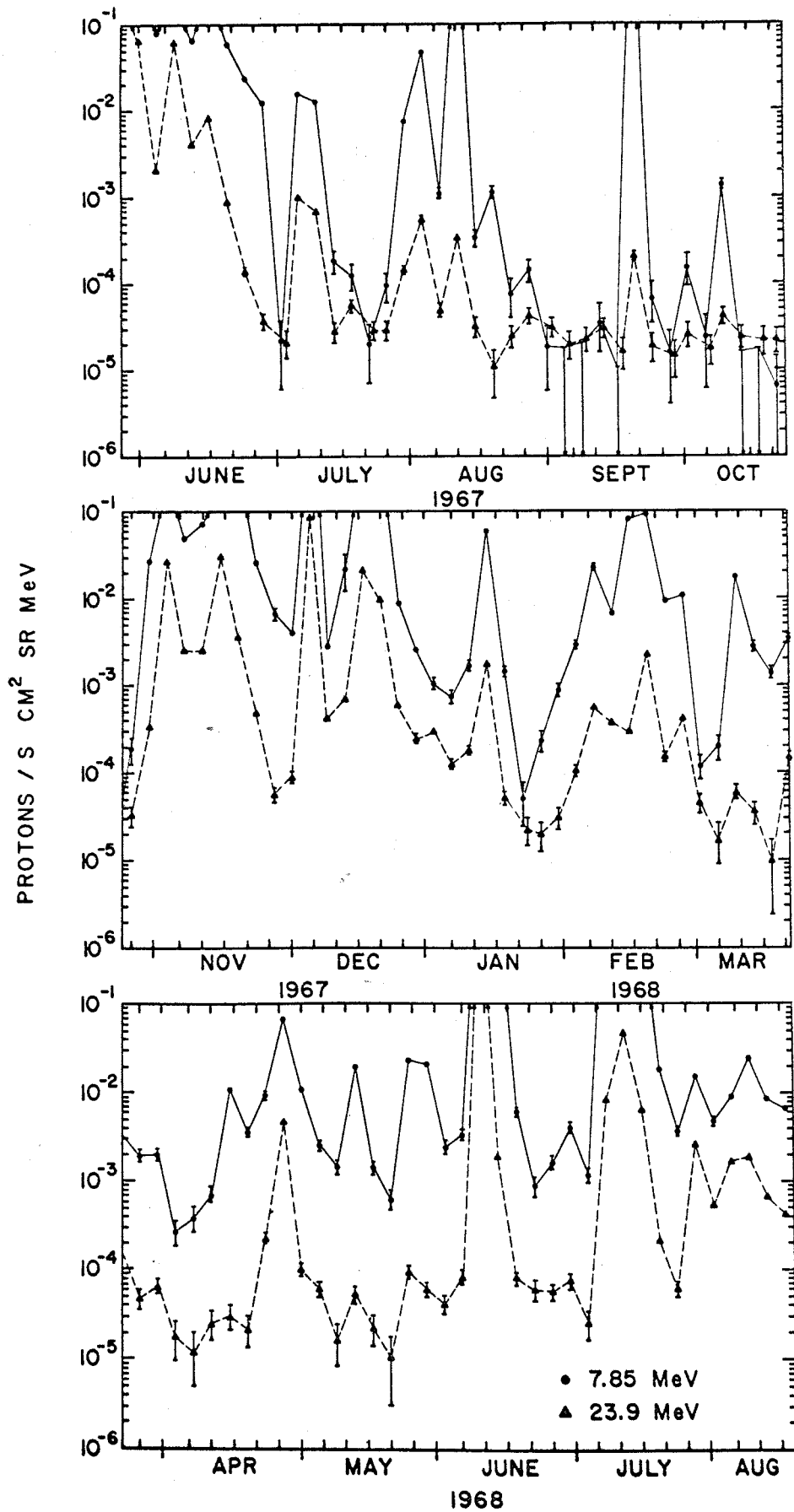
Figure 19. IMP-IV 96 hour average proton fluxes.
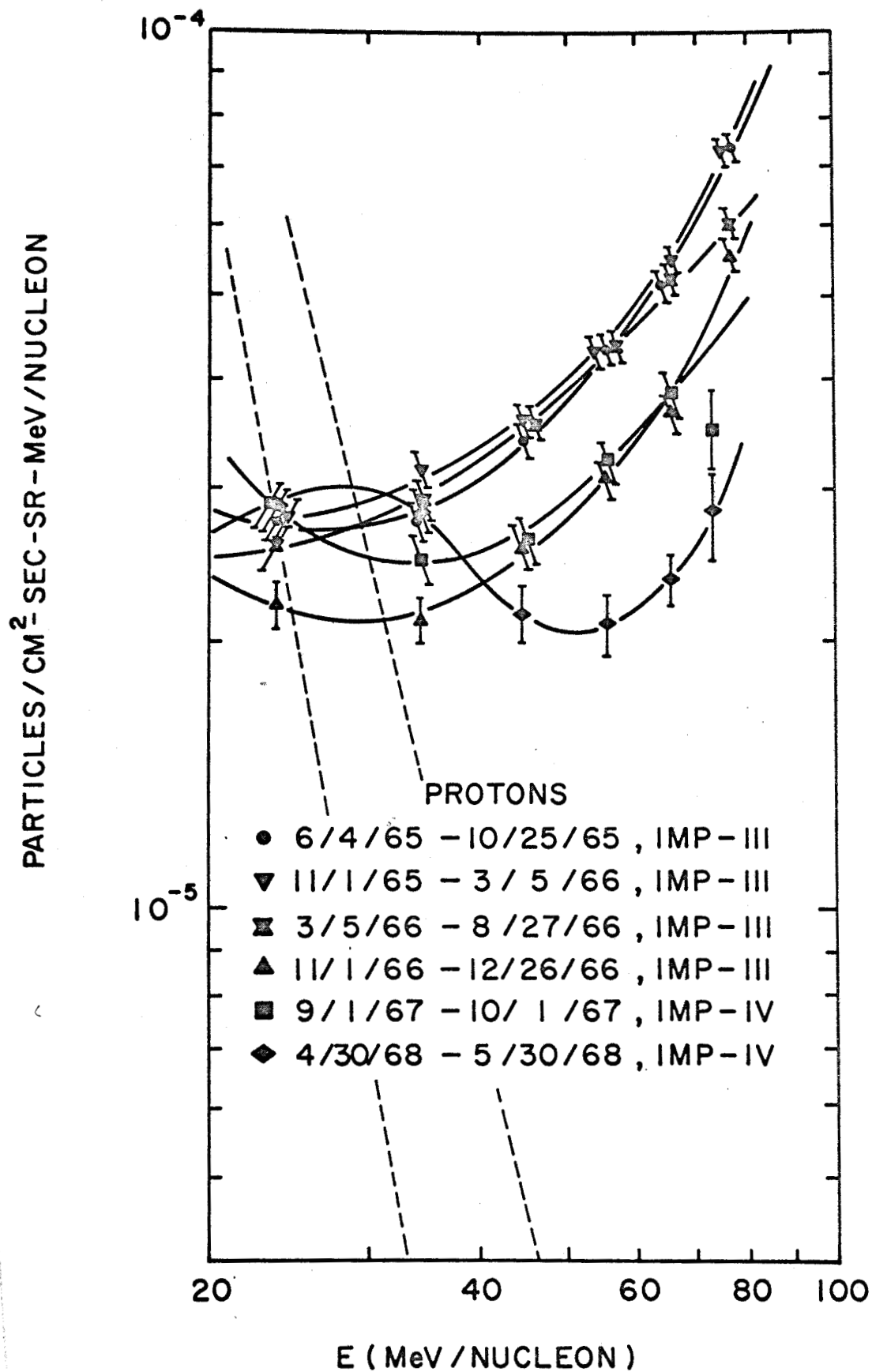
Figure 20. Quiet time proton energy spectra.
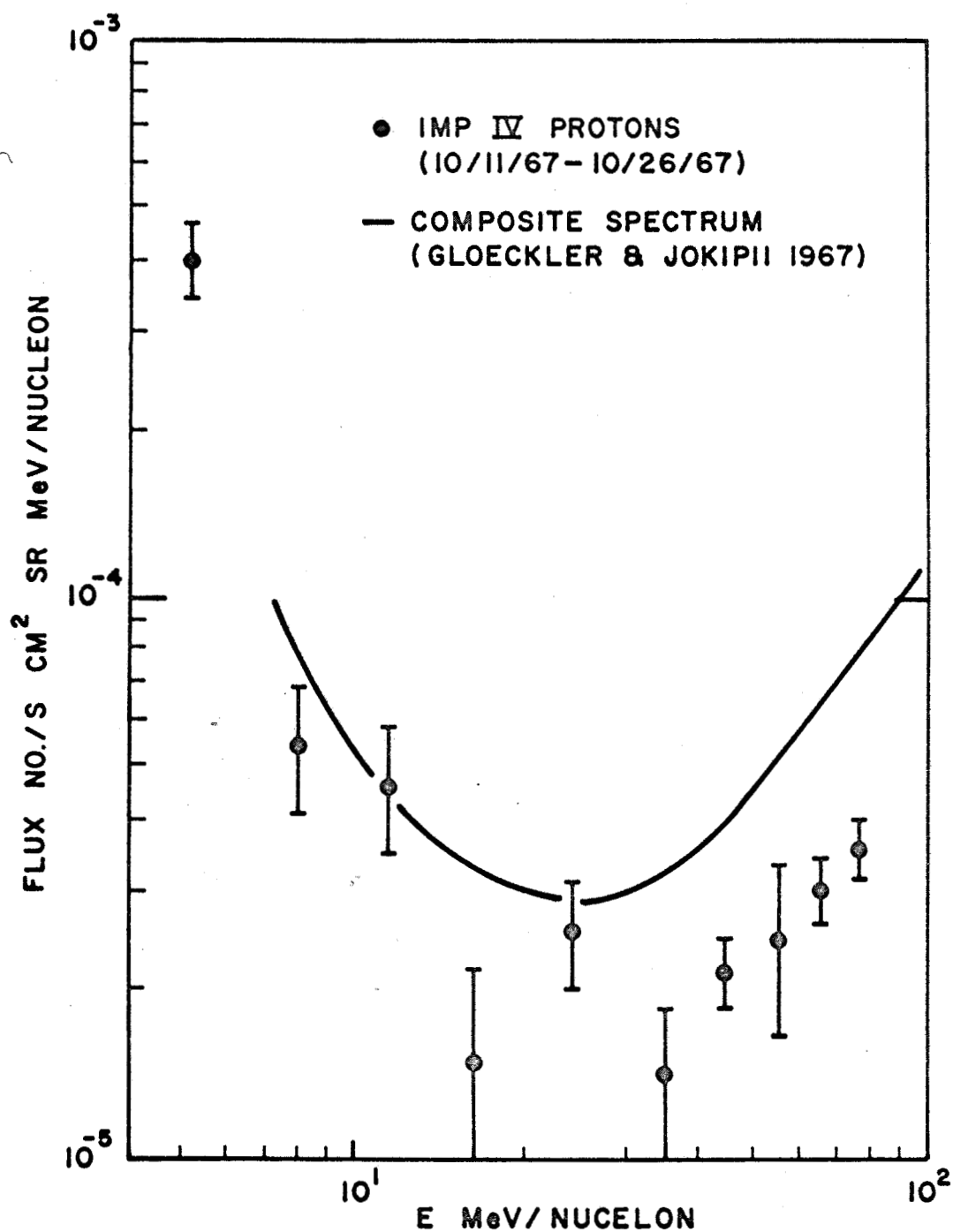
Figure 20(b). Quiet time proton energy spectra.
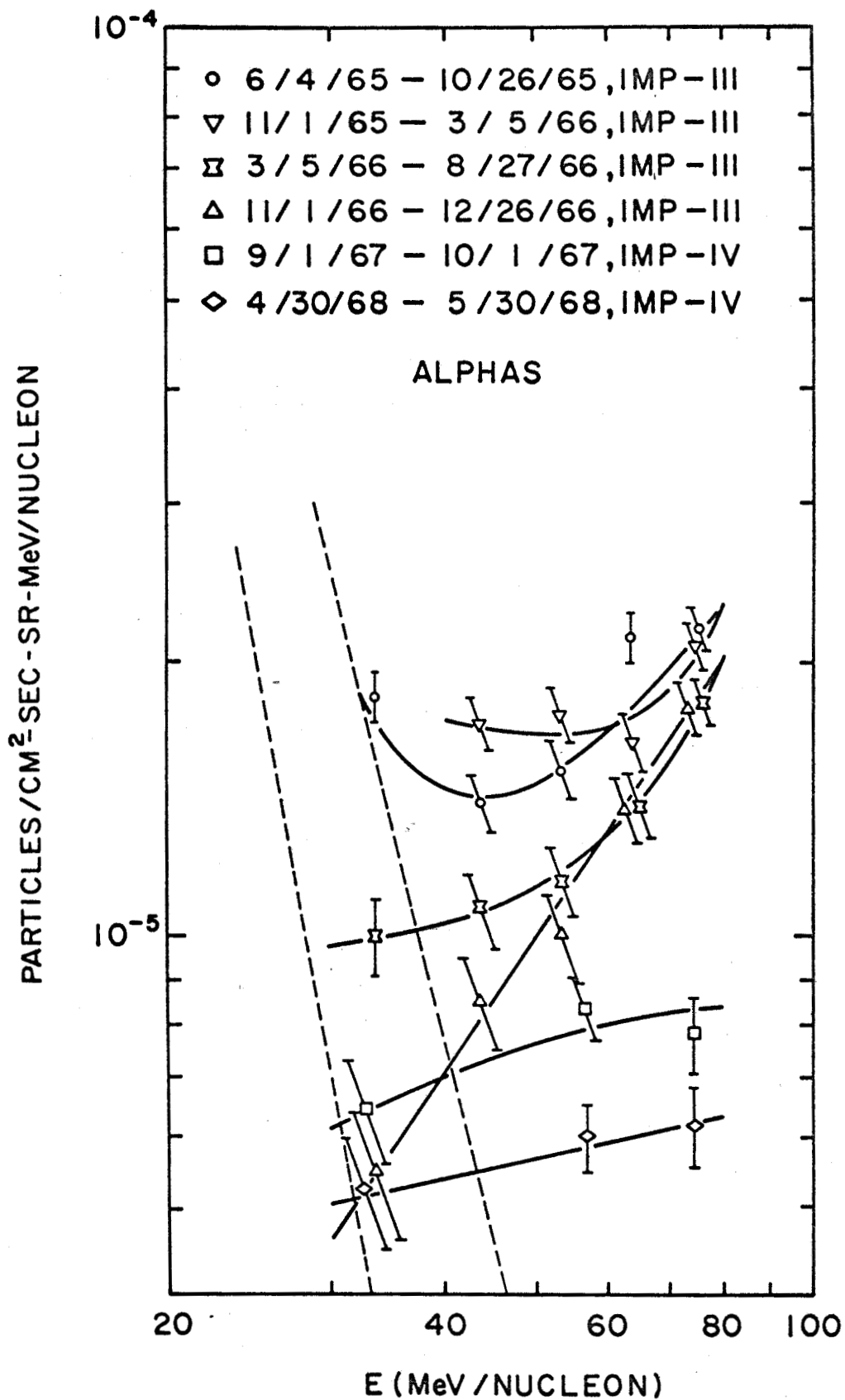
Figure 21. Quiet time alpha particle energy spectra.
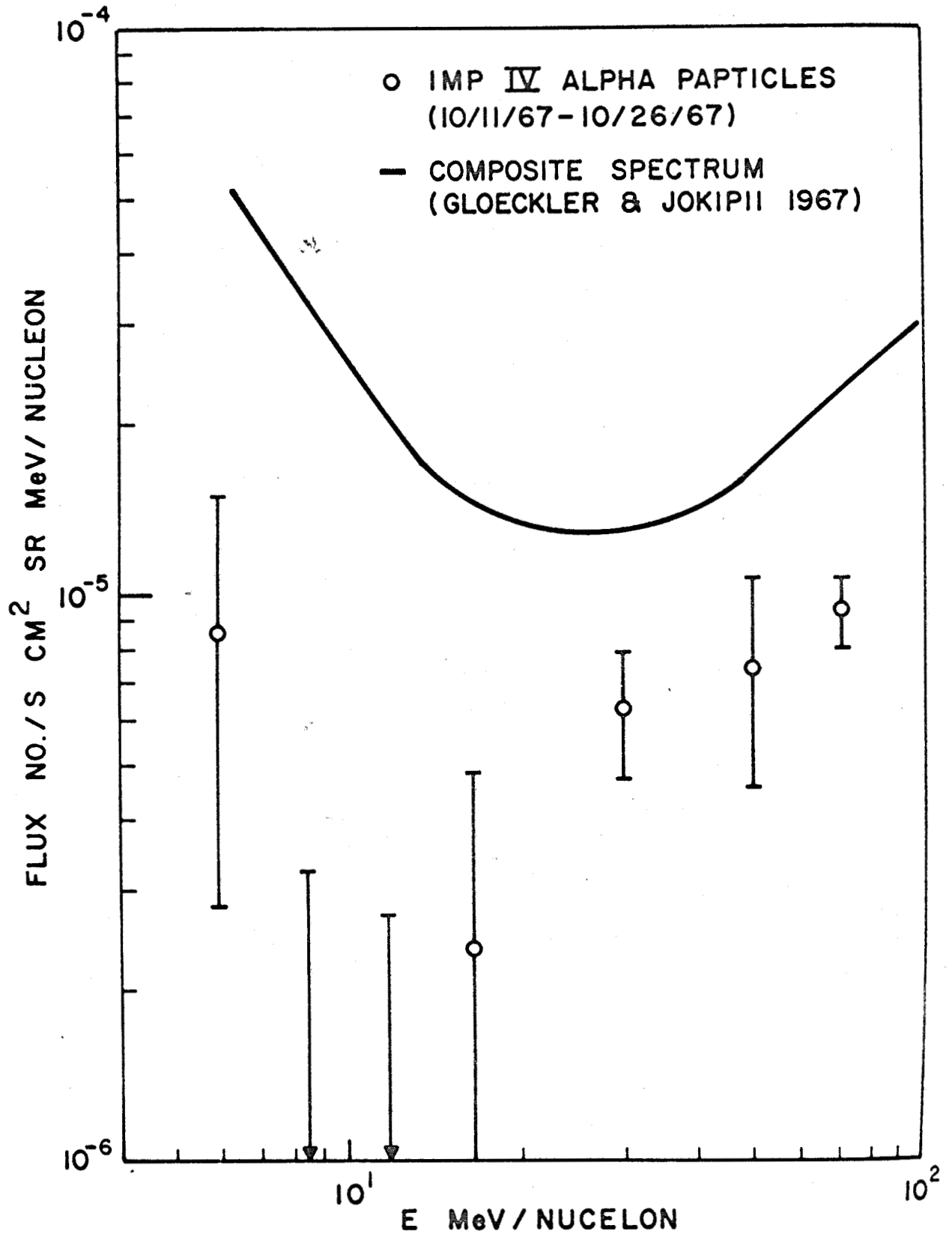
Figure 21(b). Quiet time alpha particle energy spectra.
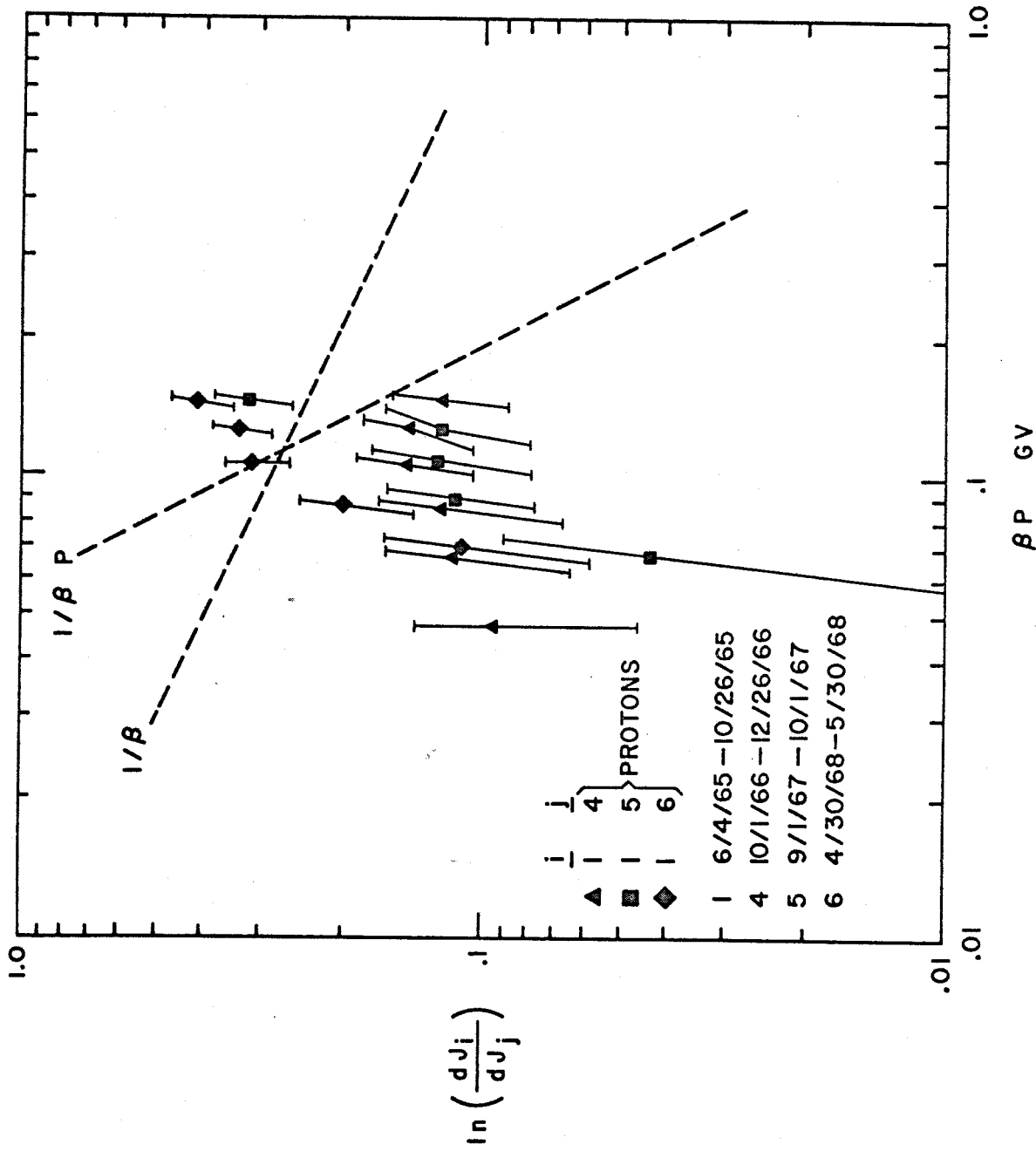
Figure 22. Modulation of proton energy spectra since solar minimum with respect to the solar minimum spectrum.
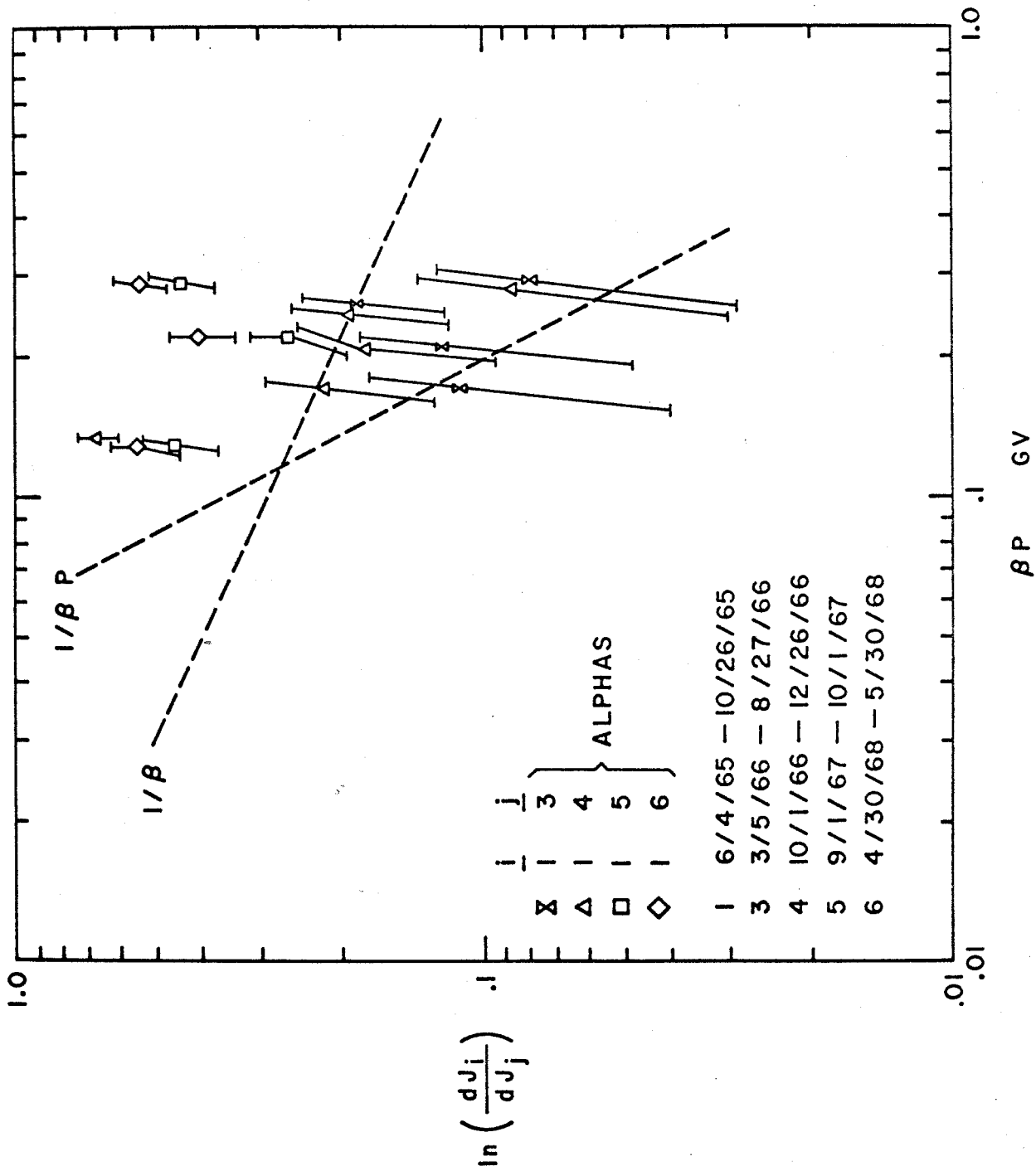
Figure 23. Modulation of the alpha particle energy spectra since solar minimum with respect to the solar minimum spectrum.

Figure 23. Modulation of the alpha particle energy spectral shape with respect to the solar minimum spectrum.
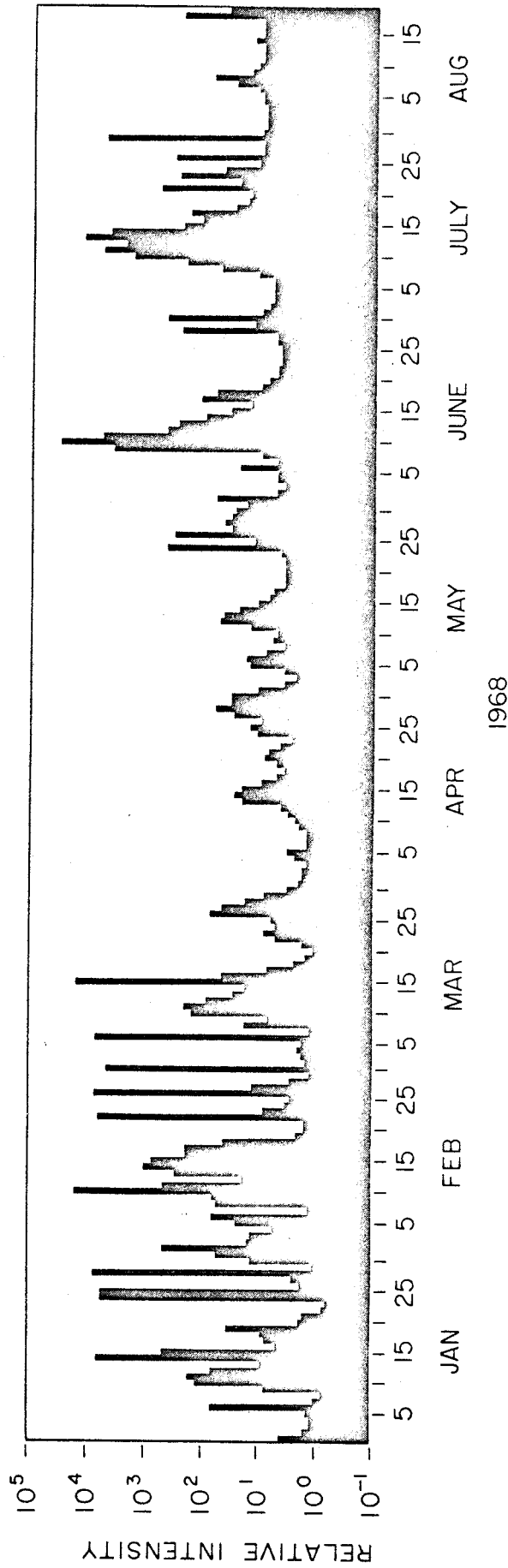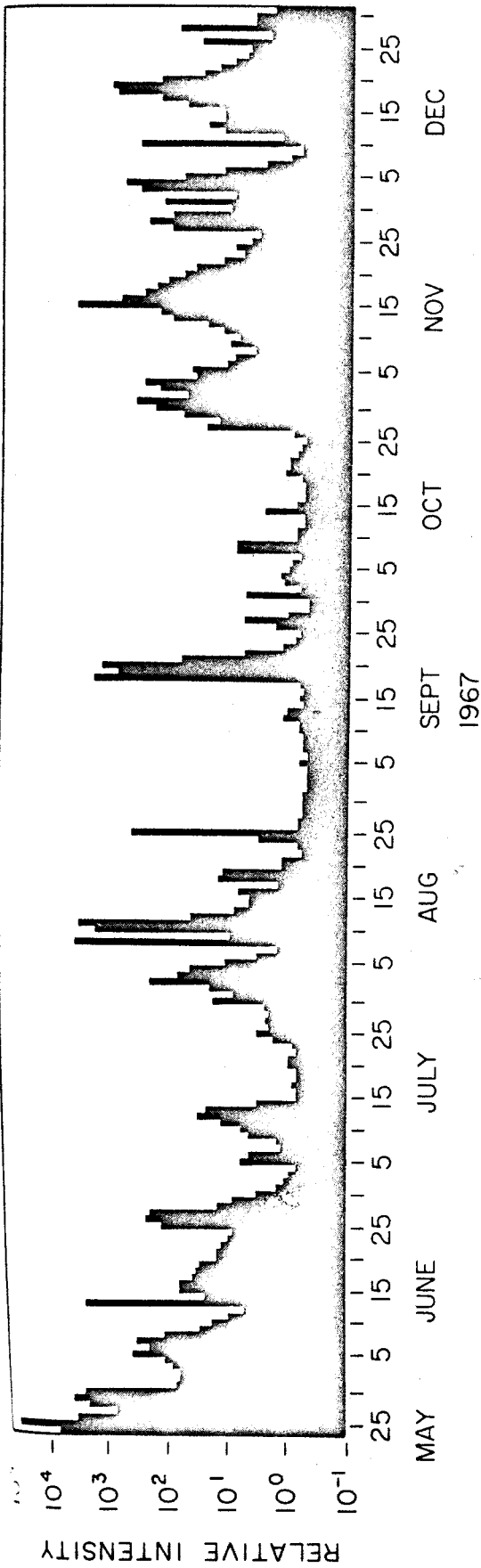
Figure 24. Time history of the 24 hour relative particle fluxes from the IMP-IV discriminator level 6.
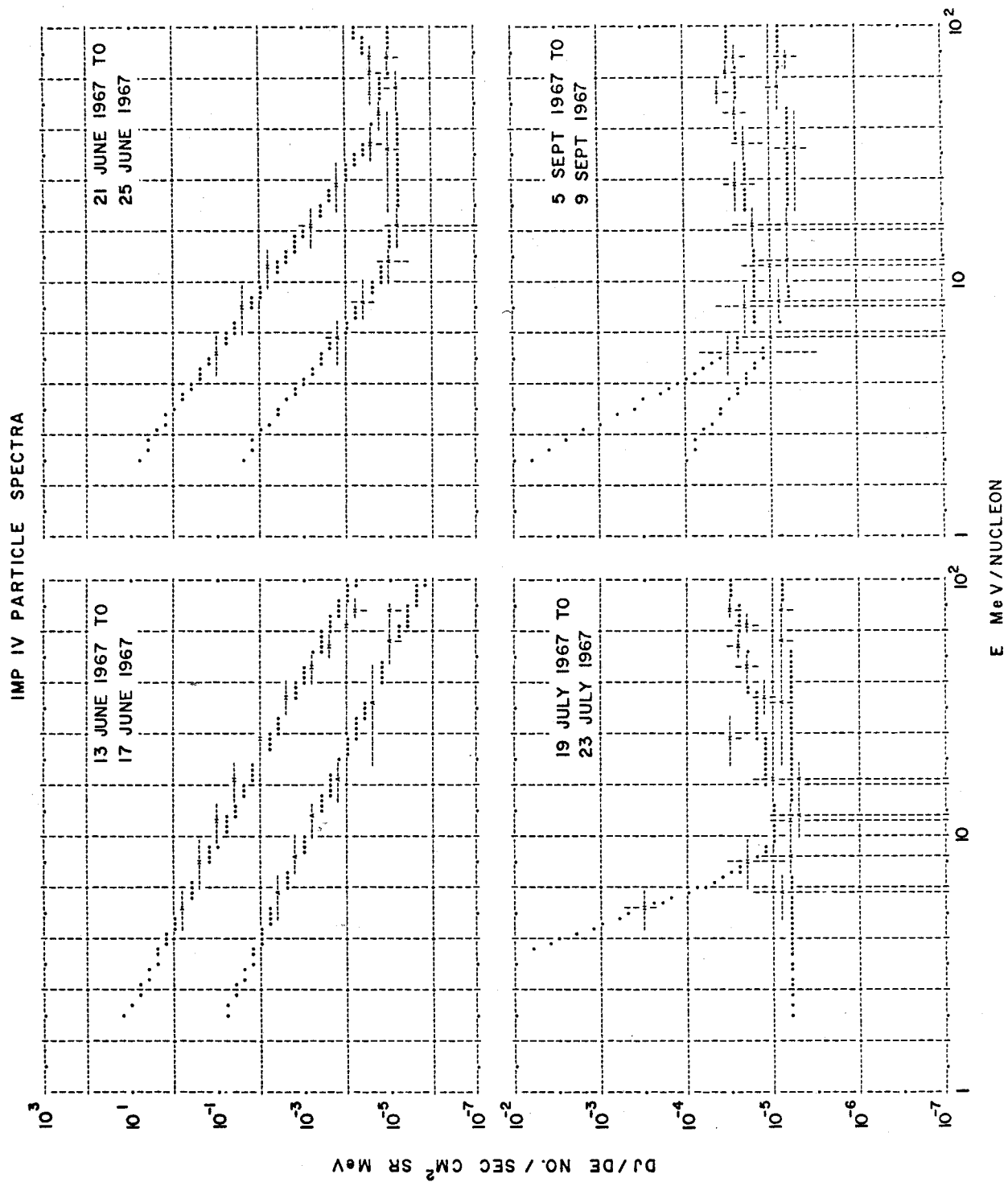
Figure 25. Representative 96 hour proton and alpha particle energy spectra with the least squares fit to the two component function.

Figure 25. Representative 96 hour proton and alpha particle [illegible] spectra with the least squares fit to the two component function.

IMP IV PARTICLE SPECTRA

13 JUNE 1967 TO 17 JUNE 1967

21 JUNE 1967 TO 25 JUNE 1967

19 JULY 1967 TO 23 JULY 1967

5 SEPT 1967 TO 9 SEPT 1967

E MeV/NUCLEON

DJ/DE (He⁴) / DJ/DE (H)
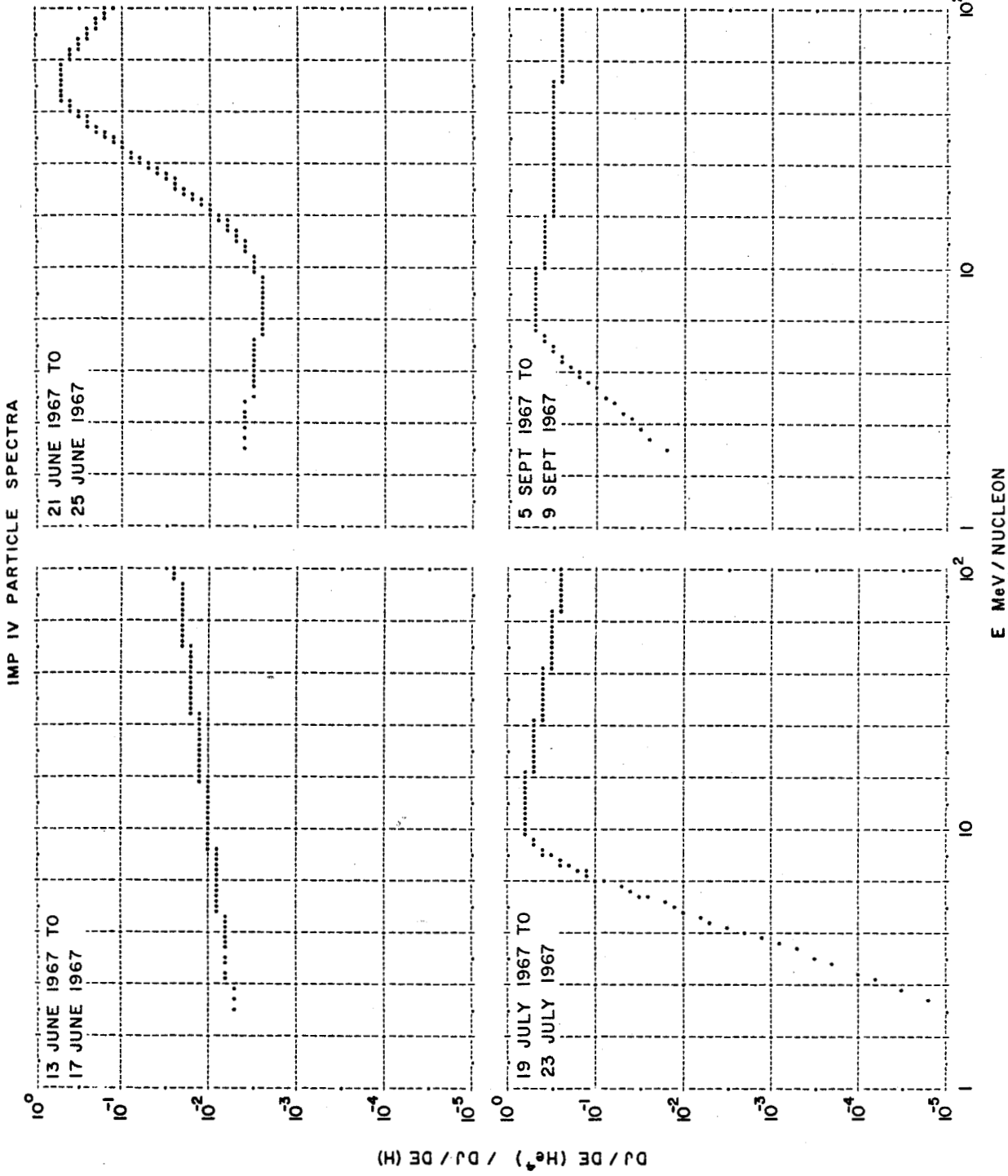
Figure 26 (a). Representative alpha particle to proton ratios of the 96 hour spectra.
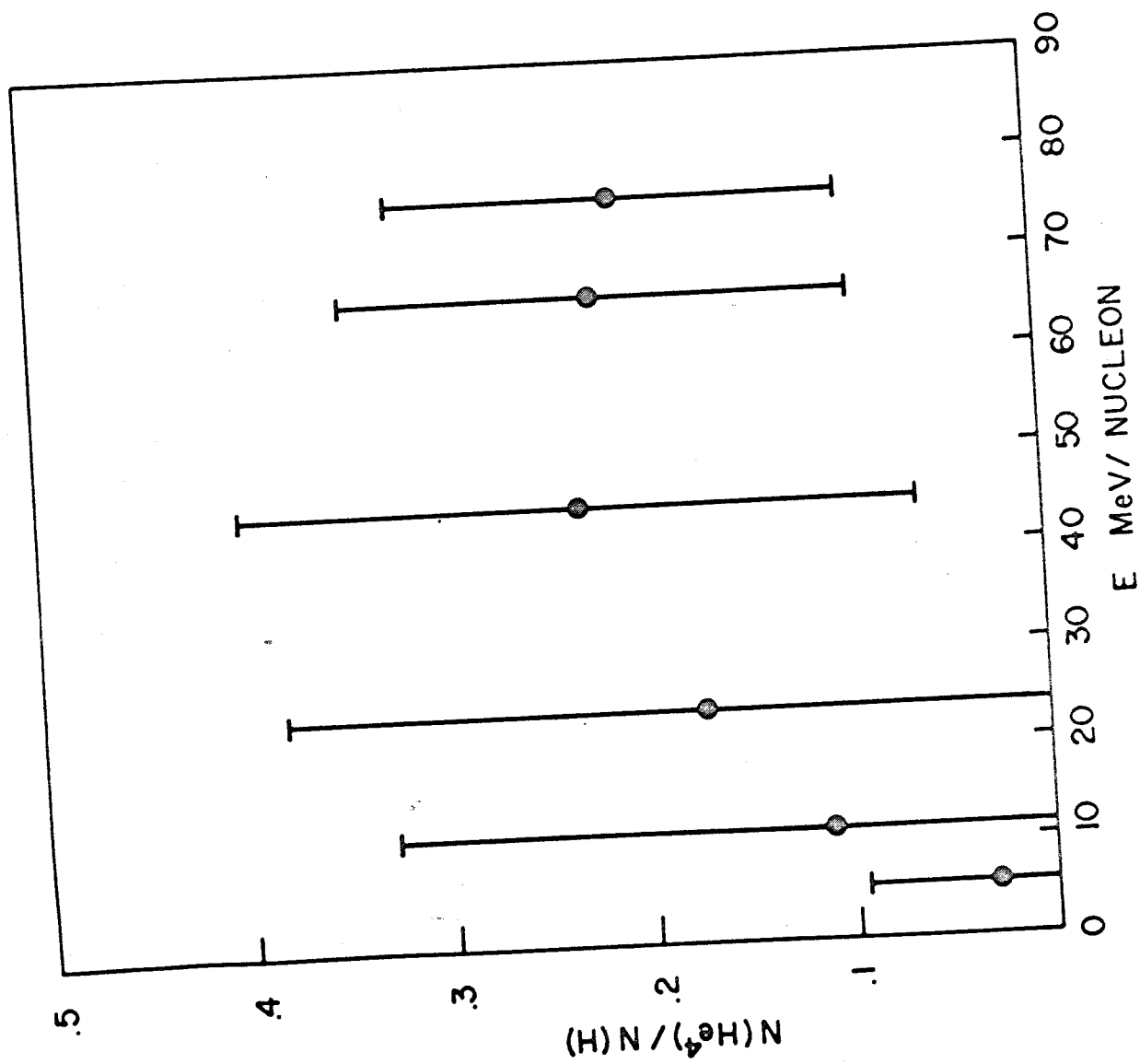
Figure 26 (b). Averages of alpha particle-to-proton ratios at discrete energies from 24 May 1967 to 20 August 1968 showing standard deviations.

PROTONS

dJ/dE (E = 5.2 MeV)

dJ/dE (E = 76.4 MeV)
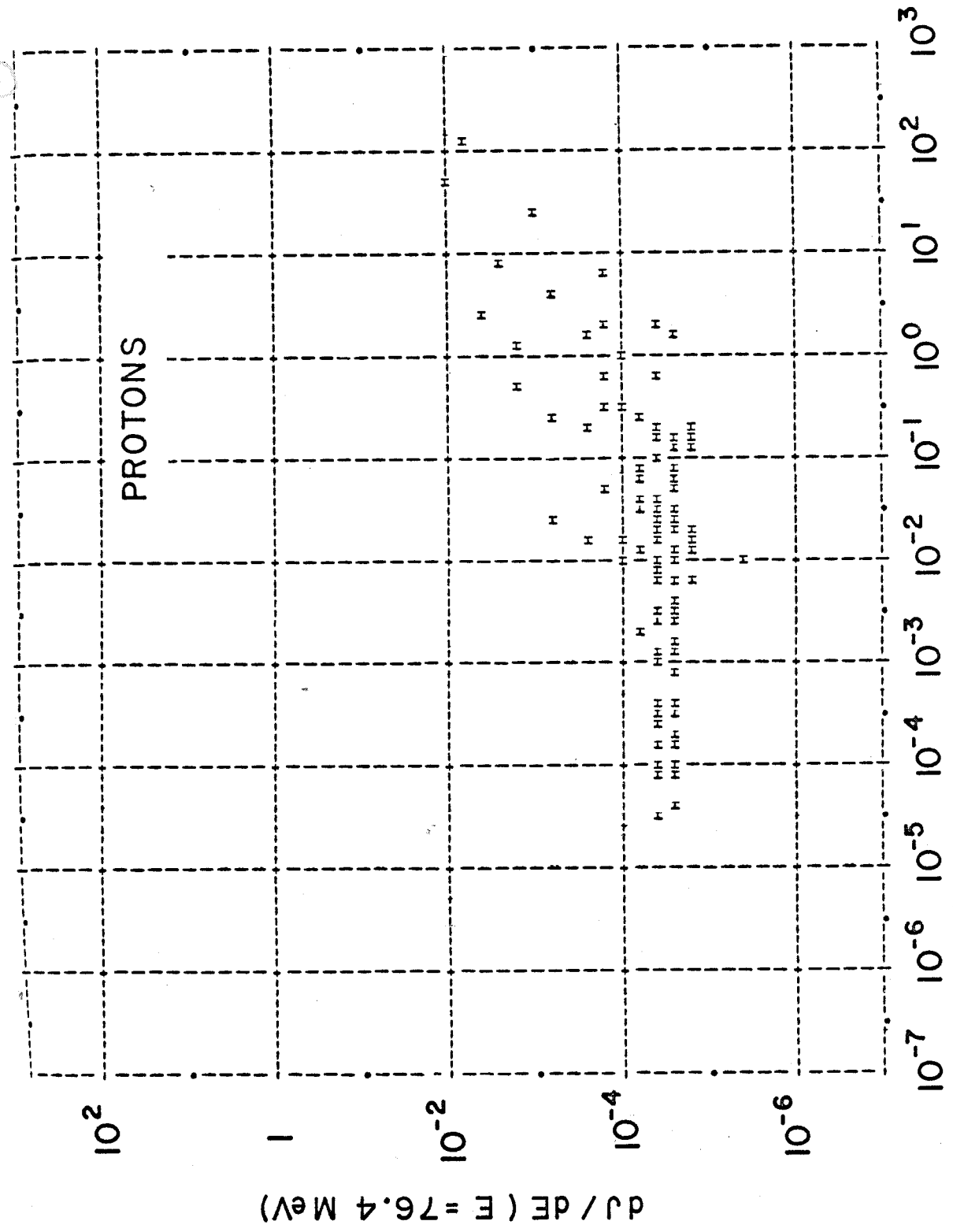
Figure 27. 76.4 MeV versus 5.2 MeV proton fluxes.
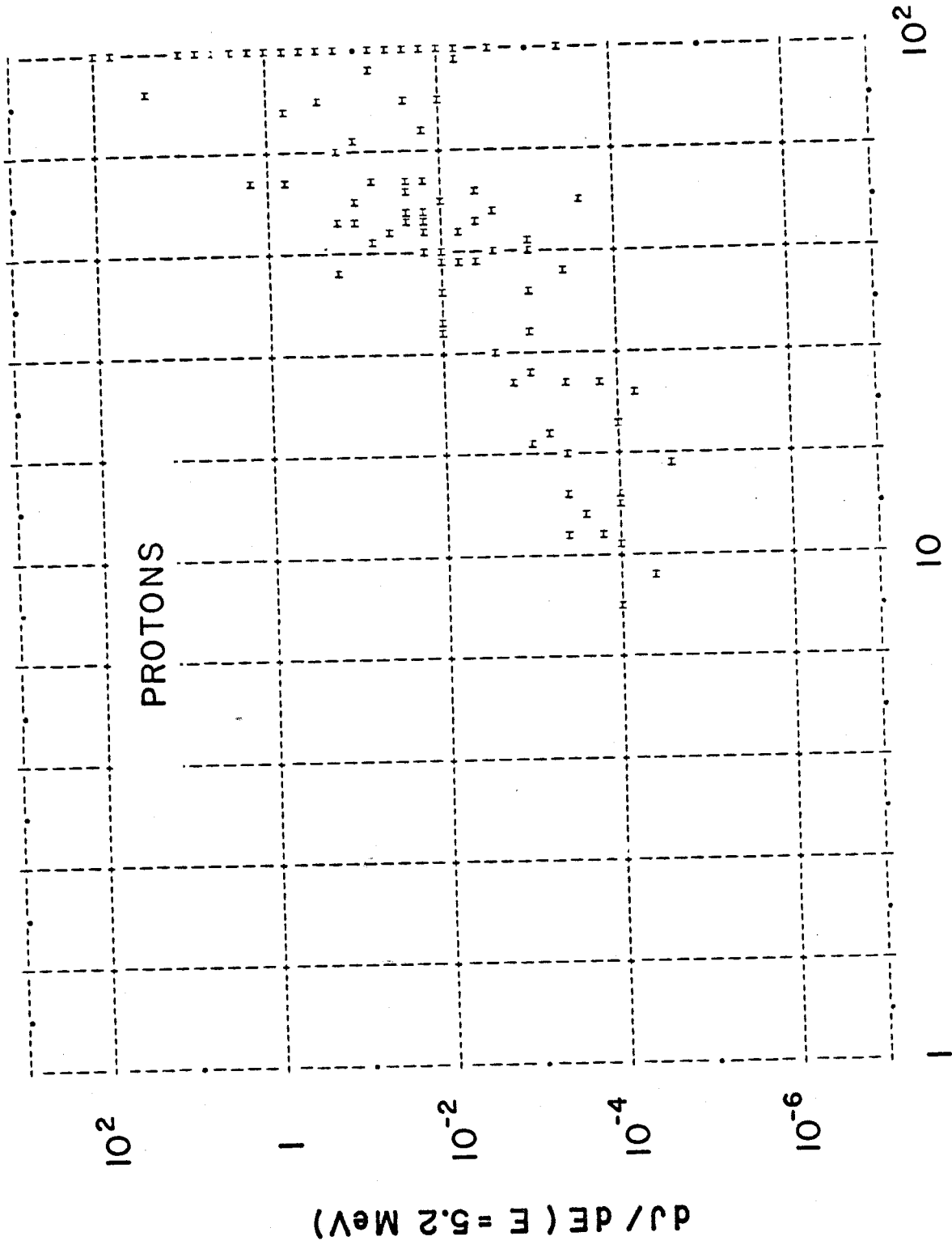
Figure 28. 5.2 MeV proton flux versus the energy at which minimum flux occurs.

PROTONS

ENERGY AT MINIMUM FLUX

dJ/dE ($E = 76.4$ MeV)
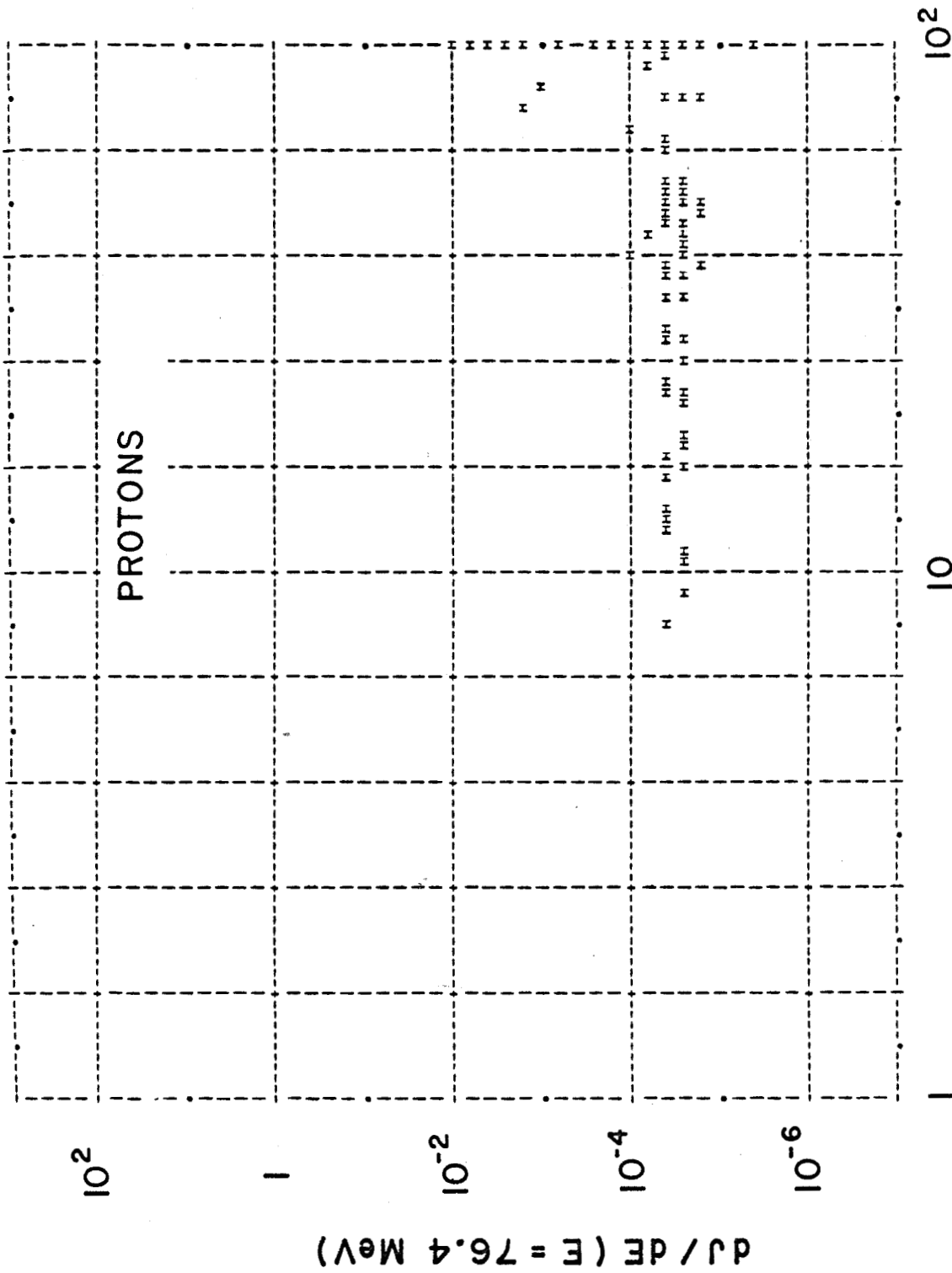
Figure 29. 76.4 MeV proton flux versus the energy at which minimum flux occurs.
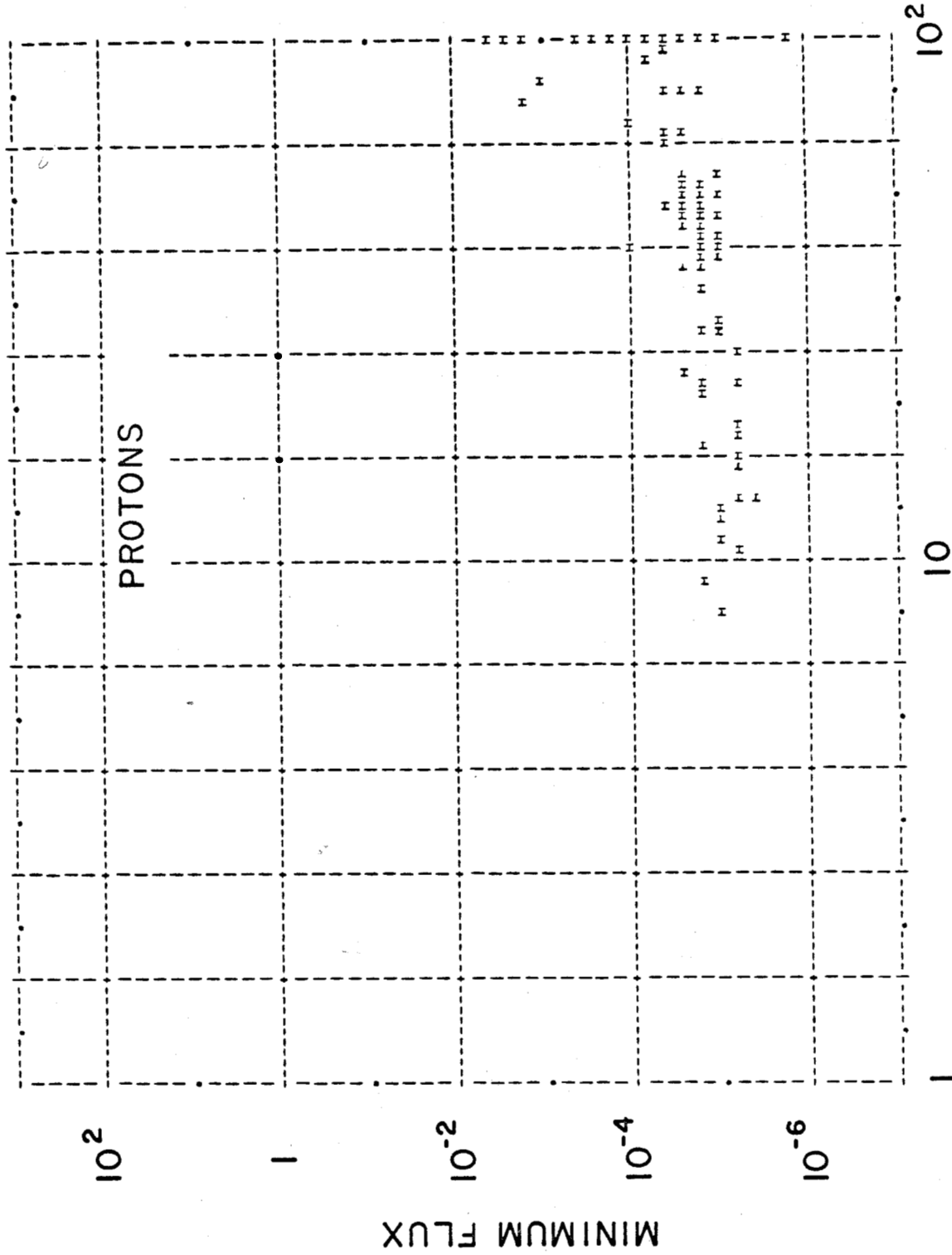
Figure 30. Minimum proton flux versus the energy at minimum flux.

Figure 30. Minimum proton flux versus the energy at minimum flux.
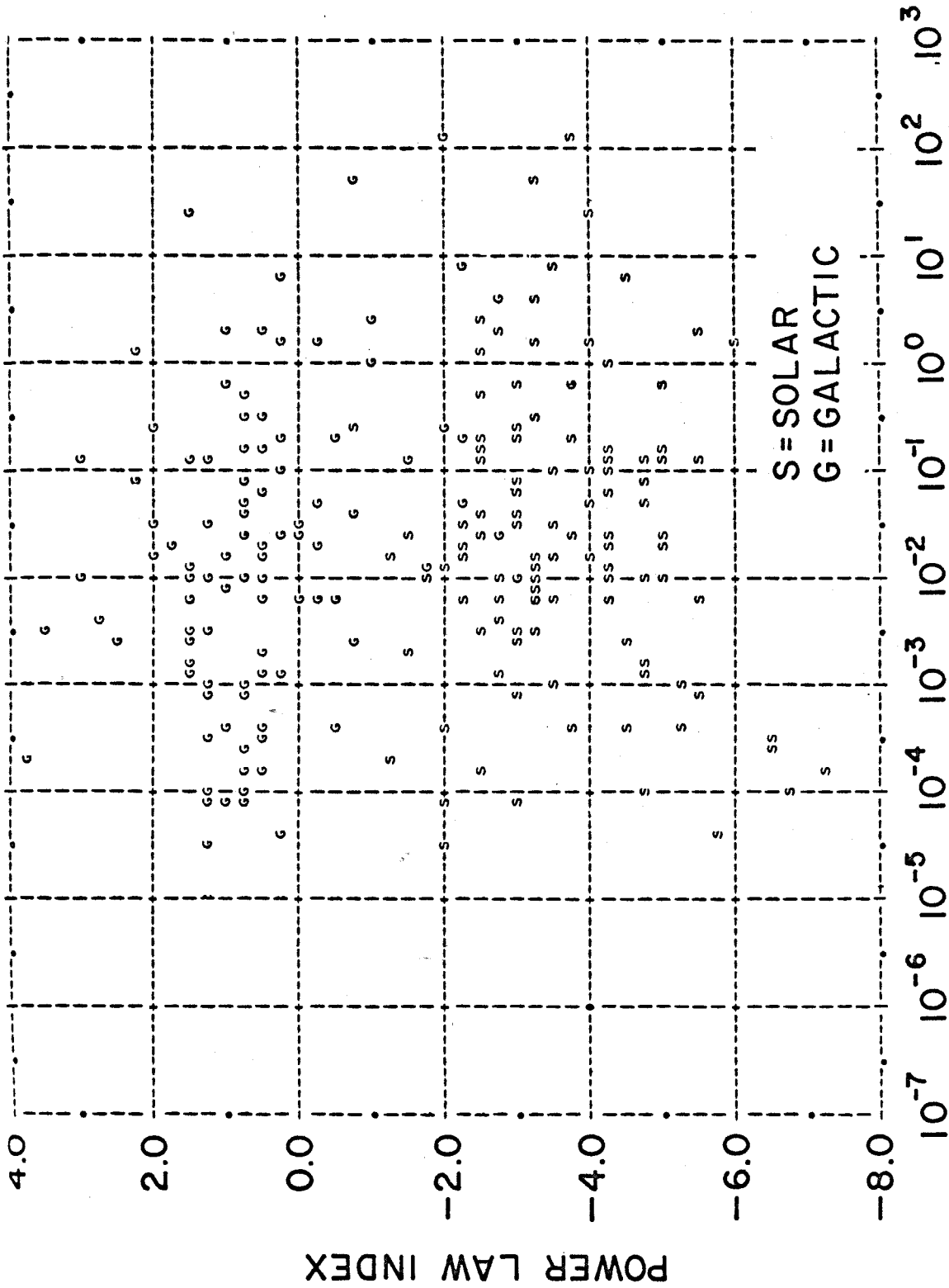
Figure 31. The computed power law indices versus the 5.2 MeV proton flux.
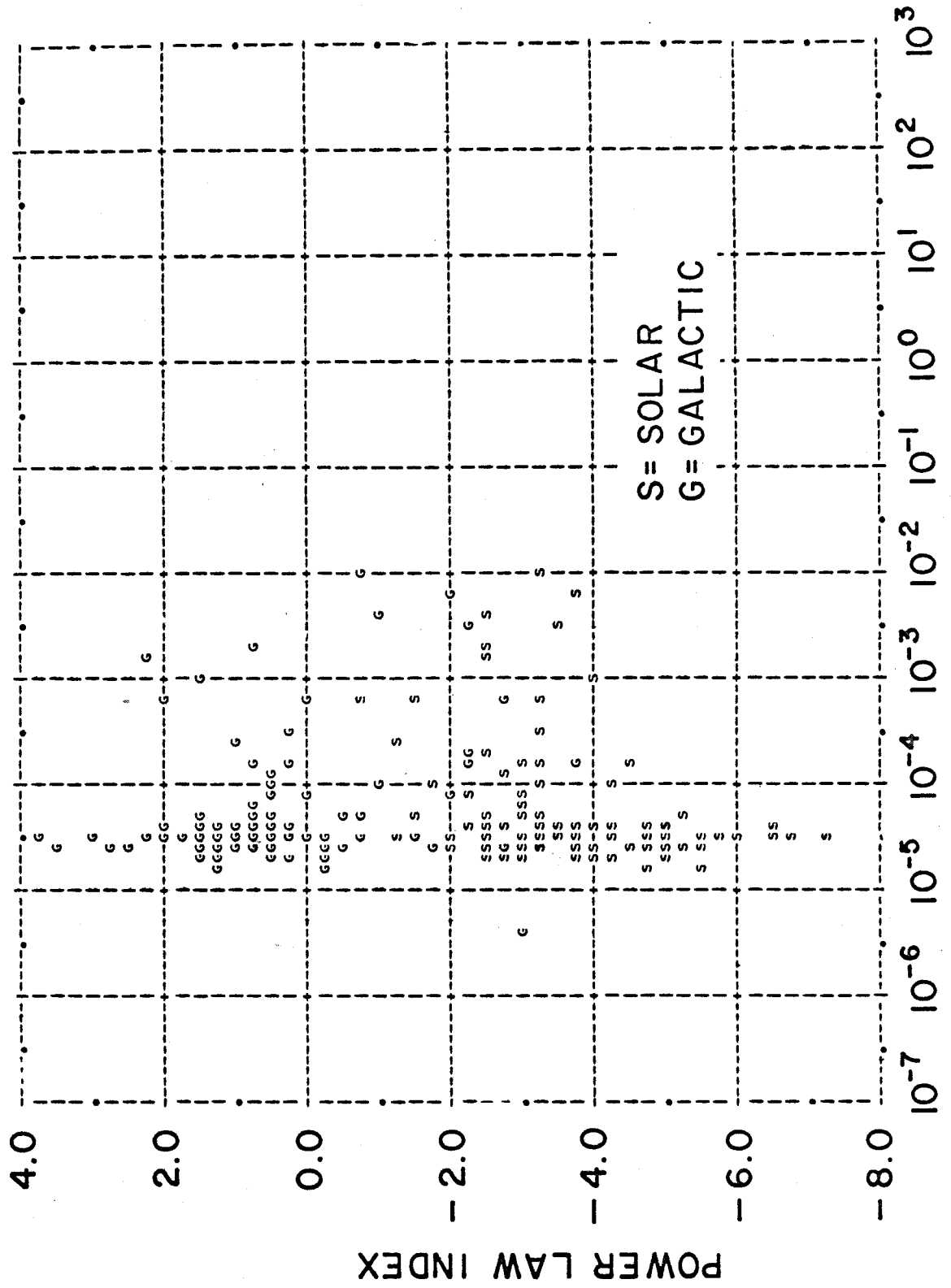
Figure 32. The computed power law indices versus the 76.4 MeV proton
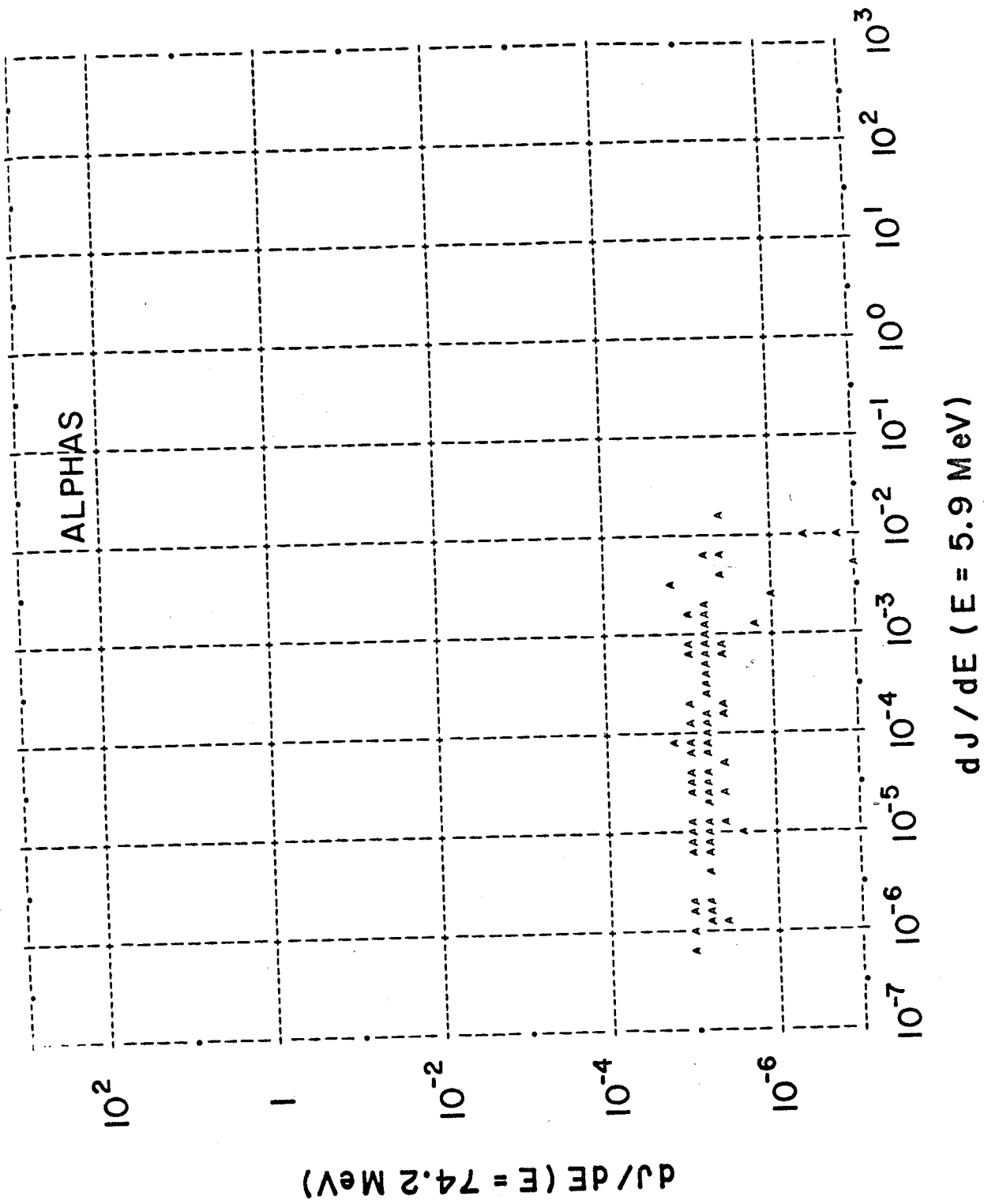
Figure 33. 74.2 MeV/nucleon versus 5.9 MeV/nucleon alpha particle fluxes.
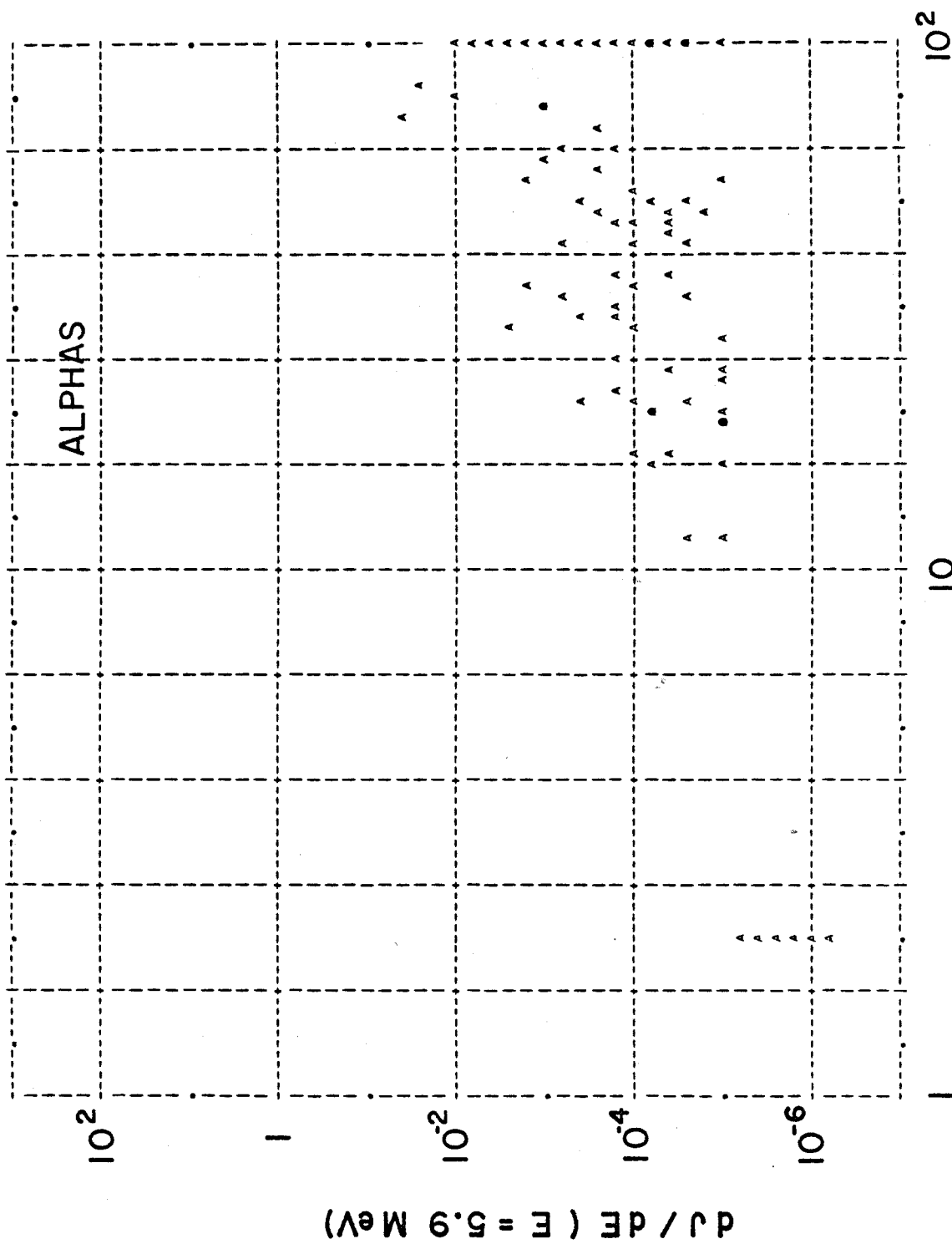
Figure 34. 5.9 MeV/nucleon alpha particle flux versus the energy/nucleon at which the minimum flux occurs.
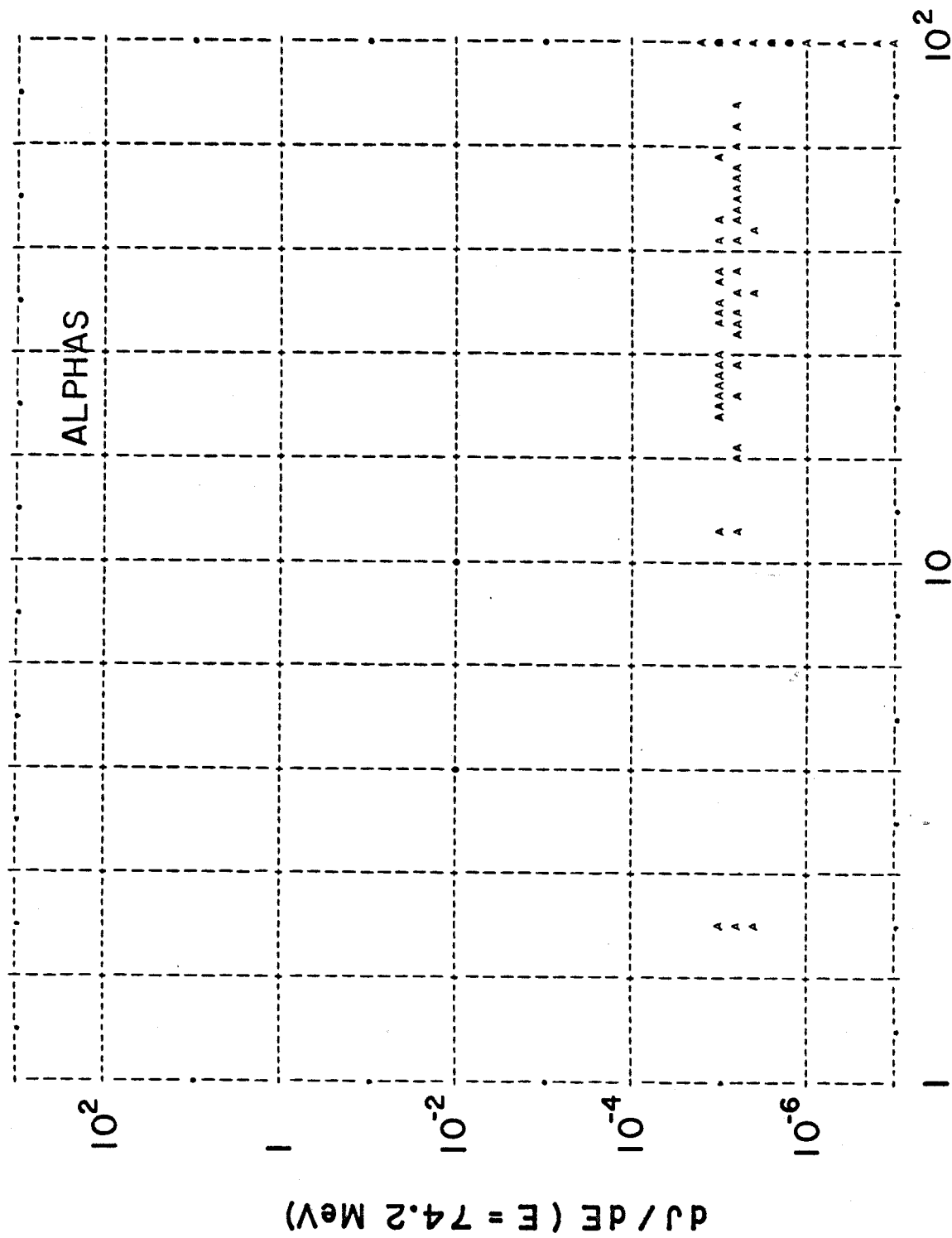
Figure 35. 74.2 MeV/nucleon alpha particle flux versus the energy/nucleon at which the minimum flux occurs.
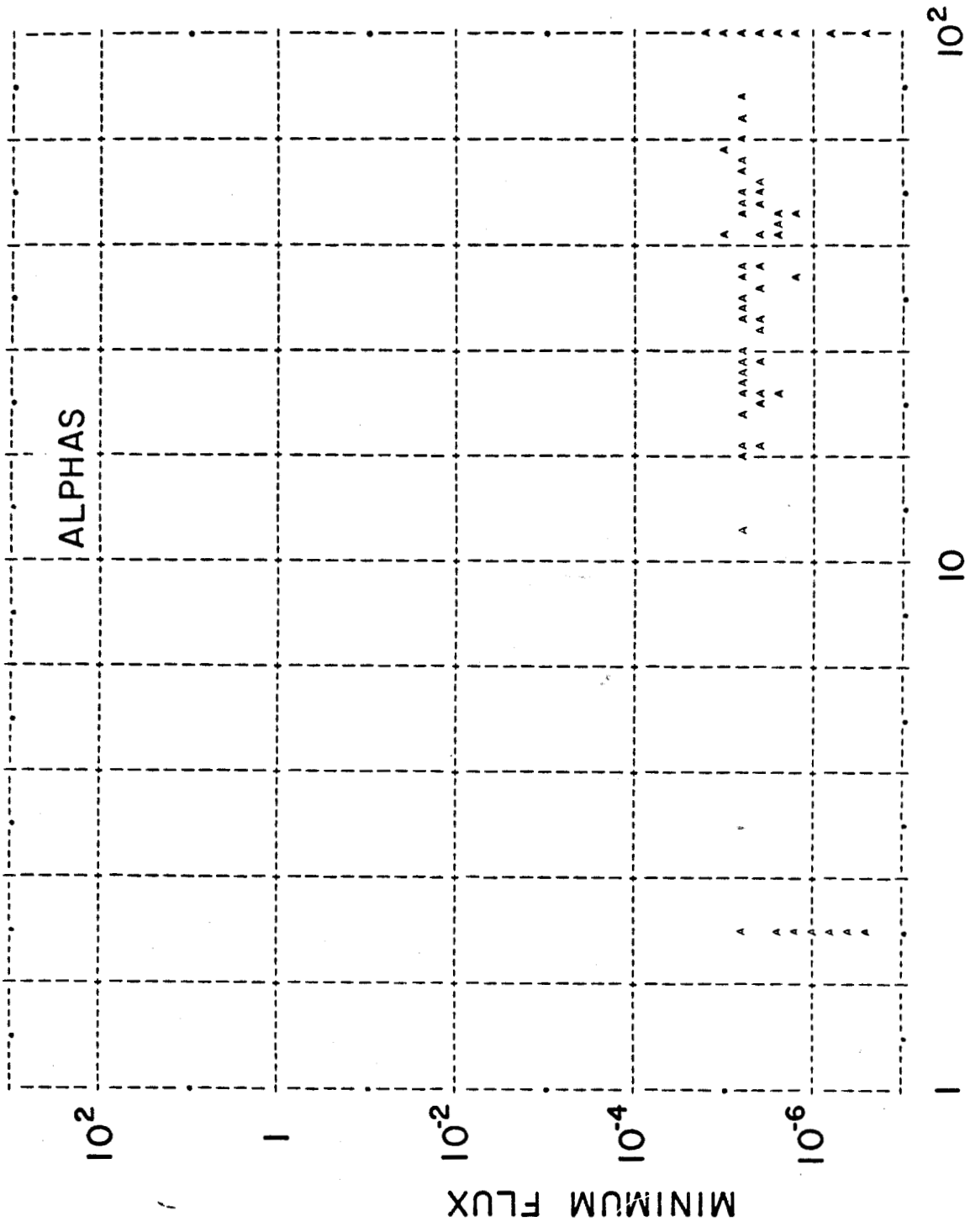
Figure 36. The minimum alpha particle flux versus the energy/nucleon at minimum flux.

Figure 36. The minimum alpha particle flux versus the energy/nucleon at minimum flux.
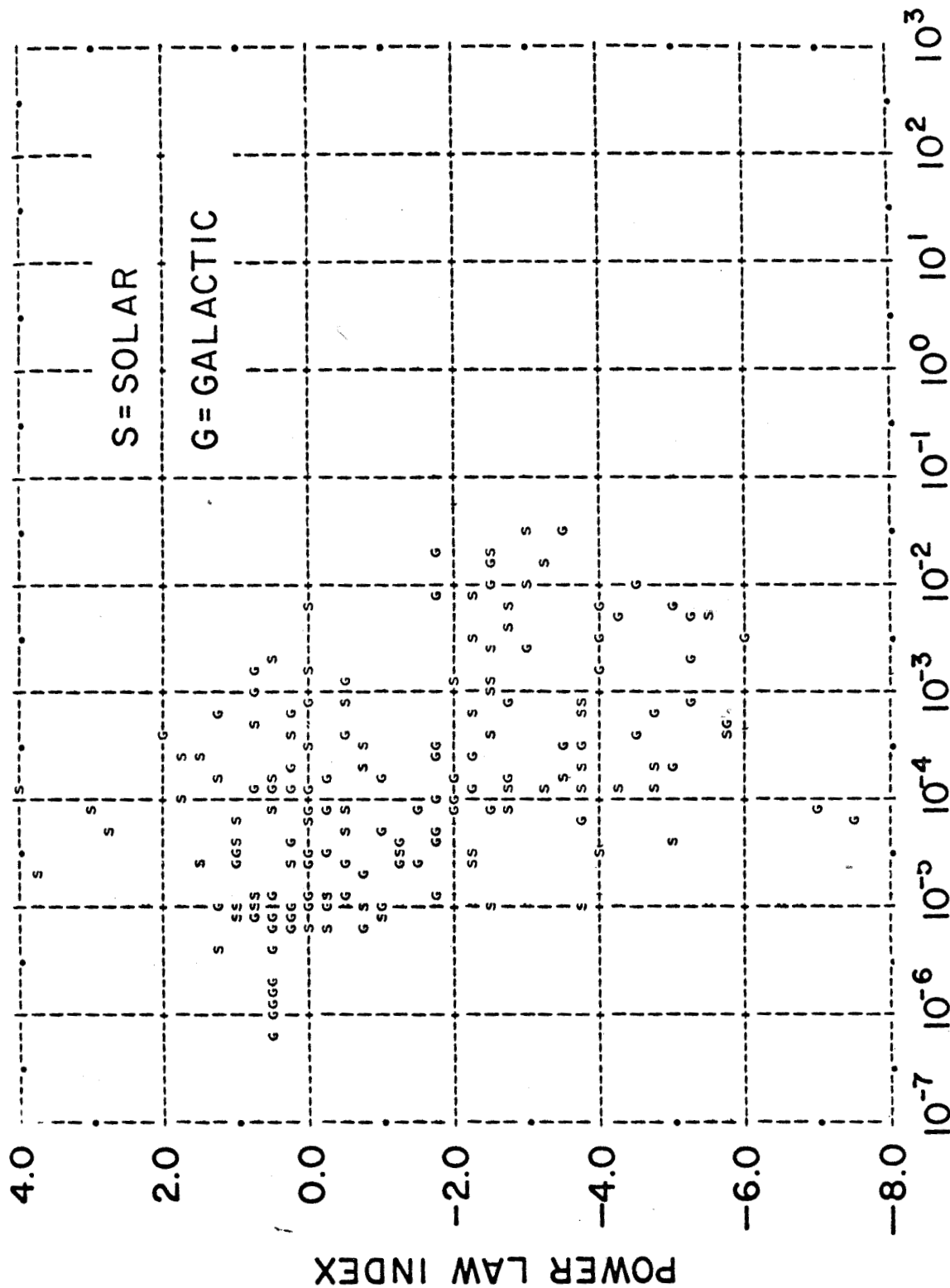
Figure 37. The computed power law indices versus the 5.9 MeV/nucleon alpha particle fluxes.
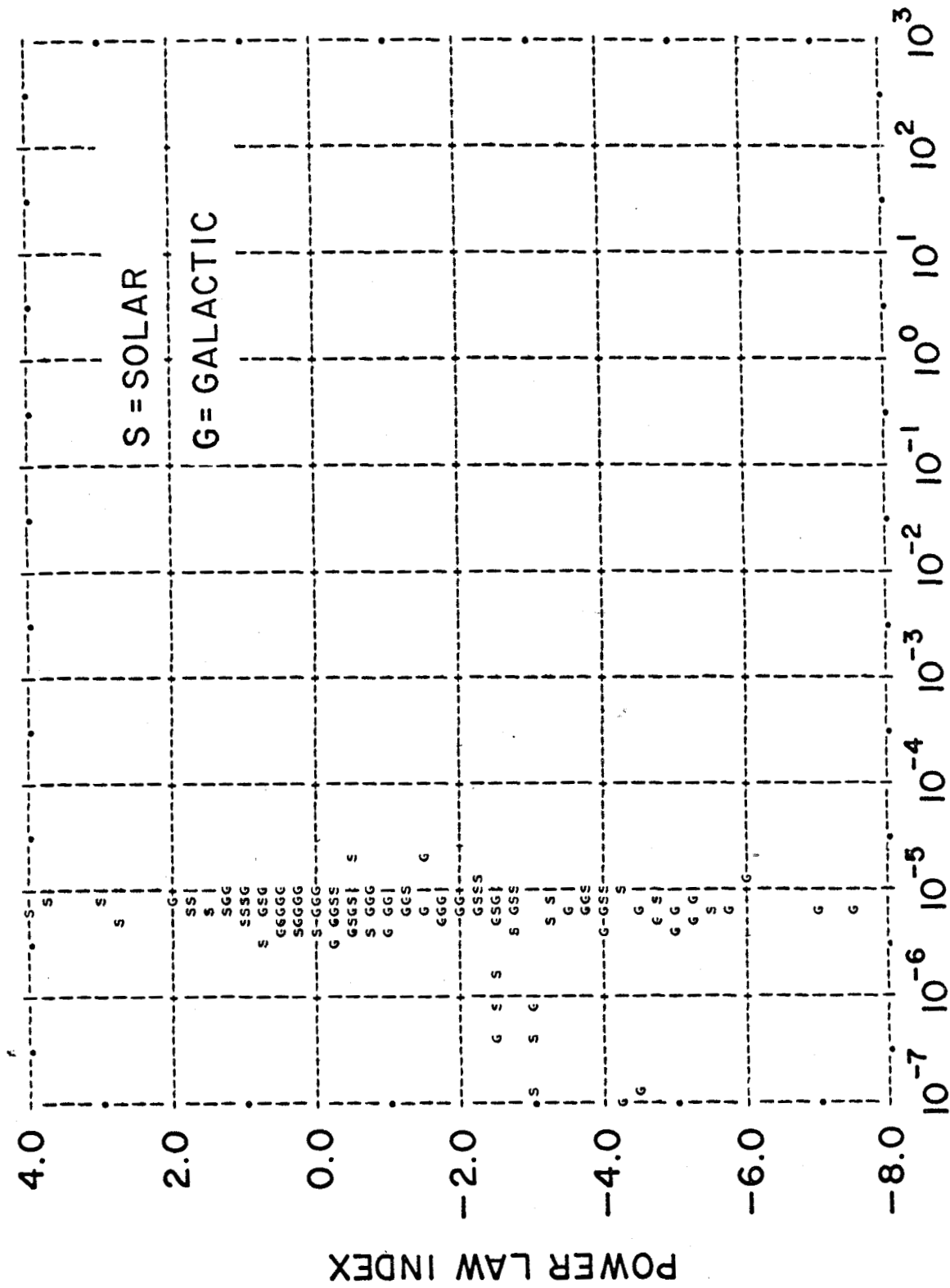
Figure 38. The computed power law indices versus the 74.2 MeV/nucleon alpha par⋯ e fluxes.
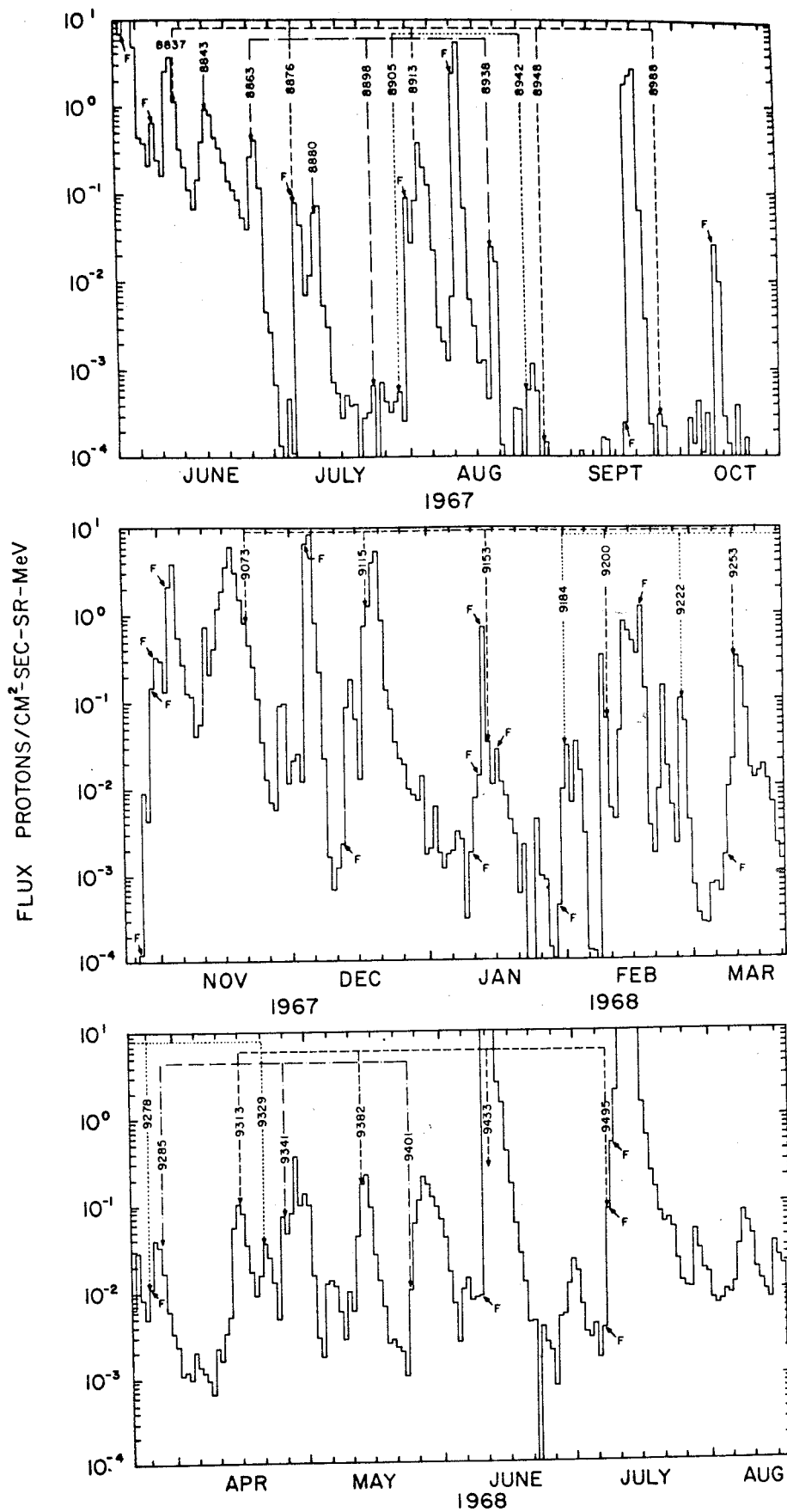
Figure 39. The 24 hour average proton fluxes at 5.2 MeV for IMP-IV. The times large confirmed solar flares occrrred are marked F. Central meridian passage of calcium plage regions are marked by the plage region number. Recurring regions are connected by horizontal lines.
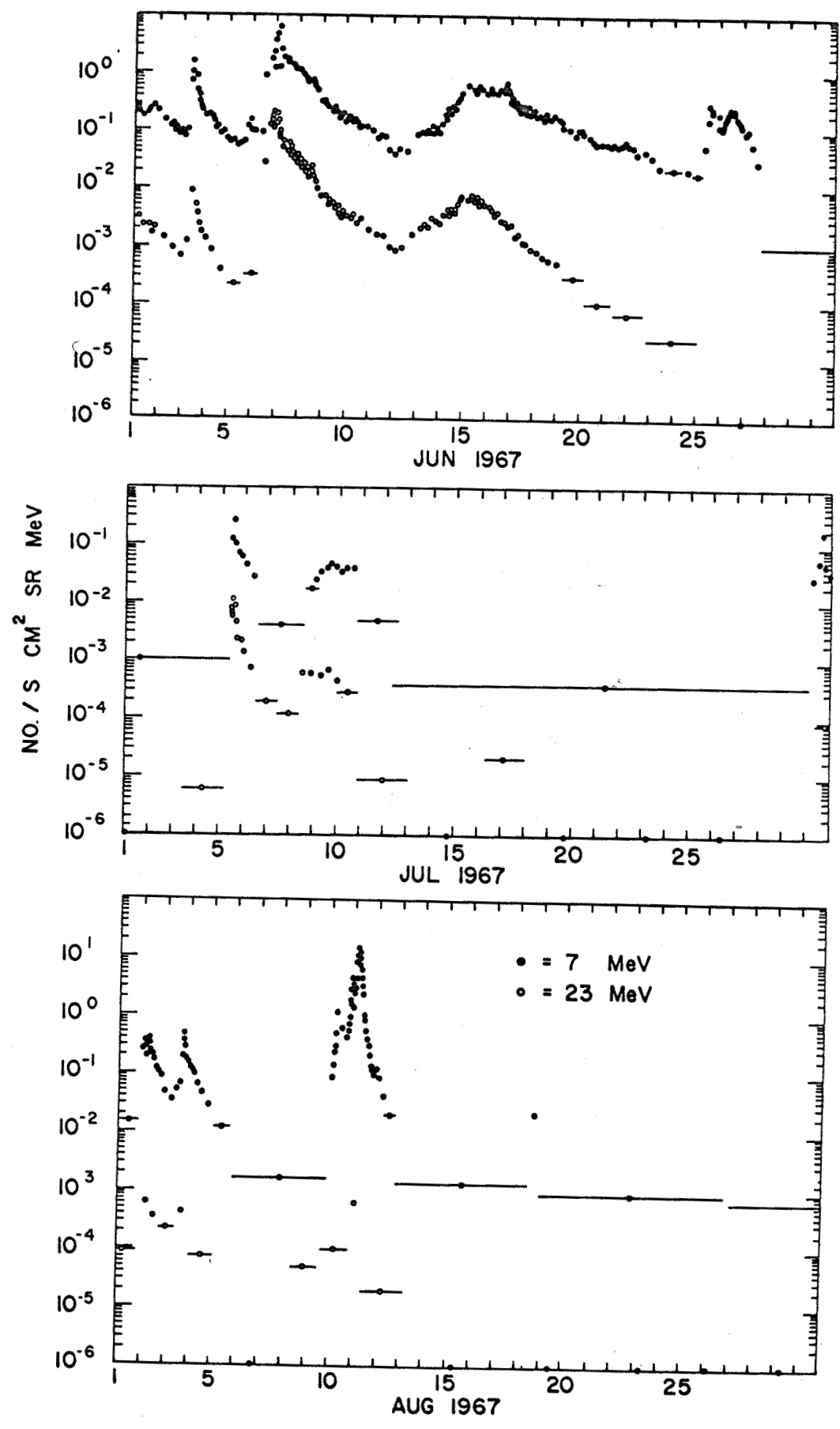
Figure 40. 10% variable time averages of proton fluxes for 3 months of IMP-IV data showing solar proton increases caused by corotating regions.
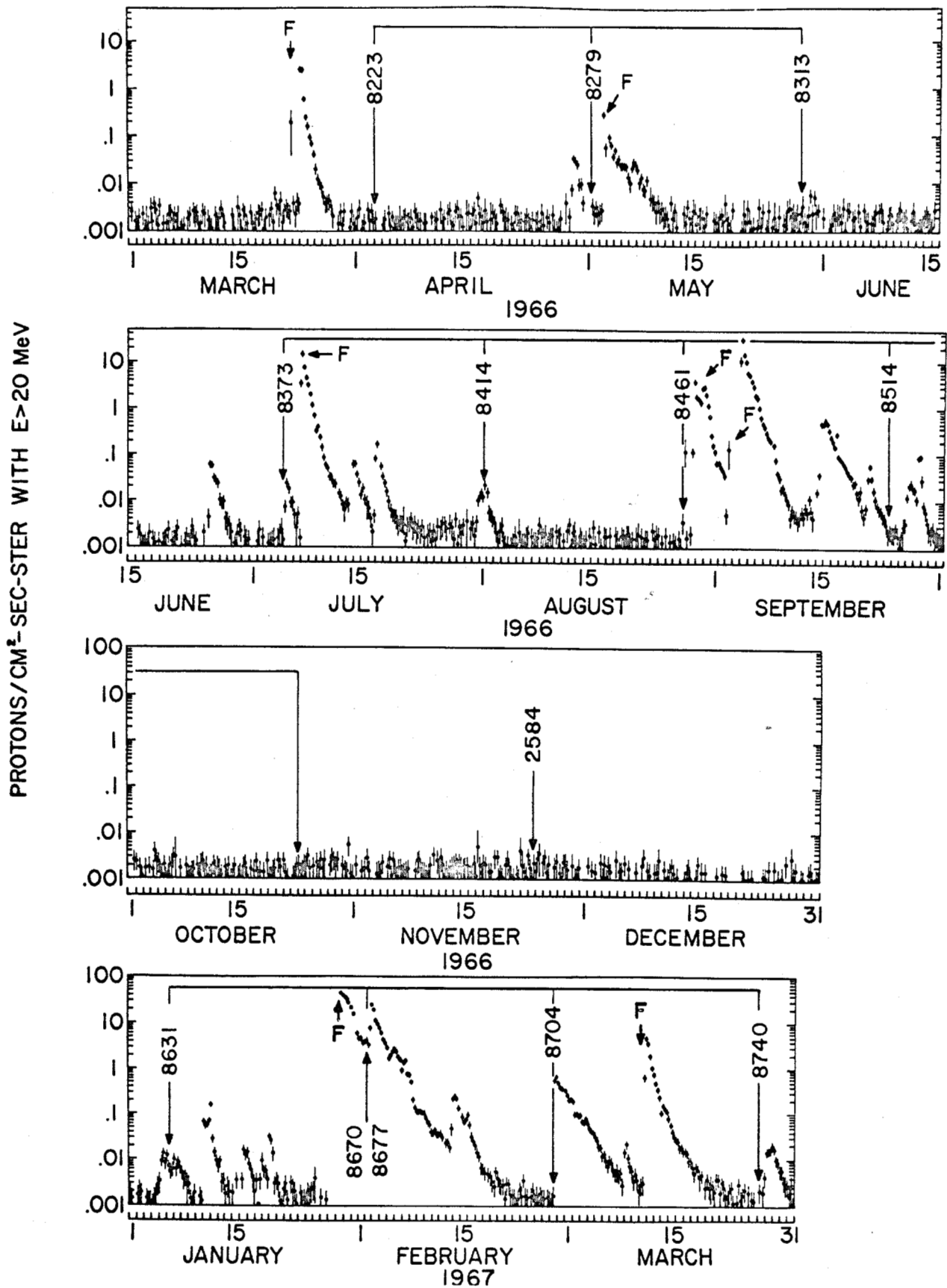
Figure 41. 6 hour integral proton fluxes for energies >20 MeV from IMP-III. The times of meridian transit for returning calcium plage regions are marked with the region numbers. Flare times are marked with an F.

1967	May 3	1	1547	1602	m	3	H,B
			1548.0	1603.5	dk	3	B
	May 19	1	1535	1555	m	3	H
			1537.2	1545.8	dk	3	B
	May 20	1	1520	1536	m	3	H
			1527.0	1553.0	dk	2	B
	May 21	1	1923	1945	m, dk	3	H
	May 23	1	1838	1842	dm	3	H
			1838	1905	m	3	H
			1843.4	1900.0	dk	3	B
			1846	1905	dk	2	H
	May 26	1	0204.5	0212	m	2	C
			0212	0228	m	1	C
			0204.15	0228	dk	1	C
	May 28	1	0539	0556	m	2	C
			0545	0552	dk	1	C
	June 3	1	0243	0250	m	2	C
			0244	0256.5	dk	2	C
	June 13	1	2034.7	2041.1	dk	1	B
	June 18	1	1555	1602	m	2	H,B
			1600	1602.9	dk	1	H,B
	June 23	1	0050	0058	m	2	H,B
			0050	0110	m	1	C
			0053.4	0110.1	dk	3	H,B
			0054	0105	dk	1	C
	July 28	1	1607	1616	m	2	H
	July 29	1	0413	0419	m	2	C
	Aug 1	2	0120	0122	dm	3	H
			0120	0123	m	2	H
			0126	0130	m	1	H
			1735	1738	m	2	H
	Aug 15	1	0232	0240	m	1	C
			0233	0242	dk	1	C

1967	Aug 18	1	2130	2151	m	2	H
			2133	2140.2	m	1	C
			2136	2159.2	dk	2	B
	Aug 19	2	0020.8	0029	dk	2	B
			0615	0620	m	1	C
	Aug 25	1	1414	1432	m	1	H
			1417.8	1432	dk	2	B
	Aug 26	1	0017	0034	m	3	H
			0017.5	0052	m	2	C
			0021	0041.2	dk	3	B
			0021	0052	dk	2	C
	Aug 29	1	2054	2100	m	1	H
	Sept 18	1	2338	2345	dk	3	B
	Sept 29	1	1547.8	1557.4	dk	3	B
	Oct 26	1	0612.5	0617	m	2	C
	Oct 31	1	1137	1139	m	1	
	Nov 4	1	1159	1208	m	1	
	Nov 8	1	0222	0227	m	2	C
			0222	0227.5	dk	2	C
	Nov 10	1	1833	1848	m	2	H
			1834+6	1840.2	dk	3	B
	Nov 12	1	2109.8	2112.1	dk	2	
	Nov 19	1	1043	1045	m	1	
			1046	1047	m	1	
	Nov 28	1	1428.1	1441.1	dk	3	B
	Dec 3	1	0854	0904	m	1	
	Dec 11	1	2357.5	2418	m	1	C
			2357.5	2424	dk	2	C
	Dec 13	2	0950	0954	m	1	
			1351	1400	m	1	

1967

Date	No.	Start	End	Code	Num	Type
Dec 16	1	0253.5	0320	m	2	C
		0253.5	0326	dk	2	C
Dec 17	1	1834	1841	m	2	H ⌉
		1843	1854	m	2	H ⌋
		1854.6	1900	dk	3	B
Dec 20	2	1524.6	1534	dk	2	B
		1814.5	1818.4	dk	3	B
Dec 27	1	0840	0857	m	1	

Date	No.	Start	End	Code	Num	Type
1968 Jan 2	1	0529	0544	m	2	C
		0532	0544	dk	2	C
Jan 4	1	2242	2248	m	3	H
Jan 5	1	−0459	0505	m	1	C
		0501	0506	dk	2	C
Jan 10	1	2152	2158	m	2	H
Jan 11	1	1702	1703	dm	1	H
		1703	1717	m	2	H
		1706	1710	dk	2	H, B
Jan 12		1812	1816	m	2	H
		1821	1823	m	2	H ⌉
		1822	1823	dk	2	H ⌋
Jan 14	1	2017	2032	m	2	H
		2019.3	2021	dk	?	Sg
		2019.5	2042.7	dk		B
Jan 15	1	0014	0020	m	1	
		0016	0038	dk	2	
Jan 17	1	0557.5	0602	m	1	C
		0557.5	0610	dk	2	C
Jan 29	1	1542.8		cm, dm		
		1540	1547	m	3	H

1968							
	Feb 1	4	1309	1311	dk		S$_g$
			1356.3	1400	dk		S$_g$
			1820	1824	m	2	H
			1919	1923	dm	3	H ⎤
			1921	1924	m	3	H ⎦
	Feb 2	1	0545.5	0547	m	2	
	Feb 8	1	1400		dm		
			1402	1405	m	3	H
	Feb 10	1	1624	1634	m	2	H
			1623.3	1625.3	dk		S$_g$
			1624.9	1632.2	dk	3	B)
			1624	1634	dk	2	H)
			1638	1640	m	1	H
			1638	1640	dk	1	H
	Feb 15	1	1505	1515	m	2	H
	Feb 16	1	2350	2353	m	2	H
	Feb 17	1	0300		cm		
			0258		dm		
			0259.5	0306.5	m	2	C
			0259.5	0306.5	dk	2	C
	Feb 21	1	2020	2022	dk		S$_g$
			2025	2030.6	dk		S$_g$
			2025.2	2038	dk	3	B
	Feb 25	1	0400	0422	m	1	C
	Feb 27	1	1949	1957	m	2	
1968	Mar 14	1	1012	1017	m	3	W
	Mar 21	5	1423	1440	m	3	H ⎤
			1441	1449	m	2	H ⎤
			1438.7	1454	dk	5	B ⎦
			1442	1447	dk		S$_g$ ⎦
			1525	1528	m	3	H)
			1916	1931	m	3	B ⎤
			1924.8	1933	dk	2	H ⎦
			2207	2212	m	2	H
			2215	2219	m	1	H
			2235.5	2240.3	dk	3	B

Year	Date		Time 1	Time 2			
1968							
	Mar 22	1	1200	1201	dm	1	W
	Mar 28	1	0331	0341	m	2	C
			0331	0346	dk	2	C
	Mar 30	2	1423	1425	dm	2	H
			1423	1432	m	2	H
			1526	1528	m	1	W
1968	April 1	1	1311.5	1318.5	m	3	W
	April 15	1	1326	1332	m	2	H
	April 19	1	1655	1700	dk		Sg
	April 26	1	1529	1534	dk	2	B
1968	May 3	1	2125		cm		
			2124		dm		
			2127	2133	dm	2	H
			2127	2143	m	3	H
			2128.5	2147	m	2	C
			2139.7	2146	dk	2	B
	May 8	1	1416		cm		
			1415		dm		
			1416	1419	dm	3	H
			1416	1419	m	2	H
			1416.1	1426	m	3	W
			1419	1434	m	1	H
	May 10	1	1941	1946	m	2	H
	May 21	1	2024	2036	dk	3	B
	May 31	1	before 2140	2144	m	1	B
			2140.4	2158	dk	2	B
1968	June 1	1	1628		cm		
			1627		dm		
			1630	1633	dm	2	H
			1631	1639	m	2	H
			1637.5	1643.6	dk	2	B
	June 3	1	2351.4	2359.1	dk	3	B

1968							
June 9	1	0107	0122	m	1	C	
		0112	0122	dk	1	C	
		0119	0119.5	m	2	C	
		0119	0119.5	dk	2	C	
June 11	1	0935		cm, dm			
		0936.7	0942.3	m	2	W	
June 17	1	0301.5	0326	m	1		
June 25	1	0608.5	0609.5	m	1		
June 26	1	2302	2306	m	2		
		2303	2306	dk	1		
		2303.3	2312.3	dk	3	B	
		2302	2316	m	2	C	
		2302	2316	dk	2	C	
July 2	1	0036.2	0037.7 g	dk	3		
July 5	1	2055.5	2114	dk	2	B	
July 7	1	0320	0329	m	1	C	
July 8	1	1708		cm			
		1707		dm			
		1910	1727	dm	3	H	
		1709	1732	m	3	H	
		1712	1732	dk	3	H	
		1715	1719	dk		Sg	
		1715.5	1751.4	dk	3	B	
Aug 3	1	0312		cm, dm			
		0316	0406	m	2	C	
		0318.5	0406	dk	2	C	
Aug 7	1	0241.5	0243	m	2	C	
		0253	0258	m	1	C	
Aug 11	1	2205	2211	m	2	H	
		2207	2210	dk	1	H	
		2205	2213.5	m	2	C	
		2206.5	2216	dk	2	C	
		2206.3	2210.5	dk		Sg	
		2208.3	2220	dk	3	B	
Aug 13	1	1257.5	1303	m	3	W	
		1300	1302	dm	2	H	
		1258	1308	m	2	H	

1968	Aug 14	1	1339	1348	m	2	H
			1340	1355	m	2	W
			1342	1354	dk		Sg
			1352	1400	dk		Sg
	Aug 21	1	0154	0200	m	1	C
	Aug 23	1	2348.5	2359	m	2	C
	Aug 29	1	0103	0118	m	1	C
			0106	0106	dk	1	
	Sept 1	1	1626.5	1635.7	dk	3	B
	Sept 4	1	0041	0054	m	2	H
	Sept 8	1	0339.5	0400	m	1	C
	Sept 9	1	1752	1800	m	2	H
	Sept 26	1	0034.2	0047	m	2	C
			0038	0047	dk	2	C
	Sept 29	1	1626.6	1636.2	m, dk	3	B
			1626	1636	dk		Sg
			1634	1644	dk		Sg
	Oct 2	1	2022	2029	m	1	H
			2024.6	2031.7	m	2	B
	Oct 3	1	2359.2	2427	m, dk	1	C
	Oct 4	1	2131.5	2143	m	2	C
			2133.5	2134.5	dk	2	C
			2132	2155	m	2	H
			2133	2138	dk	1	H
	Oct 6	1	1730	1744	m	3	H
			1733	1744	dk	2	H
			1731	1744.3	m		B
			1732.5	1741	dk		Sg
	Oct 11	1	1719	1722.8	dk		3
	Oct 23	1	2358	2417	m	2	C
			2409	2422	dk	2	C

1968	Oct 24	1	2057	2120	m	2	H
			2058.3	2119.4	m		B
			2058	2120	m	2	C
			2104	2120	dk	2	C
	Oct 28	1	1636	1642	m	2	H
			1638	1642	dk	2	H
			1638.1	1643.5	dk	3	B
	Oct 30	1	2359	2405	m	2	C
			2400	2405	dk	2	C
	Oct 31	1	0017.5	0021	m	2	C
			0017.8	0021	dk	1	C
	Nov 1	3	0851.7	0900.5	m	2	W
			1708	1709.5	dk		Sc
			2007	2011	m	2	H
	Nov 2	3	1003.5	1017.5	m	2	W
			1439.2	1444.2	m,dk	3	B
			1504	1518.2	mdk	3	B
	Nov 4	2	0231.5	0232.5	m	2	C
			0517	0550	mdk	3	C
	Nov 18	1	1026.5	1105	dm	3	W
	Dec 2	1	2114	2115	dm	2	H
			2114	2141	m	3	H
			2117	2141	dk	2	H
			2115	2143	m	2	C
			2116	2147	dk	2	C
			2116	2133.2	mdk	3	B
	Dec 11	1	1154	1155	m	2	W
	Dec 12	1	2314	2315	dm	2	H
			2314	2322	m	2	H
	Dec 13	1	0428	0444	m	2	C
	Dec 14	1	1010.2	1010.5	m	2	W
	Dec 23	1	1119.8	1126.5	m	2	W

1968	Dec 24	2	0642.5	0652	m	2	C
			2224	—	m	1	C -
			2230.5	2242	m	2	C
			2235	2247	dk	2	C
			2231	2242	m	2	H
			2233.7	2243.3	m,dk	3	B -
	Dec 25	1	0650.5	0658	m	2	C
	Dec 27	1	1055.5	1115	m	3	W
	Dec 28	1	2137	2144	m	1	C
	Dec 30	1	1433	1437	m,dk	2	B
1969	Jan 13	1	2105	2347	dk	3	B
	Jan 17	1 -	1705.6	1720	m	3	H
			1709	1720	dk	3	H
			1710	1715	dk		Sg
	Jan 18	1	0203.5	0210.5	m	2	C
	Jan 28	1	1819	1823	dk		Sg
	Feb 1	1	2138.5	2201	m	2	H
	Feb 2	1	0513	0520	m	1	C
	Feb 8	4	0021	0024	m,dk	1	C
			0418	0422	m	1	C
			1207.4	1221.5	m	3	W
			1752.8	1809	m	2	H -
			1757	1809	dk	2	H
			1754.3	1804.1	m,dk	3	B
			1757.2	1803	dk		Sg
	Feb 9	2	1435	1438	m	1	H
			1440.7	1444.6	m,dk	2	B
			1726	1728	dm	3	H -
			1726	1745	m	3	H
			1728	1745	dk	3	H
			1727.3	1739.4	m,dk	3	B
			1728	1733	dk		Sg
			1728	1739	dk		Sg -

1969	Feb 23	1	0447	0456	m	3	C
	Feb 24	1	2311.5	2329	m	2	C
			2315.5	2327	dk	2	C
			2316	2321.5	m, dk	3	C
	Feb 26	1	0425.5	0441	m	3	C
			0428.5	0444	dk	3	C
	Feb 27	1	1403	1405	dk		Sg
			1404.3	1432	m	2	W
			1404.5	1421	m	2	H
			1405.7	1514.4	m, dk	3	B
	Mar 1	1	2142	2151	dm, m	3	C
			2142	2159	m	2	B
			2149	2159	dk	2	B
	Mar 2	3	0258	0308	m	2	C
			0305	0307	dk	1	C
			0326.5	0329.5	m	1	C
			1115	1121	m	2	W
	Mar 3	1	2221.5	2231	m	3	C
			2221.7	2239	m	3	H
			2223.9	2238.3	m, dk	3	B
	Mar 12	1	1740.8	1741.4	dm	3	H
			1740.8	1759	m	3	H
			1742.3	1759.7	R, dk	3	B
			1745.5	1748	dk		Sg
	Mar 13	1	2117	2121	dk		Sg
	Mar 16	1	1930.1	1932.5	dk		Sg
	Mar 17	1	2340	2344	m	2	H
			2340	2344.5	m	2	C
	Mar 18	2	0651	0654	m	1	C
			2016.8	2019.2	dk		Sg
	Mar 21	2	0150	0203	m	2	C
			0154	0210	dk	2	C
			1319	1334	dk		Sg
			1332.3	1345	dk	3	Sg
			1334	1346	m	2	W

I

Boulder

University of Colorado
7.6 - 41.0 mHz

180 mHz → 10 m
40 mHz → 7.5 m

			start UT	end UT	intensity scale	frequency range
1967	May 3	Type II	1548.0	1603.5	3	11-41 mHz
		Type IV	1603.5	1650.3	2	13-41 mHz
	May 18	Type IV	1848.4	2040.0	2	20-41 mHz
	May 19	Type II	1537.2	1545.8	3	15-41 mHz
		Type IV	1537.2	1615.0	3	11-41 mHz
		IV	1615.0	1910.0	3	20-41 mHz
	May 20	IV	1513.5	16.00	3	9-41 mHz
		II	1527.0	1553.0	3	10-41 mHz
		IV	1600.0	1645.0	2	22-41 mHz
	May 21	IV	1922.1	2008.2	3	9-41 mHz
		IV	2008.2	2180.6	3	20-41 mHz
	May 23	IV	1837.0	1900.0	2	24-41 mHz
		II	1843.4	1900.0	3	11-41 mHz
1967	June 9	II*	2525.0	2543.0	1	22-41 mHz
	June 13	II	2034.7	2041.1	1	27-39 mHz
	June 18	II	1600.0	1602.9	1	32-41 mHz
	June 22	II	2453.5	2510.0	3	16-41 mHz
		IV	2510.0	after 2603	2	21-41 mHz

* maybe what they label as
"continuum" - a continuum burst
associated with Type II storms,
often with reverse drift
bursts, sometimes with
storms in metric λ

type IV ≡ continuum burst following a
major outburst of II or III associated
with flares.

intensity:
1 3×10²² - 2×10²¹
2 2×10²¹ - 8×10²⁰   watt Hz⁻¹
3 8×10²⁰ - 1.1×10²⁰   m²

1967	June 23	IV	1900.9 — 2105.8	3	18-41 mHz
	June 28	IV	before 2041.0 — 2220.0	3	20-41 mHz
1967	July 5	IV	1907.3 — 2120.0	2	26-41 mHz
	July 11	IV	2037.0 — 2150.0	1	26-41 mHz
	July 12	IV	1805.0 — 1836.0	1	27-41 mHz
	July 23	IV	2120.4 — 2303.8	3	26-41 mHz
	July 25	IV	2312.5 — 2615 after	3	22-41 mHz

not observing

may 26	1450 - 0630
June 6	1911 - 1950
June 8	1810 — 2133
June 21	1259 - 2000
June 25	1646 - 1721

routinely observe
1400-2400 UT daily

HARVARD RADIO ASTRON. STATION
FT. DAVIS, TEXAS

1967	May 3	IV	1541 – 1552	2	m, dm
		II	1547 – 1602	3	m
	May 19	IV N	1533 – 1537	2	dm
		IV N	1531 – 1550	2	m
		II	1535 – 1555	3	m
	May 20	II	1520 – 1536	3	m
	may 21	II	1923 – 1945	3	m, dk
		IV	1923 – 2100	2	m, dm
	May 23	II	1838 – 1842	3	dm
		II	1838 – 1905	3	m
		II	1846 – 1905	2	dk
		IV	1839 – 2252	3	dm
		IV	1839 – 2320	3	m
		IV	1846 – 2300	2	dk
	May 25	IV	before 1230 – 1520	3	dm
		IV	before 1230 – 1600	3	m
		IV	1520 – 1600	2	dm
		IV	1600 – 1640	2	m
		IV	1600 – 1640	1	dm

N - intermittent activity

1967	June 18	II	1550 — 1602	2	m
	June 23	II	0050 — 0058	2	m
1967	July 28	II	1607 — 1616	2	m

KULGOORA SOLAR OBS.

1967	May 26	II	0204.5 — 0212	2	m
		II	0204.5 — 0228	1	dk
		II	0212 — 0228	1	m
	May 28	II	0539 — 0556	2	m
		II	0545 — 0552	1	dk
1967	June 3	IV	0235 — 0450	3	m
		II	0243 — 0250	2	m
		II	0244 — 0256.5	2	dk
	June 23	II	0050 — 0100	1	m
		II	0054 — 0105	1	dk
1967	July 29	II	0413 — 0419	2	m

TIMES OF NO OBSERVERS

1967 May 1 0706 - 1245   1967 June 1 0639 - 1230

2   0702 - 1245
3   0645 - 1245
4   0701 - 1245
5   0659 - 1245
6   0658 - 1245
7   0703 - 1245
8   0425 - 0458   0645 - 1245
9   0701 - 1245
10 0701 - 1245
11 0701 - 1245
12 0651 - 1245
13 0432 - 0450   0705 - 1245
14 0700 - 1245
15 0648 - 1245 -
16 0702 - 1245
17 0705 - 1245
18 0700 - 1245
19 0700 - 1245
20 0700 - 1231
21 0700 - 1230
22 0700 - 1231
23 0652 - 1230
24 0630 - 1230
25 0712 - 1230
26 0654 - 1230
27 0705 - 1231
28 0711 - 1230
29 0656 - 1230
30 0700 - 1400
31 0629 - 1400

seems
representative

no obscures duty from

Culgoora   0000 - 0700
              2000 - 2400

Harvard   0000 - 0130   UT
              1230 - 2400

Boulder   1230 - 2400

Sagamore   1100 - 2200

Weissnau   ~0730 - 15:30

1967

Date						
May 3	IV	1541	1552	2	#	m,dm
	II	1547	1602	3	#	w
	II	1548	1603.5	3	B	w
	IV	1603.5	1650.3	2	B	w
May 18	IV	1848.4	2040.0	2	B	w
May 19	IV	1531	1550	2	H	w
	IV	1535	1537	2	H	dm
	II	1535	1555	3	H	w
	II	1537.2	1545.8	3	B	w
	IV	1537.2	1615.0	3	B	w
	IV	1615.0	1910.0	3	B	w
May 20	IV	1613.5	1600	3	B	w
	II	1520	1536	3	H	w
	IV	1527	1553.9	3	B	w
	IV	1600	1645.0	2	B	w
May 21	IV	1922.1	2008.2	3	B	w
	II	1923	1945	3	#	m,dk
	IV	1923	2100	2	#	m,dm
	IV	2006.2	2130.6	3	B	w

Year						
1967						

Date						
May 23	IV	1537.0	1906.0	2	m	B
	II	1838	1842	3	dm	#
	II	1838	1905	3	m	#
	IV	1839	2252	3	dm	#
	IV	1839	2320	3	m	#
	II	1843.4	1900.0	3	dk	B
	II	1846	1905	2	dk	#
	IV	1846	2300	2	dk	#
May 25	IV	before 1230	1520	3	dm	#
	IV	before 1230	1600	3	m	#
	IV	1520	1600	2	dm	#
	IV	1600	1640	2	m	#
	IV	1600	1640	1	dm	#
May 26	II	0204.5	6212	2	m	C
	II	0204.5	0228	1	dk	C
	II	0212	0228	1	m	C
May 28	II	0539	0556	2	n	C
	II	0545	0552	1	dk	C
June 3	IV	0235	0450	3	n	c
	II	0243	0250	2	m	c
	II	0244	0256.5	2	dk	c

1967

Date		Before	After		No.			
June 9	II*	2525.0	2543.0		1		m	B
June 13	II	2034.7	2041.1		1		m	B
June 18	II	1550	1600		2		m	H
	II	1600.0	1662.9		1		m	B
June 23	II	0050	0100		1		m	C
	II	0050	0058		2		m	H
	II	0054	0105		1		dt	C
	II	0063.5	0110.0 after		3		m	B
	IV	0110.0	0203		2		m	B
	IV	1900.1	2105.8		3		m	B
June 28	IV	before 2041.0	2220.0		3		m	B
July 5	IV	1907.3	2120.0		2		m	B
July 11	IV	2037.5	2150.0		1		m	B
July 13	IV	1805.0	1836.0		1		m	B
July 23	IV	2120.4	2303.8		3		m	B
July 25	IV	2312.5	after 2615		3		m	B

1967							
July 28	II	1607	1616	2	m	#
July 29	II	0443	0411	2	m	c
Aug 1	III	0059	0159	1	m	c
	III	0059	0122	1	dk	c
	II	0120	0122	3	dm	#
	II	0120	0123	2	m	#
	II	0126	0130	1	m	#
	III	0350	0644	1	m	c
	III	0350	0634	1	dk	c
	II	1735	1738	2	m	#
Aug 9	III	0139	0203	1	m	c
Aug 12	III	0056	0511	1	m	c
	III	0056	0435	1	dk	c
Aug 15	#	0232	0240	1	m	c
	II	0233	0242	1	dk	c
	III	2300	2400	1	dk	c
Aug 16	III	0000	0213	1	dk	c

1967

Date		Time	Time				
Aug 18	III	2130	2151	2	m	#	
	II	2133	2140.2	1	m	C	
	II	2136	2159.2	2	dk	B	
Aug 19	IV	0002.8	0036	2	dk'	B	
	II	0020.8	0029	2	dk	B	
	II	0615	0620	1	m	C	
Aug 25	III	144	1432	1	N	#	
	II	1417.8	1432	2	dk	B	
Aug 26	IV	0017	0025	3	m, dm	#	
	II	0017	0034	3	m	#	
	IV 2	0017	0039	2	m, dm	#	
	III #	0017.5	0052	2	dk	C	
	III #	0021	0052	2	dk	C	
	II	0031	0041.2	3	dk	B	
	IV	0043.3	0111.2	2	m, dm	B	
	IV	0045	0052	2	m, dm	#	
	IV	0052	0113	3	m, dm	#	
Aug 29	II	2054	2100	1	m	#	
Sept 17	IV	before 1244	1433	3	dk	B	

1967

Date		Reading 1	Reading 2		Count		
Sept 18	IV	2335.4	after 2437		3	dk	B
	II	2338	2345		3	dk	B
Sept 29	II	1547.8	1557.4		3	dk	B
Oct 25	IV	1838	1405		3	m, dm	#
	IV	1420	1443		3	m, dm	H
	IV	1443	1454		2	m, dm	H
Oct 26	II	2612.5	2617		2	m	C
Nov 8	II H	6222	6227		2	m, dk	C
Nov 10	IV	1749	1834.2		1	dk	C
	II	1833	1648		3	m	H
	IV	1834.2	1912		2	dk	B
	II	1834.6	1840.2		3	dk	B
Nov 26	IV	1444	1504		1	dm	# horizontal striation 1444~1456
	IV	1568	1610		3	dm	H
	IV	1511	___		1	m	#
	IV	1617	1649		1	dm, m	H

1967						
Nov 28	II	1428.1	1444.1	3	dk	B
	IV	1526.8	1610.6	3	dk	B
Dec 11	II	2357.5	2918	1	w	C
	II	2357.5	2424	2	dk	C
Dec 13	IV	before 1356	1543	3	dk	B
	IV	1543	1617	1	dL	B
Dec 16	II H	0253.5	0320	2	w	C
	II H	0253.5	0326	2	dk	C
Dec 17	II	1838	1841	2	w	H
	II	1843	1854	2	w	H
	II	1854.6	1900	3	dk	B
	IV	1900	1908	3	dk	B
	IV	1908	1935	1	dk	B
Dec 20	II	1524.6	1534	3	dk	B
	IV	1534	1622.2	2	dk	B
	II	1814.5	1818.4	3	dk	B

1968						
Jan 2	II	0529	0544 }	2	m	C
	II	0532	0544 }	2	dk	C
Jan 4	II	2242	2248	3	m	H
Jan 5	II	0459	0505 }	1	m	C
	II	0501	0506 }	2	dk	C
Jan 10	II	2152	2158	2	m	H
Jan 11	II	1702	1703 }	1	dm	H
	II	1703	1717 }	2	m	#
	II	1706	1710	2	dk	H
	IV	1705	1845	2	dk	B
	II	1706	1710	2	dk	B
Jan 12	II	1812	1816	2	m	#
	II	1821	1823	2	m	#
	II	1823	—	1	dk	#
Jan 13	IV	1849.3	1918.5	1	dk	B
Jan 14	IV	1835.5	1911	2	dk	B

Date		Time 1	Time 2	No.		
1968						
Jan 14	II	2017	2032	3	m	H
	II	2019.3	2021		dk	Sg
	II	2019.5	2042.7		dk	B
	IV	2021	2036	2	dk	Sg
	IV	2042.7	2304		dk	B
Jan 17	II	0557.5	0602	1	m	C
	II	0557.25	0610	2	dk	C
Jan 29	II	1540	1547	3	m	H
Feb 1	II	1309	1311		dk	Sg
	II	1356.3	1400	2	dk	Sg
	II	1820	1824	3	m	H
	II	1919	1923	3	dm	H
	II	1921	1924		m	H
Feb 2	II	0545.5	0548	2	m	C
Feb 3	IV	1336	1340		dk	Sg
Feb 4	II	1347	1348.8		dk	Sg
Feb 8	II	1402	1405	3	m	H

1968						
Feb 10	II	1623.3	1625.3	3	dk	SS/B
	II	1624.9	1632.2	2	dk	#
	II	1629	1634	2	n,dk	#
	IV	1627	1714	3	dm	#
	IV	1632.2	1715	1	dk	B
	II	1638	1640	1	n,dk	#
	IV	1715	1801.1		dk	B
Feb 14	IV	1537	1545	2	dk	SS/B
	IV	1537.1	1555		dk	
Feb 15	II	1505	1515	2	n	#
Feb 16	II	2350	2353	2	m	#
Feb 17	II MB	0257.5	6306.5	2	m,dk	C
Feb 21	II	2020	2020	3	dk	SS
	II	2025	2030.6		dk	SS/B
	II	2025.2	2038		dk	
Feb 25	II	0900	0422	1	m	C

Date		Start	End	No.			
Mar 14	II 6	1012	1017	3	m	3	
Mar 20	IV	2300	after 2502	3	dk	B	
Mar 21	II	1423	1440	3	m	#	
	II	1438.7	1454	3	dk	B	
	IV	1440	1453	2	dk	Sp	
	II	1441	1449	3	m	A	
	II	1442	1447	3	d/c	Sp	
	II 6	1525	1528	3	m	B	
	II	1916	1931	2	dk	H	
	II	1924.8	1933	2	m	H	
	II	2207	2212	1	m	#	
	II*	2215	2219	3	dk	B	
	II*	2235.5	2240.3				
Mar 22	II 6	1200	1201	1	dm	W	
Mar 28	II*	0331	0341	2	m	C	
	II*	0331	0346	2	dk	C	
Mar 30	II	1423	1425	2	dm	#	
	II	1423	1432	2	m	#	
	II	1526	1528	1	m	W	
	IV	2115	2230		dk	Sp	

1968

Date		Time 1	Time 2	Count		
Apr 1	IV 8	1307.3	1311	1	w	w
	II 8	1315.5	1318.5	3	n	w
Apr 2	IV cont	1614.5	1615.5	3	n	w
Apr 15	II	1326	1332	2	n	H
Apr 19	II	1655	1700		dk	sg
	N	1700	1800		dk	sg
Apr 22	IV	1436	1630	1	dk	B
	IV	1752.5	1859	1	dk	B
Apr 26	II	1529	1534	3	dk	B
May 3	IV	1446	1446.3	2	dk	sg
	II	2127	2133	3	dm	H
	II/II	2127	2143	2	n	H
	II/II	2128.5	2147		n	C
	IV	2131	2400	1	n	C
	II	2139.7	2146	2	dk	B
May 4	IV	0000	0659	1	n	C
	IV	1200	1800		dk	sg

1968

Date						
May 8	II	1416	1419	3	dm	#
	II	1416	1419	2	m	#
	II	1461	1426	3	m	3
	II	1419	1434	1	m	#
May 10	II	1941	1946	2	m	#
May 13	IV	2131	2159.6	2	dc	B
May 21	II	2024	2036	3	dc	B
	#	2025.4	2032		dc	Sq
	#	2033	20368		dc	Sq
May 29	IV	1550	1633	2	dc	B
May 30	II	2404	2158	2	dk	B
June 1	II	1630	1633	2	dm	#
	II	1631	1630	2	m	#
	#	1637.5	1643.4	2	dk	B
June 3	II	2351.4	2359.1	3	dk	B
	IV	2355.4 .0149		2	dk	B

1968

Date						
June 8	IV	1457	1851		dk	Sg
June 9	II	0107	0122	1	m	c
	II	0112	0122	1	dk	c
	III	0119	0114.5	2	m, dk	c
	IV	0839	0940	3	dm	W
	IV	0960	0910.3		dk	Sg
June 11	II	0936.7	0942.3	2	m	W
June 26	II	2362	2316	2	m, dk	c
	II	2302	2311		dk	Sg
	II	23033	2312.3	3	dk	B
July 1	IV	1510	1527		dk	Sg
July 5	IV	2042.7	2150	1	dk	B
	II	2055.5	2114	2	dk	B
July 6	IV	0944.6	1004	3	dm	W
July 7	II	0320	0329	1	m	c

1968

Date						
July 8	II,N	1708.6	1745	3	m	W
	III	1710	1727	3	dm	H
	III	1709	1732	3	m	H
	III	1712	1732	3	dk	H
	III	1715	1719		dk	Sg
	III	1715.5	1751.4	3	dk	B
	IV	1715.8	1906	3	dk	B
	IV	1750	1745	3	dm	H
	IV	1739	1746	3	dk	H
	IV	1732	1830		m	Sg/H
	IV	1903	1920	2		Sg
July 12	W	1404	1445		dk	Sg
Aug 3	H	0316	0406	2	m	C
	H	0318.5	0406	2	dk	C
Aug 7	II	0291.5	0293	2	m	C
	H	0253	0258	1	m	C

1968						
Aug 11	II	2205	2211	2	m	#
	II	2207	2210	1	dk	#
	II	2205	2213.5	2	m	c
	II	2206.5	2216	2	dk	c
	II	2206.3	2210.5		dk	sg
	II	2208.3	2220	3	dk	B
Aug 13	IV	1254.2	1255.7	2	m	w
	II	1257.5	1303	3	m	w
	II	1300	1302	2	dm	#
	II	1258	1308	2	m	#
Aug 14	II	1339	1348	2	h	#
	II	1346	1355	2	m	w
	II	1342	1354		dk	sg
	II	1352	1400		dk	sg
Aug 16	IV	1125	1900		dk	sg
Aug 18	II	1337.1	1347	2	m	w
Aug 21	II	0154	6200	1	m	c
Aug 23	II	2349.5	2359	2	m	c

1968	Date		Time	Time	Count		
	Aug 29	II	0103	0118	1	m	c
	Sept 1	II	1626.5	1635.7	3	dk	B
		IV	1629	1745		dk	Sg
		IV	1635.7	1837.6	3	dk	B
	Sept 4	IV	0033	0054	2	m,dm	H
		II	0041	0054	2	m	H
	Sept 8	II	0339.5	0400	1	m	c
	Sept 9	II	1752	1800	2	m	H
	Sept 26	II	0034.2	0047	2	m	c
		II	0038	0047	2	dk	c
	Sept 29	II	1626	1636	3	dk	Sg/B
		II	1626.6	1636.2		m,dk	B
		II	1634	1644		dk	Sg
		IV	1636.2	1650	3	m,dk	B

1968

Date						
Oct 2	IV	2018.2	2054	2	m	B
	II	2022	2029	1	n	A
	II	2024.6	2031.7	2	m	B
	IV	2054	2200	1	m	B
Oct 3	II	2359.5	2227	1	m, dk	C
Oct 4	II	2131.5	2143	2	m	C
	II	2133.5	2134.5	2	dk	C
	II	2132	2155	2	m	H
	II	2133	2138	1	dk	H
	IV	2135	2145	2	dm	H
	IV	2135	2155	3	m	H
Oct 6	II	1730	1744	3	m	H
	II	1733	1744	2	dk	H
	II	1731	1744.3		m	B
	II	1732.5	174		dk	Sg
	IV	1744.3	1758		n	Sg
Oct 11	II	1719.8	1722.8		dk	Sg

Date						
1968						
Oct 23	II	2358	2417	2	m	C
	II	2469	2422	2	dk	C
Oct 28	IV	0003	0055	1	m, dk	C
	IV	2055	2100	3	dm	H
	IV	2059	2106	3	m	H
	II	2057	2120	2	m	H
	II #	2058	2120	2	m, dk	C
	II N	2104	2120	2	dk	C
	II	2058.3	2119.4	2	m	B
	IV	2119.4	2200	3	m	B
	N	2129	2227	1	m	C
Oct 27	IV	1307	1534	2	dm	B
	IV	before 1312	1651	3	m	B
	N	before 1330	1830		m, dm	H
Oct 28	II	1636	1642	2	m, dk	H
	II	1638	1642	2	dk	#
	II	1638.1	1643.5	3	dk	B

P168

Date		Time	Time	Count	Code	Symbol
Oct 29	IV	1225	1540	3	dm	3
	IV	1252	2200		dk	Sg B
	IV	before 1311	1524	3,2	m	±
	IV	before 1328	1440	2,1	m, dm	±
	IV	1440	1516	3	m, dm	3
	IV	1516.7	1539	3	dm	±
	IV	1516	1547	3	dm	#
	IV	1516	1538		m	
Oct 30	IV	1255 before 1328	1545	2	m	3
	IV		1917	2	dm	±
	IV	1350	1630		dk	Sg
	IV	2145	2340	2	dm	#
	II	2359	2405	2	m	C
	II	2400	2405	2	dk	C
Oct 31	IV	0002.5	0035	1	m	C
	II	0017.5	0021	2,1	m, dk	C
	IV	2247	2315	2,2	dm	#
	IV	2247	2307	3	m	M

1968						
Nov 1	II	0851.7	0900.5	2	m	3
	IV	0853	0915	1	dw	3
	IV	0925	0952	2	dw	3
	II	1708	1709.5		dk	S??
	IV	1717	1723		dk	S-4
	II	2007	2011	2	m	
Nov 2	IV	1001.2	1028.4	3	dw	3
	II	1003.5	1017.5	2	m	3
	II	1439.2	1444.2	3	m,dk	B
	II	1504	1518.2	3	m,dk	B
	IV	1518.2	1607	3	m,dk	B
Nov 4	II	0231.5	0232.5	2	m	c
	II H	0517	0550	3	m,dk	c
Nov 11	IV	1457.4	1538	2	m,dk	B
Nov 18	IV	1026.5	1050	3	dw	3
	II	1026.5	1105	3	dw	3

1968

Date						
Dec 2	II #	2114	2115	2	dm	#
	III	2114	2141	3	m	#
	II	2117	2141	2	dk	#
	II #	2115	2143	2	m	C
	II #	2116	2147	2	dk	C
	II	2116	2133.2	3	m, dk	B
	IV	2117.5	2152	3	m, dk	B
Dec 11	IV	1144	1210	2	m	3
	II	1154	1155	2	m	3
Dec 12	II #	2314	2315	2	dm	#
	II #	2314	2322	2	m	#
Dec 13	II #	0428	0444	2	m	C
Dec 14	II	1610.2	1012.5	2	m	3
Dec 23	II	1119.8	1126.5	2	m	3
Dec 24	II	0622.5	0652	2	m	C
	III	2224	2224.5	1	m	C
	IV	2229	23478	3	dk	B
	II #	2230.5	2242	2	m	C
	II #	2235	2247	2	dk	C
	II	2231	2242	2	m	#
	II	22337	2203.3	3	m, dk	B

1968						
Dec 25	II	0659.95	0658	2	m	C
Dec 27	II	1055.5	115	3	m	3
	IV	1100	1400		dk	Sg
Dec 28	II	2137	2144	1	m	C
Dec 30	II	1433.6	1437	2	m, dk	B
1969						
Jan 13	IV	2105	2347	3	dk	B
	II	2229.4	2249.8	3	dk	B
Jan 17	IV	1705.2	1709	3	dk	Sg
	IV	1705.4	1737		m, dk	B
	II 6	1716	1715	3	dk	Sg
	II	1705.6	1720	3	m	H
	II	1709	1720		dk	H
Jan 18	II	0203.5	0210.5	2	m	C
Jan 23	IV	1100	1500		dk	Sg
Jan 28	II	1819	1823		dk	St

Date		Time 1	Time 2	No.	Wx	Code
1969						
Feb 1	II	2158.5	2201	2	m	H
	II	2138.5	2203	2	m	C
Feb 2	II	0513	0520	-	m	C
Feb 8	II	0021	0024	-	m, dk	C
	II	0418	0422	1	m	C
	IV	1205	1210	1	m	W
	II	12074	1226.5	2,3	m	W
	IV	1504.8	1504.7	1	dw	W
	II	1752.8	1809	2	m	H
	II	1757	1809	2	dk	H
	II	1754.3	1804.1	3	m, dk	B
	II	17572	1805		dk	Sβ
	IV	1804.1	1814	3	m, dk	B
	IV	1814	1900	2	m, dk	B
Feb 9	II	1435	1435	-	m	H
	II	1440.7	1444.6	2	m, dk	B
	II	1726	1728	3	dw	H
	II	1726	1745	3	m	H
	II	1728	1745	3	dk	H
	II	17243	1734.4	3	m, dk	R
	II	1728	1733		dk	Sβ
	IV	1728	1739	3	dk	Sβ

1969

Date		Time	Time		Code	
Feb 15	IV	1445	1527		dk	Sg
Feb 23	II	ca47 0457	0456	3	m.	C
Feb 24	IV	2307.7	at14 2430	3	m, dk	8
	IV	2308	2400	3	dm, m	H
	III	2315.5	2329 ?	2	m	C
	III	2315.5	2327	2	dk	C
	II	2316	2321.5	3	m,dk	C
Feb 25	IV	6000	0015	3,2	dm, m	H
	IV	0904	1130	3	m	W
	IV	1651	1702	3	dm, m	H
	IV	1937	1948	3	dm	H
	IV	1934	1946	3	m	H
Feb 26	II	ca25.5	ca25.5 0441	3	m	C
	II	ca28.5	ca44	3	dk	C

1969						
Feb 27	II	1403	1405	dk		Sg
	II	1409.3	1432	w	2	w
	II	1404.5	1421	w	2	H
	IV	1405.3	1458	m,dk	3	B,B
	II	1405.7	1514.4	m,dk	3	B
	IV,N	1407	1454	dw	2	H
	IV,N	1409	1450	n	2	H
	IV	1458	1525	dk		Sg
	IV		1531	m,dk	2	B
Mar 1	II	2142	2151	dm,m	3	d
	II	2142	2159	m	2	B
	II	2149	2159	dk	2	B
Mar 2	II	0258	0308	m	2	C
	II	0305	0307	dk	1	d
	II	0326.5	63245	m	1	d
	II	115	1121	m	2	w
Mar 3	II	2221.5	2231	m	3	d
	II	2221.7	2222.9	n	3	H
	II	2223.9	2233.3	m,dk	3	B

Date						
1269						
Mar 11	IV	1751	1806		dk	Sg
Mar 12	I	1740.8	1741.4	3	dm	11
	II	1740.8	1759	3	2	14
	IV	1741	1747	3	dm	11
	IV	1741	1748	2	m	H
	II	17423	1759.7	3	m,dk	B / Sg
	IV	1745.5	1748		dk	Sg
	IV	1756.5	2000		dk	
	IV	1759.7	2035	3	m,dk	B
Mar 13	II	2417	2121		dk	Sg
Mar 16	II	1930.1	1932.5	2	dk	Sg
	IV	2006	2129		m,dk	B
Mar 17	II	2340	2344.3	2	m	11
	II	2340	2344.5	2	m	C
Mar 18	II	1590	0654	1	m	C
	II	2016.8	2014.2		dk	Sg
Mar 20	IV	1100 before 1315	1800		dk	Sg
	IV	1730		3	dk	B

1969

Date		Start	End			
Mar 21	I	0150	0203	2	~	c c 3
	II	0154	0210	2	dk	c d
	IV	0821.5	0824.2	2	~	3 B
	IV	before 1315	1840	3	m, dk	Sg
	III	1319	1334		dk	3
	II	1323.5	1345	3	m	Sg
	II	1332.3	1345	3	dk	3
	II	1334	1346	2	m	Sg
	II	1345	2300		dk	3
Mar 22	IV	0643.5	0655	2	m	c c
	II	0644.5	06475	2	h	c
	II	0646.5	0655	2	m	c
	III	0653	0655	1	dk	3
	II	0646.6	0657	3	m	
Mar 23	IV	1500	1800		dk	Sg
Mar 27	II	1326	1330.3	2	dk	Sg
	IV	1329	343	2	dk, m	H
	II	1331	1339	3	m	h B
	IV	1336.7	1515		m, dk	Sg
	II	1503	1508.5		dk	

1969

Mar 30

II	"	6250.5	0318	)		1	dk	c
II	H	6257	0259			ı	dk	c
II		6367	0318			ı	dk	c

1967	May 3	IV	1541	1541	.	cm, dm	H			
		IV	1541	1552	2	m	H			
		II	1547	1602	3	m	H, B	107000 Ⓐ	1543→1608 } type IV	
		II	1548.0	1603.5	3	dk	H, B	2800 Ⓑ	1543→1544	
		IV	1603.5	1650.3	2	dk				
	May 18	IV	1848.4	2040.0	2	dk				
	May 19	IV	1533	1537	2	m	H			
		IV	1531	1550	2	m	H			
		II	1535	1555	3	m	H	Ⓐ 1527.4→1532.7		
		II	1537.2	1545.8	3	dk	B	Ⓑ 1524.5→1533		
		IV	1537.2	1615.0	3	dk	B			
		IV	1615.0	1910.0	3	dk				
	May 20	IV	1513	1513		cm, dm				
		IV	1513.5	1600.0	3	dk		1513.7→1520.4	III	1B flare SID 1
		II	1520	1536	3	m	H	1513.5→1520.6		
		II	1527.0	1553.0	2	dk	B			
		IV	1600.0	1645.0	2					
	May 21	IV	1922.1	2008.2	3	dk	B	Ⓐ 1922.7→1925.3	III	2N flare SID 2
		IV	1923	2100	1	m	H	Ⓑ 1922→1929.2		
		II	1923	1945	3	m, dk				
		IV	2008.2	2130.6	3	dk				
	May 23	IV	1537.0	1900.0	2	dk				
		II	1838	1905	3	m	H	Ⓑ 1835.5→1952	IV	2b flare SID #3
		II	1846	1905	2	dk	H			
		II	1843.4	1900.0	3	dk	B			
		IV	1839	2320	3	m	H			
		IV	1846	2300	2	dk	H			
		IV	1900.0	2052.2	2	dk	B			
		IV	2052.2	2400	3	dk	B			
	May 24	IV	1813.0	1913.2	3	dk				
	May 25	IV	1230	1600	3	m				
		IV	1207			dm				
		IV	1600	1640	2	m				
	May 26	II	0204.5	0212	2	m		0158→0214.3 (9400 MHz)		2N flare SID 2
		II	0204.5	0228	1	dk		0155→0214.6 (2000 MHz)		
		II	0212	0228	1	m				
	May 29	IV	1904.4	2036.0	2	dk				
	May 28	II	0539-0556	m c				0529.3→0541.8 17000 MHz	II	2B flare SID 3
		II	0595-0552	dk c				0528.8→0541.7 5000 MHz		

from S 6D

								MHZ			
1967	June 3	IV	0235	0450	m	3					
		II	0243	0250	m	2					
		II	0244	0256.5	dk	2					
	June 18	II	1555	1602	m	2	H, B				
		IV	1600	1602.9	dk	1	H, B				
	June 23	II	0050	0058	m	2	H, B	9400	0037→0046.3	III	1 N flare
		II	0053.5	0110.0	dk	3	H B	3750	0037→0046.3		
		II	0050	0100	m	1	C				
		II	0054	0105	dk	1	C				
		IV	0100	0203	dk	2					
		IV	1901	2105.8	dk	2	B				
	June 28	IV	<2041.0	2220.0	dk	2					
1967	July 5	IV	−1907.3	2120.0	dk	2					
	July 23	IV	2120.4	2303.8	dk	3		8800	2113→2114.7		
								B	2113→2114.7		
	July 25	IV	2312.5	2400 after	dk	3		9400	2314→2317.9	III	
								B	2316.2→2318		
	July 26	IV	0000	0215 after	dk	3	B				
	July 28	II	1607	1616	m	2		9139	1604→1621	III	
								B	1603→1605		
	July 29	II	0413	0419	m	2		9400	0355→0422		
								3750	0405→0440		2h flare
1967	Aug 1	II	0120.5		dm			9400	0117.5→0118.4	III	
		II	0120	0123	m	2		2700	0117→0118.5		
		II	0126	0130	m	1					
		II	1735	1738	m	2		8800	1729→1731.2	III	2B flare
								3000	1730→1731.4		SID 2
	Aug 15	II	0232	0240	m	1		9400	0250−0410	III/II	
		II	0233	0242	dk	1		3750	0210−0400		
	Aug 18	II	2130	2151	m	2		10700	2119.7→2128.7		SID
		II	2133	2146.5	m	1		2800	2120→2129		2−
		II	2136	2159.2	dk	2					
	Aug 19	IV	0002.8	0036	dk	2		9400	→2401.5		2N flare
		II	0020.8	0029	dk	2		2700	2359→2401		
		II	0615	0620	m	1					

MHZ

Year	Date	Type						MHz		
1967	Aug 25	II	1414	1432	m	1		8800	1405–1421.5	1B flare
		II	1417.8	1432	dk	2		2800	1412–1413	S10 1
	Aug 26	IV	0013		cm					1B
		IV	0016		dm			9400	0013–0025 ⎱ IV	flare
		IV	0017	0025	m	3		2700	0014–0016.7 ⎰	
		II	0017	0034	m	3				
		IV	0017	0039	m	2				
		II	0017.5	0052	m	2	Herringbone			
		II	0021	0052	dk	2	Herringbone			
		II	0021.3	0041.2	dk	3				
		IV	0043.3	0111.2	dk	2		2700	0045.5—0051.5	
		IV	0045	0052	m	2				
		IV	0052	0115	m	3				
	Aug 29	II	2054	2100	m	1		8800	2050.8–2051	1B flare
								2800	2046—2053.2	S10 2-
1967	Sept 17	IV	before 1244	1433	dk	3	B			
	Sept 18	IV	2335.4	after 2437	dk	3	1	9400	2320–2355	2b
		II	2338	2345	dk	3		2700	2320–2358.0	flare
	Sept 29	II	1547.8	1557.4	dk	3		200	1541.1–1543.2	
1967	Oct 25	IV	1338	1405	m	3		3000	1335–1345 IV	
		IV	1480	1443	m	3				
		IV	1443	1454	m	2				
	Oct 26	II	0612.5	0617	m	2		9375	0612.5–0613 ⎱ III	1B flare
								3100	0609–0610.5 ⎰ V	
	Oct 27	IV	1320	1335 g	m	11				S10 1
	Oct 31	II	1137	1139	m	1		9139	1125–1126.8 ⎱ III	2N flare
								3000	1124–1125.2 ⎰	
1967	Nov 2	IV	0854	0910 g	m	1		15000	0857–0858 ⎱ IV	2B flare
								3000	0854.0–0856.3 ⎰	S10 2+
	Nov 4	IV	1152	1156 b	m	1		9100	1152.2–1153.27 ⎱ V	1B flare
		II	1159	1208 jg	m	1		3000	1151.9–1153.9 ⎰	S10 1-
	Nov 8	II	0222	0227	m	2	Herringbone			
		II	0222	0227.5	dk	2	" "			

MHz

1967										
Nov 10	IV	1749	1834.2 dk	1			2800	1821 – 1834		SID 1
	II	1833	1848	2						
	IV	1834.2	1912 dk	2						
	II	1834.6	1840.8 dk	3						
Nov 12	II	2109.8	2112.1 g dk	2						
Nov 19	II	1042	1045 7 m	1			9100	1023.2 – 1049.2		
	II	1046	1047 8 m	1			3000	1025 – 1033		
Nov 25	IV	1138	1139 b m	1			239	1137.1 – 1137.3 III		Sa flare
Nov 26	IV	1444	1504 m	1	hard					
	IV	1508	1610 m	2						
	IV	1617	1649 m	1						
Nov 28	II	1428.1	1441.1 dk	3						
	IV	1528.8	1610.6 dk	3			4995	1533.7 – 1537.6 III		

1967										
Dec 3	II	0854	0904 g m	1						
Dec 11	II	2357.5	2418 m	1			9400	2350 – 2355.0		1B flare
	II	2357.5	2424 dk	2			2000	2346 – 2355.3		SID 1
Dec 13	II	0950	0954 m	1			9100	0944.7 – 0947.8 } II		SN flare
	II	1351	1400 m	1			3000	0943.8 – 0945.8 }		
	IV	1356	1543 dk	3						
Dec 16	II	0253.5	0320 m	2	Herringbone	9400	0246 – 0251.9		3N flare
	II	0253.5	0326 dk	2	"	2000	0246 – 0347		SID 1
Dec 17	II	1838	1841 m	2			15400	1834.8 – 1839.5		SID 1
	II	1843	1854 m	2			2800	1834 – 1839.5		
	II	1854.6	1900 dk	3						
	IV	1900	1908 dk	3						
Dec 20	II	1524.6	1534 dk	2						
	IV	1534	1622.12 dk	2						
	II	1814.5	1818.4 dk	2						
Dec 27	II	0840	0847 m	1			15000	0838 – 0838.5 } II		1N flare
							3000	0838.0 – 0839.2 }		

ν

Year	Date									
1968	Jan 2	II	0529	0544	m	2	9400	0521-0522.4	III	1B flare S+B 2
			0532	0544	dk	2				
	Jan 4	II	2242	2248	m	3	2700	2238-2239.5	III	2B 1-S1D
	Jan 5	II	0459	0505	m	1	9700	0456-0458	III	2B 1-S1D
		II	0501	0506	dk	2				
	Jan 10	II	2152	2158	m	2	2700	2145-2148		
	Jan 11	II	1703	1717	m	2	15400	1700-1700.8	II	1B 1+ S1D
		II	1706	1710	dk	2	2800	1659-1701		
		IV	1705	1845	dk	2				
		II	1706.9	1710	dk	2				
	Jan 12	II	1812	1816	m	2	15400	1809.5-1809.8		2B 1+ S1D
		II	1821	1823	m	2	2800	1806.5-1810		
		II	1822	1823	dk	2				
	Jan 14	IV	1835.5	1911	dk	2				
		II	2017	2022	m	2	15400	2009.9-213.3		2B
		II	2019.5	2042.7	dk	3	2800	240.5-2012		2+ Sid
		IV	2042.7	2304	dk	2				
	Jan 15	II	0014	0020	m	1	9400	-0012.8		
		I	0014	0038	dk	2	3750	-0013.0		
	Jan 17	II	0557.5	0602	m	1	(3750	0539-0540.8)		
		I	0557.5	0610	dk	2				
	Jan 29	II	1542.8		cm		2800	1534-1535		1B
		II	1542.8		dm		15400	1538.6-1539.3	III	1+ sid
			1540	1547	m	3	2800	1537-1539		
1968	Feb 1	I	1820	1824	m	2	15400 / 2800	1814.1-1815.6 / 1813-1815		
		I	1921	1924	n	3	15400 / 2695	1917.7-1917.9 / 1916d-1917.7		1N 1 sid
	Feb 2	II	0545.5	0548	n	2	35000	0542.5-0542.95		1B
							3750	0540-0542.6	III	1 sid
	Feb 8	II	1400		dm					
		I	1402	1405	m	3	3000	1408-1404.4	II	
	Feb 10	II	1626	1634	m	2	7000	1608-1628		2N
		I	1628	1634	dk	2	2695	1604-1629		2+ sid
		IV	1627	1714	m	2				
		IV	1632.2	1715	dk	2				
		II	1638	1640	m	1				
		II	1638	1640	dk	1				

1968	Feb 14	IV	1537.1	1555	dk	2			
	Feb 15	II	1505	1515	m	2	4995	1501-1501.4 }	1+ sid
		IV	1507	1526	m	2	3000	1456.0-1500.7)	
	Feb 16	II	2350	2353	m	2	9400	2347-2347.7)	
							2700	2347.5 - 2347.8	
	Feb 17	II	0300		cm				
		III	0258		dm		35000	0255-0256.2 } III	1B
		III	0259.5	0306.5	m	2	3750	0251-0255.6)	1- sid
		III	0259.5	0306.5	dk	2	3750	0300 - 0301.3	
	Feb 21	II	2028.2	2038	dk	2			
	Feb 25	II	0400	0422	m	1	9500	0353 - 0357.2 }	1B
							3750	0347 -0356.7)	1+ fbre
	Feb 27	II	1949	1957	m	2	8800	1950.6 -1953.5	sn
							2800	1950 -1950.5	

1968	Mar 14	II	1012	1017	m	3	2950	1009.5-1011.8 III	1 F
	Mar 20	IV	2300	after 2502	dk	2			
	Mar 21	II	1423	1440	m	3	15400	1422.5 - 1433.5 } III	
		II	1438.7	1454	dk	3	3000	1423.1 - 1430.6)	
		II	1441	1449	m	2			
		II	1916	1931	m	3	15400	1914.6 -1915.1 } III	SB
		II	1924.8	1933	dk	2	2800	1913 - 1914.8)	2- sid
		II	2207	2212	m	2	9400	2201 - 2208.8)	
		II	2215	2219	m	1	2800	2202 - 2204)	1- sid
		II	2235.5	2240.3	dk	3	2800	2221 -2222 M	
	Mar 30	II	1423	1432	m	2	2800	1423 -1423.2	

1968	Apr 1	IV	1307		cm, dm		15400	1307.2-1308.1 } III	Sb
		IV	1307.3	1311.6	m	1	300	1307.1-1308.1)	
		II	1311.5	1318.5 b	m	3			
	Apr 15	II	1326	1332	m	2	no		
	Apr 19	IV	1650	1818	dk	3			
	Apr 22	IV	1436	1630	dk	1			
		IV	1752.5	1859	dk	1			
	Apr 26	II	1529	1534	dk	2	no		

1968

Date		Time	Time	Type	#		Freq	Range		
May 3	II	2125		cm			15400	2125.7–2128.2	III	1B
	II	2124		dn			2800	2125.5–2128		3 sid
	II	2127	2143??	m	3			–2132		
	II	2139.7	2146	dk	2					
May 4	IV	0000	0659	m	1	C				
May 8	II	1416		cm			15400	1416.3–14127	III	
	II	1415		dn			2800	1415–1418		
	II	1416	1419	m	2					
	II	1416.1	1426	m	3					
	II	1419	1434	m	1					
May 10	II	1741	1746	m	2		15400	1937.1–1138.5	III	Sb
							2800	1936.3–1187.5		
May 13	IV	2131	2159.6	dk	2					
May 19	IV	0453	0515.5	m	1					
May 21	II	2024	2036	dk	3		no			
May 30	II	before 2140	<144	m	1	EB	no			
	II	2140.4	2158	dk	2	EB				

1968

Date		Time	Time	Type	#		Freq	Range		
June 1	II	1628		cm			19600	1628.0–1629.5	III	Sb
	II	1627		dn			2800	1627.9–1629	II	1-sid
	II	1631	1639	m	2					
	II	1637.5	1643.4	dk	2					
June 3	II	2351.4	2359.1	dk	3	?	9400	2382–2344		IN
	IV	2355.4	0149	dk	2		2800	2332–2335.8		1 side
June 9	II	0107	0122	m	1					
	II	0112	0122	dk	1		no			
	II	0119	0119.5	m	2					
	II	0119	0119.5	dk	2					
	IV	0839	0940	dk	2					
June 11	II	0935		cm, dkn			19000	1934.5–1930.0	III	1B
	II	0936.7	0942.3	m	2		3000	0934.4–0936.2		1t sid
June 17	II	0301.5	0326	m	1		9400	0245–0325		
							3750	0245–0325		
June 25	II	0608.5	0609.5	m	1		no			

1968										
	June 26	II	2302	2306	m	2		no		
		II	2303	2306	dk	1				
		II	2302	2316	m	2				
		II	2302	2316	dk	2				
		II	2303.3	2312.5	dk	3				

1968	July 2	II	0036.2	0037.7g	dk	3		no		
	July 5	II	2055.5	2114	dk	2?		no		
	July 7	II	0320	0329	m	1		no		
	July 8	II	1708		cm		19000	1708.5 - 1711.1 II	3B
		II	1707		dm		2800	1704	IV 3B
		II	1709	1732	m	3	2800	1708 - 1711.5 IV 3+ sid
		II	1712	1732	dk	3		
		IV	1715.8	1906	dk	3		
		IV	1239		cm			
		IV	1739	1746	m	3		
		IV	1903	1926	m	2		
	Aug 3	II	0312		cm		9400	0312 - 0317.2 II 2 N
		II	0312		dm		3750	0312 - 0317.0 II 2+ sid
		II	0316	0406	m	2		
		II	0318.5	0406	dk	2		
	Aug 7	II	0241.5	0243	m	2		no	
		II	0253	0258	m	1		
	Aug 11	II	2205	2213.5	m	2	2800	2145 - 2155
		II	2206.5	2216	dk	2		
	Aug 13	IV	1254.2	1255.7	m	2	22000	1254.0 - 1254.5 1N
		II	1257.5	1303	m	2	3600	1253.6 - 1254.5 III 1+ sid
		II	1258	1308	m	2		
	Aug 14	II	1339	1348	m	2	22000	1326.3 - 1338.3 III 1B
		II	1340	1355	m	2	2800	1326 - 1338.5 III 3 sid
	Aug 21	II	0154	0200	m	1	9400	0148 - 0148.5 II 1N
							200	0153.8 - 0154 II 2 sid
	Aug 23	II	2349.5	2359	m	2	no	
	Aug 29	II	0103	0118	m	1	no	
			0106	0106	dk	1		

1968

	Date									
	Sept 1	II	1626.5	1635.7	dk	3		10700	1613.6 – 1637.2	
		IV	1635.7	1837.6	dk	3		2800	1615 – 1680	
								2800	1617.5 – 1619	
	Sept 4	IV	0033	0054	m	2		2800	1623 – 1623.4	
	Sept 8	II	0339.5	0400	m	1		no		
	Sept 9	II	1752	1800	m	2		15400	1747.5 – 1748.2	III 1 N
								2800	1742.5 – 1748	1 - sid
	Sept 26	II	0034.5	0047	m	2		9400	0026 – 0035.2	III 2 B
		II	0038	0047	dk	2				
	Sept 29	II	1636.6	16362	dk	3		15400	1619 – 1621	III, I III 2 sid
		IV	1636.2	1650	dk	2		2695	165.9 – 1620.5	2 B 2 sid
								10700	1634.4 – 1635.1 II	
1968	Oct 2	IV	2018.2	2054	m	2		15400	2012.3 – 2013.4	III 1 N sid 2
		II	2022	2029	m	1		2800	2012 – 2014	
		IV	2054	2200	m	1				
	Oct 3	II	2359.5	2429	m	1		9400	2344 – 2420	II 2 B
			2359.5	2427	dk	1		2800	2343 – 2404.5	2 - sid
	Oct 4	II	2131.5	2143	m	2				
		II	2133.5	2134.5	dk	2		2800	2138 – 2139.5 IV	
		IV	2135	2155	m	2				
	Oct 6	II	1730	1744	m	3		8800	1734.6 – 1734.9	SN
		II	1733	1744	dk	2		2800	1734.5 – 1735.15	
		IV	1744.3	1758	m	2				
	Oct 11	IV	1457.4	1538	m, dk	2		- no -		
	Oct 23	II	2358	2417	m	2		9400	2354	III 2 B
		II	2409	2422	dk	2		3250	2354 – 2403.8	2 sid
	Oct 24	IV	0003	0055	m	1				
		IV	0003	0055	dk	1				
		IV	2059	2106	m	3		2800	2045 – 2134.5	
		II	2058	2120	m	2				
		II	2104	2120	dk	2	terry ghous		2124 – 2134.5	
		IV	2129	2237	m	1				
	Oct 27	IV	1306		ch, dm			15400	1306.2 – 1318.3	2 N
		IV	before 1312	1651	m	3		3000	1306.1 – 1319.2	3 - sid
		IV	before 1330	1830	m	3				
	Oct 28	II	1636	1642	m	2		10700	1629.3 – 1630	- 1 sid
		II	1638	1642	dk	2		2800	1629 – 1636	
	Oct 29	IV	before 1328	1440	m	3				
		IV	1440	1516	m	2				
		IV	1516		m, dk					
		IV	1516	1538	m	3				

1968	Oct 30	IV	1255	1545	m	2		17000	2353 – 2411.4		3B
		IV	Nue/1328	1917	m	2		2700	2343 - 2350		2↑sid
		IV	2145	2340	m	2					
		II	2359	2405	M	2					
		I	2400	2405	dk	2					
	Oct 31	IV	0002.5	0035	m	2					
		II	0017.5	0021	m	2		9400	2231 – 2259.4	IV	2B
		II	0017.5	0021	dk	1		2700	2247 - 2301		1↑sid
		IV	2247	2307	m	3					
	Nov 1	II	0851.7	0900.5	m	2					
		II	2007	2011	M	2		2800	2009 - 2011.6		
	Nov 2	II	1003.5	1017.5	M	2		19000	0949.0 - 0955.7		2B
		IV	1054.6	1100.7	m	2		3000	0949.2 - 1012.6		3- sid
		II	1439.2	1404.2	m dk	3					
		II	1504	1518.2	m dk	3		15400	1455.8 - 1522.3		
		IV	15 M		em			4995	1451.7 – 1522		
		IV	1514		dk						
		IV	1518.2	1607	m dk	3					
	Nov 4	II	0231.5	0232.5	m	2					
		II	0517	0550	m	3	H	17000	0514		
		II	0517.5	0550	dk	3		3100	0514 - 0523		2 sid
								9400	0539 - 0548		
	Nov 11	IV	1457.4	1538	m dk	2					
	Dec 2	II	2114	2141	m	3		2700	2105 – 2116	II	1N
		II	2117	2141	dk	2					1↑sid
		IV	2117.5	2152	m dk	3					
	Dec 11	IV	1144		ch dim						
		IV	1144	1210	m	2		19000	1148.4 – 1153.9	IV	1↑sid
		II	1154	1155	m	2		3000	1145 - 1154.6		
	Dec 12	II	2314	2322	m	2		9400	2310 - 2310.8	II	
								2000	2309 - 2311.6		
	Dec 13	II	0428	0444	m	2		3750	0424 - 0425.2	III	
	Dec 14	II	1010.2	1010.5	m	2		dw only			
	Dec 23	II	1119.8	1126.5	m	2		9500	1112.3 - 1112.6	III	1N
	Dec 24	II	0642.5	0652	m	2		9100	0652.2 - 0637.3	III	SN
		II	2224	2224.5	m	1		2950	0634.0 - 0636.3		
		IV	2229	2247.8	m	3					
		II	2230.5	2242	m	2					
		II	2235	2247	dk	2		2700	2229 - 2228.7	III	1B
											1- sid

Year	Date		Time1	Time2		#	Value	Range		Code
	Dic 25	II	0650.5	0658	m	2	9400	0646-0648		1N
							3100	0641-0648		
	Dic 28	II	2137	2144	m	1	nothing			
	Dic 30	II	1433.6	1437	m	2	nothing			
		II	1433.6	1437	dk	2				
1969	Jan 13	IV	2105	2347	dk	3	nothing			
		II	2229.4	2244.8	dk	3				
	Jan 17	IV	1705.4	1737	m, dk	3	35000	1704.5 - 1704.6		Sb
		II	1705.6	1720	m	3	2800	1204-17048	II	1 sid
		I	1709	1720	dk	3				
	Jan 18	II	0203.5	c210.5	m	2	17000	0201.3 - 0201.8	III	
							3750	0201 - 0201.7		
	Feb 1	II	2138.5	2201	m	2	2700	2130c - 2136.5	III	1B
										3 sid
	Feb 2	II	0513	0520	m	1	9400	0510-0512.2		2B
										1 sid
	Feb 8	II	0021	0024	m, dk	1				
		II	0418	0422	m	1	17000	0415.3 - 1415.7		SN
		IV	1205	1210	m	2				
		II	1207.4	12215	m	2	3000	1204.5 - 1206	III	Sb
		II	1752.8	1809	m	2	3000	1204.6 - 1206.1		
		II	1757	1809	dk	2	154000	1750.4 - 1251.2		
		II	1757.2	1803	dk	1	2800	1750.2 - 1757		
		IV	1804.1	1814	mdk	3	154000	1754.4 - 1755a		
		IV	1814	1900	mdk	2	2800	1255 - 1756		
	Feb 9	II	1435	1438	m	1	19000	1430.5 - 1432	III	Sb
		II	1440.7	1444.6	mdk	2	3000	1431.3 - 1432.6		2 sid
		II	1726	1745	m	2	15800	1723.8 - 1524.2	35000	1724.2 - 1725.1
		II	1728	1745	dk	3	2700	1721.9 - 1723.6	2800	1722-1724.5
	Feb 23	II	0447	0456	m	3	9400	0442 - 0455.4	SN	
	Feb 24	IV	2307.7	2430	mdk	3	9400 -	2307- 2314.0	IV	2B
		II	2311.5	2329	m	2	2700 -	2304 - 2313		2 sid
		II	2315.5	2327	dk	2				
		II	2316	23215	mdk	3				
	Feb 25	IV	0000	0015	m	2				
		IV	0904	1130	m	3				
		IV	1645		cm					
		IV	1650		dm					
		IV	1651	1702	m	3				
		IV	1939	1946	m	3				

LITHOGRAPHED IN U.S.A · ADDISON WESLEY PUBLISHING COMPANY, INC. READING, MASS · A/W Datagram® 10FLV